Multiscale Modeling and Theoretical Design of Dielectric Elastomers

Submitted in partial fulfillment of the requirements for
the degree of
Doctor of Philosophy
in
Computational Mechanics

Matthew Grasinger

B.S., Civil Engineering, University of Pittsburgh
M.S., Civil Engineering, University of Pittsburgh

Carnegie Mellon University
Pittsburgh, PA

December, 2019

Acknowledgements

I would like to acknowledge the Dean's fellowship, the Summer Journeyman fellowship, and the Neil and Jo Bushnell fellowship for choosing to support me at different times throughout my PhD work. In addition, this research was financially supported by National Science Foundation (Mechanics of Materials program: 1635407, 1150002; Manufacturing Machines and Equipment program: 1635435; XSEDE program: TG-DMR120046), Office of Naval Research (Applied and Computational Analysis program: N00014-14-1-0715, N00014-18-1-2528; Directed Energy program: N00014-18-1-2856), Air Force Office of Scientific Research (Computational Mathematics program: FA9550-12-1-0350), and Army Research Office (Numerical Analysis program: W911NF-12-1-0156, W911NF-17-1-0084).

I would like to thank my committee members, Matteo Pozzi, M. Ravi Shankar (University of Pittsburgh), Jaroslaw Knap (Army Research Laboratory), and Carmel Majidi (MechE), for their time, patience, and their insightful feedback. Their influence has helped to, not only improve this thesis significantly, but also to improve my abilities as a researcher. Also my heartfelt gratitude to my adviser, Kaushik Dayal. Kaushik has gone above and beyond as an adviser to guide both my research, and the start of my career. He has also taught me many things, but most importantly, he has taught me how to work carefully.

I cannot thank my in-laws, my parents, and my wife enough. Your support has meant everything to me. I imagine this thesis would be very blank without you.

Also,

To Shelby and Anthony.

Abstract

Dielectric elastomers (DEs) are a promising material for use in robotic, biomedical, energy, aerospace and automotive technologies. However, currently available DEs are limited by weak electromechanical coupling and our general understanding of DEs could improve. In this work, a multiscale model of dielectric elastomers is developed. At the molecular scale, an electrostatic response of a single DE monomer is assumed and, using statistical mechanics, the thermodynamics of a DE chain is investigated. This chain scale model leads to an important insight: the role of electrostatic torque on polymer chains in the electromechanical coupling of dielectric elastomers. This chain torque occurs because there is a connection between a chain's end-to-end vector and its polarization. At the continuum-scale, this macromolecular phenomena manifests itself in the form of a deformation dependent susceptibility. Not only are novel modes of electromechanical coupling discovered, but also lessons learned from (standard) isotropic dielectric elastomers are then used to guide an in-depth analysis of the implications of designing and manufacturing anisotropic dielectric elastomers. The work in theoretical design reveals how the deformation and usable work derived from (anisotropic) dielectric elastomer actuators may be increased by as much as $75 - 100\%$ relative to standard, isotropic dielectric elastomers.

Keywords: Dielectric elastomers, Multiscale modeling, Statistical mechanics, Material design

Contents

List of Figures

Chapter 1

Introduction

Dielectric elastomers (DEs) are a class of soft materials that deform and can provide actuation when subject to electrical loads. A key characteristic to actuation with DEs is that, as opposed to more traditional types of actuation, one does not need gears, bearings, and other rigid, moving parts. Instead, the type of actuation DEs provide are more closely related to that of muscles and other biological tissues. For this reason, DEs could be an ideal material for biologically inspired robots and newer, more advanced prosthetics [BC04, CKSLA11, KT07]. In addition, DEs have many advantages for applications in energy-harvesting devices, micropumps, and other, more general, types of actuation in aerospace and automotive technologies. The key advantages of DEs are that they are generally inexpensive, lightweight, easily shaped, pliable, and can undergo significant deformations [BC04]. However, despite these advantages, DEs are limited by weak electromechanical coupling so that large voltages are often required to achieve meaningful actuation [BC04]. A better understanding of these materials–in particular, how molecular and macromolecular properties affect the bulk material response–would not only aid in design with currently available DEs, but also potentially lead to the development of more advanced DEs with stronger electromechanical coupling. Manufacturing technologies are rapidly improving; thus, it is the overarching goal of this work to: (1.) develop a model which connects the molecular- and macromolecular-properties of a given DE to its performance as an actuator and/or energy harvester and, importantly, (2.) use the multiscale model to develop insights and predictions into

how novel DEs with enhanced electromechanical coupling may be designed and manufactured.

1.1 Statistical mechanics

The approach in developing the multiscale DE model is one that is familiar in the context of elastomers: the free energy of the cross-linked polymer network is assumed to be approximately given by the sum of the free energies for each of the chains in the network, as if they were in isolation from each other (see [Tre75], Section 4). This assumption, namely that the interactions between chains in the network are negligible, is one that has been successfully used in modeling the elasticity (and, subsequently, electroelasticity) of elastomers [Tre75, AB93, CDd16, F$^+$06, Wei12]. Roughly speaking, this assumption is valid for many elastomers because the number of monomers per chain is large enough (e.g. estimates are $100 - 10000$ [F$^+$06]) and the density of elastomers is small enough such that monomers from different chains tend to be far away *enough* from each other to not interact strongly. This simplifies the problem considerably, as one only needs to know the free energy of a single chain for general conditions as opposed to explicitly modeling the system as a whole.

There is a rich history of using statistical mechanics to study polymer elasticity; and the reason why is a fundamental one: the elasticity of polymer chains is primarily due to entropy. Polymer chains consist of monomers bonded end-to-end, and, in many cases, the energy required to deform a monomer is much greater than the energy associated with rotating neighboring monomers about their shared bond [Wei12, Tre75]. If the monomers are approximately rigid and the energy associated with the rotation of bonds is negligible, then all possible chain configurations (i.e. microstates) have the same energy. In this case, the microscopic state of the system does not spend most of its time in a deep energy well, as it would in a crystalline material. Instead, it more readily explores phase space and a statistical mechanics approach becomes quite necessary.

What is meant by *entropic elasticity* can perhaps best be seen through a simple example. First, we define the *end-to-end vector* of a chain, which is the vector which connects the beginning of the chain to its end. Then consider the two microstates of a chain, (a) and (b), shown in Figure 1.1. During the

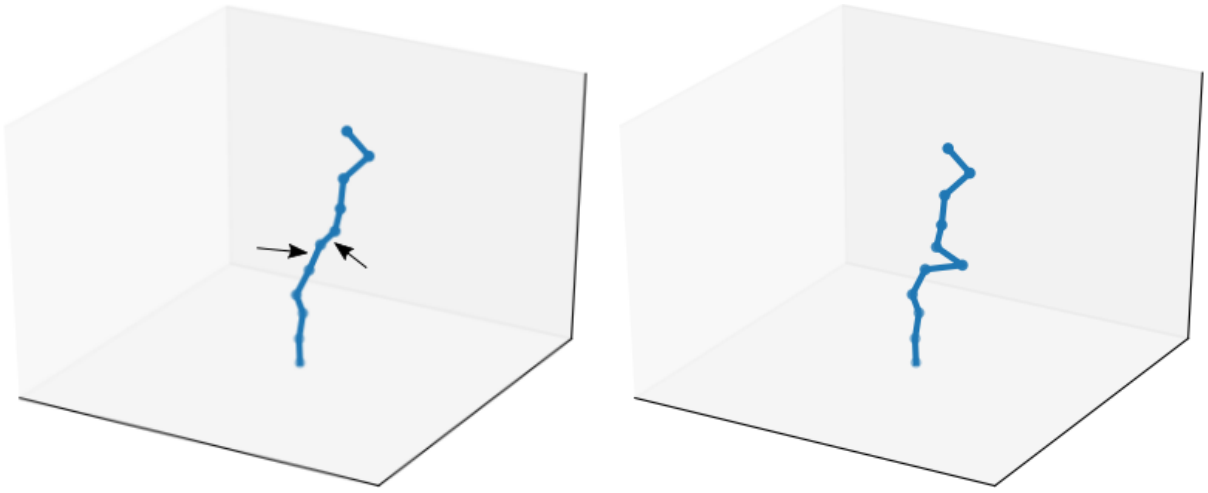

Figure 1.1: Example of what is meant by entropic elasticity. When thermal motion occurs, neighboring monomers may vibrate out of sync such that they are moving in opposite directions (left). This motion causes a rotation about their shared bond which then shortens the chain (right).

course of the thermal motion of the monomers in the chain, it will likely happen that two neighboring monomers will, at some point, vibrate out of sync such that they are moving in different directions (see Figure 1.1 (a)). Since the monomers are effectively rigid, their motion in different directions causes a rotation about their shared bond–which then shortens the chain (Figure 1.1 (b)). We say that the shorter chain has a higher entropy because there are a greater number of microstates (i.e. ways in which the monomers may be arranged) which correspond to the end-to-end vector of the shorter chain than the longer chain. While Figure 1.1 shows a single instance of a chain shortening due to thermal motion–and thereby increasing its entropy–along a polymer chain, at temperatures of interest this is happening many times per second, at different bonds along the chain, and in every chain in the network. In this way, there is a deep connection between the temperature, the entropy, and the elasticity of both an individual chain, and the polymer network which the chains make up. Notice that in Figure 1.1 an increase in thermal motion (i.e. an increase in temperature) increases the stiffness of the chain. In fact, for the same reason, polymers contract when heated, as opposed to many other materials (e.g. crystals, liquids, gasses, etc.) which expand when heated. For a more detailed discussion, see [Tre75, Wei12].

Now imagine a situation similar to Figure 1.1, but the direction that the monomers are in at any given moment are biased such that they prefer to be in some directions relative to others. Then there would be a complex interplay between the strength of the biasing, the biased directions, and the effective

elasticity of the chain. This is exactly what occurs in dielectric elastomer chains. When an electric field is applied, bound charges (of opposite sign) in the monomers of a DE chain are stretched relative to each other and an electric dipole forms. The direction of the dipole depends on the direction of the monomer, and the dipole prefers to align with the electric field. This causes an energetic preference for monomers to be in certain directions as opposed to others. Because the elasticity of the DE chain is still deeply rooted in entropy, a statistical mechanics approach (especially in the context of multiscale modeling) is still necessary. However, the monomer electrostatics (and the directional biasing that it causes) makes the problem a much more difficult one to solve.

The problem of deriving the free energy of a dielectric elastomer chain for general electrical and mechanical conditions is addressed in Chapter 2. First, the theoretical details and a derivation of classical polymer chain elasticity–without chain polarization or electrostatics–is given in Section 2.1. This is followed by a discussion of how to introduce electrostatics into the formulation and the mathematical difficulties that ensue (see Section 2.2). More specifically, since one of the goals of this work is to connect molecular-scale properties to macroscopic behavior, the free energy is derived for chains that consist of different types of monomers with different types of electrical responses. To accomplish this, the Hamiltonian for a monomer is formulated in terms of its polarization properties; that is, how its electric dipole forms in response to an applied electric field. Then, given the Hamiltonian, a statistical mechanics theory for DE chains is developed.

1.2 Network theory

As mentioned previously, the free energy of the DE network is modeled by summing over the free energies of individual chains in the network. As the end goal is a continuum-scale constitutive model, one needs to establish a correspondence between kinematics at the continuum scale and kinematics at the chain scale–at the very least. Classically, this is done using what is called a network model. Many exist in the literature, such as the 3-chain [JG43], the 4-chain model [FR43], the 8-chain model [AB93], and the full network [WVDG93]. An introduction to the basic concepts inherent in network modeling

is given in this section.

The basic idea is as follows: for each material point in the continuum body of the elastomer, we devise a number of chains to represent, on average, the chains at that material point. First, let us consider the lengths of these chains. Let b denote the length of each monomer in the chain and n denote the number of monomers per chain. Since the monomer lengths are fixed and the neighboring monomers are free to rotate about their bonds, a chain configuration is essentially a random walk of step length b and n steps. Prior to the chains being joined together in a network (i.e. prior to cross-linking), we imagine that they are free to take any configuration. If n is large, by the central limit theorem, the most likely distance of the chain beginning to the chain end (i.e. the length of its end-to-end vector) is given by $b\sqrt{n}$. What is more is that as n increases, the peak of the probability density of the chain length–which is of course at $b\sqrt{n}$–grows larger and larger such that it becomes more and more likely that chains will have length $b\sqrt{n}$. Typically, n is large enough such that the error in the constitutive relationship is negligible if one makes the simplifying assumption that all the representative chains (in the stress-free state) have length $b\sqrt{n}$ [Tre75]. Thus, in this work, as is standard [Tre75, JG43, FR43, AB93, WVDG93, MGL04], we assume the chain lengths in the stress-free, reference configuration are given by $b\sqrt{n}$.

Next, having established the lengths of our representative chains, we consider their arrangement within the network. It is important that the way in which these representative chains are chosen and their arrangement does not introduce any artificial bias into the macroscopic response that we would not expect otherwise. For instance, if we expect the material that we are modeling to be isotropic, then likewise, our representative chains should not have any directional dependence. In other words, we would prefer that the representative chains at each material point capture our knowledge–which, in many cases, is more accurately put as "our ignorance"–regarding the chain stretches and orientations in the stress-free, reference state of the elastomer. This is precisely the motivation for the so-called "full network" model [WVDG93]. Since we (1.) are modeling a material which is mechanically isotropic and (2.) we know nothing about the directions of stretch in its stress-free, reference state, *we take all chain stretch stretch directions as equally likely*. Having established this collection of reference

chains, one then takes the free energy density at a material point as the product of the average free energy over the representative chains and the number of chains per unit volume. Deformation at the continuum-scale is related to stretches at the chain-scale by what is often referred to as the *affine deformation assumption* [Tre75]. Simply put: the affine deformation assumption is such that the end-to-end vector of each chain is mapped into the current configuration by the deformation gradient (see Section 4 of [Tre75] for a detailed discussion). However, averaging over all possible chain stretch directions amounts to integrating the chain free energy function over the unit sphere. This is difficult to do in closed-form since accurate approximations of the chain free energy (even in the absence of electrostatics) have terms involving square roots and the inverse Langevin function of the integration variables.

One can strike a compromise between performing exact integration of the chain free energy function over the unit sphere and computational tractability by instead averaging over a discrete number of chains which is a "good enough" approximation of the truly frame indifferent, isotropic nature of the full network model. This apparent compromise is the motivation for the 3-chain, 4-chain, and 8-chain models, which are shown in Figure 1.2. In each case, the representative chains are arranged in a representative volume element (RVE). The RVE is a cube in the reference configuration for the 3-chain and 8-chain models. For the 3-chain model, the representative chains consist of three chains, each starting at a similar corner of the cube, and stretched along an edge of the cube; whereas, for the 8-chain model, the RVE consists of 8-chains emanating from the center of the cube to each of the eight corners. It is easy to see that using either the 3-chain or 8-chain model with the affine deformation assumption does not result in a frame indifferent constitutive model. Instead, for discrete network models, it is generally assumed that the RVE deforms in the principal frame (i.e. the frame that consists of the eigenvectors of the right Cauchy-Green tensor) and that each edge of the RVE deforms by its respective principal stretch. The reason for this assumption is two-fold: (1.) it is sufficient, when used with a discrete network model, to satisfy frame indifference (in the context of elasticity anyway) and (2.) as Arruda and Boyce [AB93, BA00] justify it, this can be considered a proper way to model the "cooperative behavior of the network". By "cooperative", we take [AB93, BA00] to mean that the

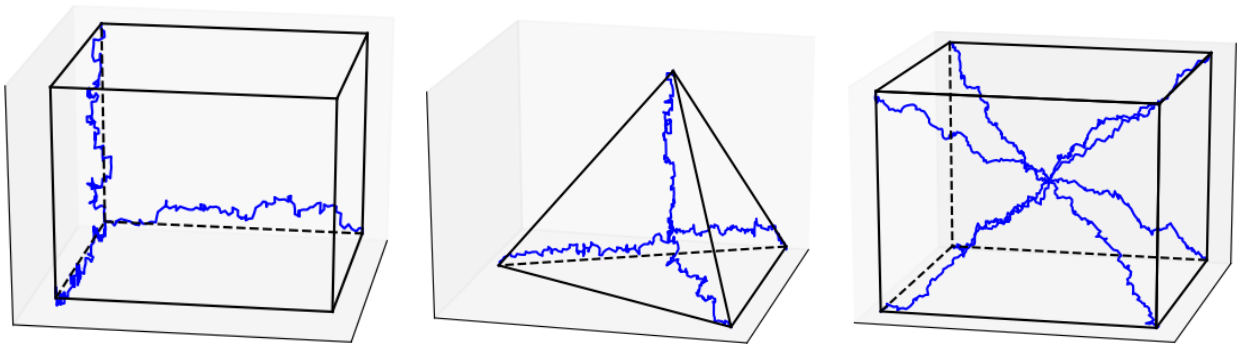

Figure 1.2: Discrete network models in the reference configuration: 3-chain (left), 4-chain (center), and 8-chain (right).

network rotates and adjusts itself, as a whole, in some sense, such that, at each material point, it is allowed to stretch in what is assumed to be its preferred frame of stretch. In the remainder of this work we refer to this as the *cooperative network assumption*. While the cooperative network assumption has not, to the author's knowledge, been observed in experiment directly, it is further motivated by the fact that, at least in the context of elasticity, it produces a constitutive model which has excellent agreement with experimental data [AB93, BA00].

To draw a comparison between the two kinematic assumptions (and two of their respective network models), consider the following: imagine that the polymer chains in our network can be approximately modeled as springs such that their energy is $\frac{1}{2}kr^2$, where k is a constant related to the spring stiffness (and is the same for all chains) and $r = |\mathbf{r}|$ is the length of the end-to-end vector of the chain. If the deformation gradient, $\mathbf{F}$, is diagonal, then the cooperative network assumption reduces to the affine deformation assumption. Thus, let us consider a deformation which does not have a diagonal $\mathbf{F}$– namely, a simple shear deformation: $\mathbf{F} = \mathbf{I} + s\mathbf{e}_1 \otimes \mathbf{e}_3$. For this $\mathbf{F}$, it is easy to average the energy over the representative chains for both the full network and 8-chain models using the affine deformation assumption and cooperative network assumption, respectively. The interested reader can verify that the network models agree, and that the average energy is given by $\frac{1}{2}kb^2n\,(1 + s^2/3)$.

This begs the question then: when do the kinematic assumptions result in different average energies and therefore predict different material behaviors? To probe this further, we visualize (Figure 1.3) the representative chains in both the reference and deformed (simple shear) configurations for the full

network and 8-chain models. Notice that the cooperative network assumption of the 8-chain model results in a rotation of the chains in the deformed configuration relative to the reference configuration, whereas the affine deformation assumption of the full network model simply shears the spherical distribution of chains. If we are only interested in an elastic response such as the one considered in the proceeding paragraph, then the rotation of the 8-chain model makes no difference. This is because the elastic energy of each of the individual chains is rotationally invariant. However, if there are some other physics involved such that a chain's energy also depends on its orientation (i.e. the energy is no longer rotationally invariant), then there are some important differences between the network models that arise. As a simple example, imagine that now the stiffness of the chains depends on their alignment with the axis $\operatorname{span}(\mathbf{e}_3)$ such that

$$\frac{1}{2}k\left(\mathbf{e}_3\cdot\hat{\mathbf{r}}\right)^2 r^2.$$

Interestingly, the average energy of the full network model and 8-chain model vary. In fact, the energy of the full network model is invariant with respect to s, whereas for the 8-chain model the average energy is

$$\frac{1}{2}kb^2n\left(1+\frac{s^3}{3}\right)\frac{1-\lambda^2+\lambda^4}{1+\lambda^2+\lambda^4}$$

where $\lambda=\frac{1}{2}\left(\sqrt{4+s^2}+s\right)$. The proceeding example was chosen because of its computational simplicity, but the idea of an alignment based energy is pervasive in physical phenomena such as electrostatics, magnetostatics, liquid crystals, as well as many others.

In Chapter 3, we use the single chain results obtained in Chapter 2 in confluence with the 8-chain model [AB93] and investigate the electromechanical coupling of (isotropic) DE networks. Various experiments are suggested and modeled which isolate some phenomena of interest, such as how chain torque contributes to electrostriction and/or body couples in DEs. As expected (based on the previous discussion), there are interesting implications associated with the cooperative network assumption such as the prediction of a novel shear mode of actuation that is possible with dielectric elastomer actuators (DEAs). In fact, an experiment involving this shear mode of actuation is suggested which would, if the actuation mode is found to exist, strengthen the argument for the cooperative network assumption in

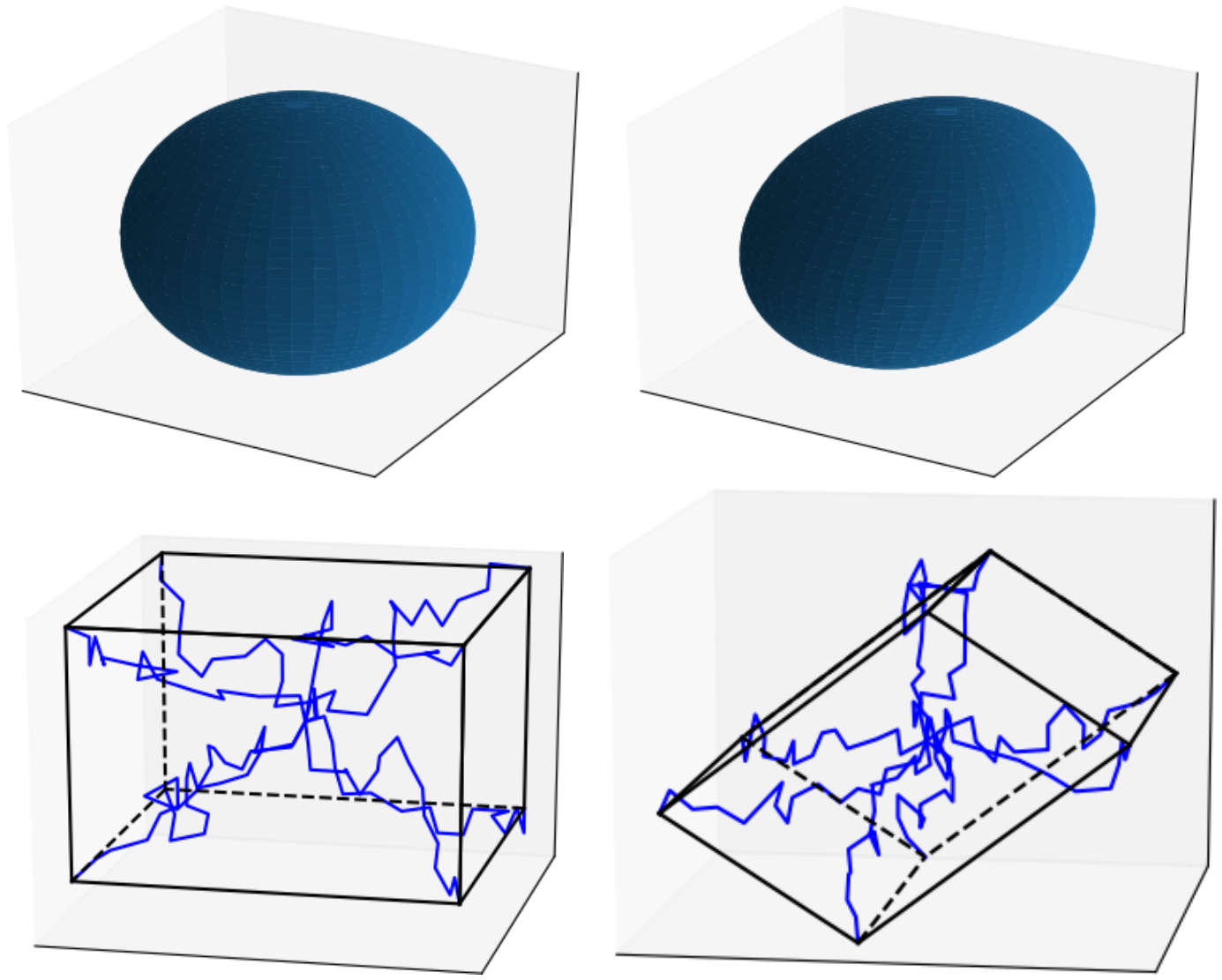

Figure 1.3: The representative chains in both the reference (left) and deformed configurations (right) for simple shear deformation with $s = 0.2$. The full network model (top)–which is depicted by a surface since the representative chains consist of a continuous distribution–utilizes the affine deformation assumption. The 8-chain model (bottom) utilizes the cooperative network assumption.

DEs.

1.3 Material design

In Chapter 4, the multiscale model and physicals insights that are developed in Chapter 2 and Chapter 3 are leveraged to make concrete suggestions and predictions about how novel, anisotropic DEs with enhanced electromechanical coupling may be designed and manufactured. First, structural, and potentially alterable, properties of the DE network are identified as design parameters: such as the density of the material (i.e. total monomers per unit volume), the density of cross-links in the network, the fraction of monomers in a chain which make up side chains–so-called "loose-end" monomers–and the orientation of chains in the network. Then equations are developed and trends are identified for how the various design parameters affect properties of the DE such as its stiffness, its susceptibility, and its deformation response and usable work output when used in a dielectric elastomer actuator (DEA). It is found that (theoretically speaking), one can see an increase of $75 - 100\%$ in the deformation and usable work output of a DEA by carefully choosing and controlling the design parameters during the manufacturing process. In particular, chain orientation is found to be important and a manufacturing process–which is analogous to poling in piezoelectrics [SA08]–is proposed, which aligns chains such as to maximize the desired electromechanical response of the material.

Chapter 2

Electroelasticity and thermodynamics of dielectric elastomer chains

The problem of the statistics of electrostatic interactions in macromolecules has been studied in [SW17]. However, the system of consideration was polyelectrolytes in solution which has two important differences from our goal in this work. First, the macromolecules considered in [SW17] consist of fixed charge distributions in the sense that the charge distributions are inseparable from the polymer and are present even in the absence of an applied electric field; whereas, in this work, we focus on electro-*responsive* materials. We emphasize responsive because the polarization vanishes in the absence of an electric field for dielectric elastomers. The second difference is that we consider polymers that are cross-linked in a network, as opposed to in solution. As a result, we need to consider ensembles with a fixed end-to-end vector, because where the chain begins and ends is dependent on the configuration of the entire network.

The electromechanical modeling of DEs can be grouped into two categories: (1) continuum based approaches where the general form of the energy density (of either a polymer chain or polymer network) as a function of mechanical and electrical loads is inferred by assuming a form of the equation, which usually depends on electroelastic invariants, that leads to behavior observed in experiments (see for example [Tou56, DO06, ZS08]) and (2) statistical mechanics based approaches that build from

molecular-scale responses up to the levels of a single chain and eventually the continuum level response. Statistical mechanics has a rich history in modeling and understanding rubber elasticity (see for example [Tre75, KG42, Wei12]); however, its use in the modeling of DEs is only recent.

In [IKW18], an DE constitutive model was developed that started by considering the polarization response of a single monomer and assumed the statistical density of monomer orientations in an DE chain are governed by non-Gaussian chain statistics (derived in [KG42]). From these assumptions, approximate DE chain statistics and polarization were derived; then, [IKW18] used directional averaging and network theory (for example [AB93, MGL04]) to arrive at a prediction of the macroscopic constitutive response. The resulting constitutive model is limited, however. The assumption that the density of monomer orientations in the chain are governed by classical (i.e. not informed by electrostatics), non-Gaussian statistics, is only valid when either (1) the electrical energy of the system is much less than the thermal energy (such that the Boltzmann factor is practically unity for all chain configurations) or (2) the chain is near to its stretched limit (such that the limited range of possible monomer orientations are all of nearly the same electrical energy).

In [CDd16], an DE constitutive model is developed using a similar approach. However, in contrast to [IKW18], the authors do not assume the density of monomer orientations is governed by non-Gaussian statistics, but instead derive the most likely density of monomer orientations; that is, the density of monomer orientations that minimizes the entropy of the chain. Such a derivation naturally involves optimization with respect to constraints; hence, the authors use the method of Lagrange multipliers. The integrals and system of equations required to determine the unknown multipliers are difficult to evaluate and solve; and so the authors assume that some of the unknown multipliers are small and use Taylor expansions to simplify the calculations. This results in an approximate density of monomer orientations that is exact when there is no stretch in the chain. However, the simplifying assumption that is made corresponds, physically, to the assumption that the tension in the chain is small. This assumption could prove inaccurate for finite, or even small, stretches for certain chain orientations with respect to the applied electrical field, especially when the electric field strength is large. In addition, for DEs used as actuators or for energy-harvesting, the chain tension is not guaranteed to be small. Lastly,

note that an approximate chain free energy was not derived in either [IKW18, CDd16]–although such a development could prove useful in understanding the physics of DEs and modeling their behavior using Finite Elements.

In the present work, we employ the maximum-term approach [Hil86] to derive a most likely density of monomer orientations and an approximation of the DE chain free energy. Although, as in [CDd16], the Lagrange multipliers are not determined exactly, we investigate their character using numerics (e.g. numerical integration, Newton-Raphson method, and numerical optimization); and then proceed to derive closed-form approximations in the limits of (1) the electrical energy as small compared with thermal energy and (2) the limit of small chain tension. Lastly, using physical intuition and the exactly known solutions of the unstretched and fully stretched chain limits, we derive closed-form approximations that remain accurate for many different electrical inputs, chain orientations, and chain stretches. Figure 2.1 shows a rough schematic of the limits in which closed-form approximations have been developed. The y-axis, labeled $|\kappa|$, represents the magnitude of the electrical energy with respect to the thermal energy. The x-axis, labeled $|\boldsymbol{\tau}|$, represents the dimensionless tension in the DE chain. The approximation labeled (1) corresponds to the monomer density function derived in [KG42] (also revisited in Section 2.1) and used in [IKW18] to model DE chains; (2) corresponds to the limit explored in [CDd16] and subsequently in Section 2.5; (3) corresponds to the limit investigated in Section 2.4; and Section 2.6 aims to develop an approximation that is valid at (4), (2), and in the space between.

2.1 Inverse Langevin chain statistics, revisited

In this section, we revisit the work of Kuhn and Grün [KG42] (see also: [Tre75], Ch. 7) regarding the statistical mechanics of a polymer chain with the aim to later generalize it to the case of a dielectric elastomer chain with combined mechanical and electrical loading. This section will be structured as follows: definitions and assumptions for the model of a polymer chain will be explicitly stated; the thermodynamics of polymers and the thermodynamic implications of the model assumptions will be presented; the Helmholtz free energy of the chain will be derived; and finally, the force-length rela-

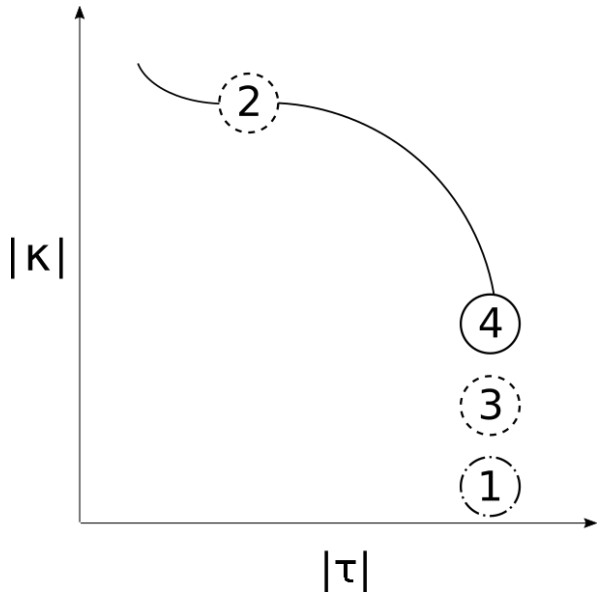

Figure 2.1: Schematic of the limits for which closed-form approximations have been developed. The axis labeled $|\kappa|$ represents the magnitude of the electrical energy with respect to the thermal energy and the axis labeled $|\tau|$ represents the dimensionless tension in the DE chain. The approximation labeled (1) corresponds to the monomer density function derived in [KG42] (also revisited in Section 2.1) and used in [IKW18] to model DE chains; (2) corresponds to the limit explored in [CDd16] and subsequently in Section 2.5; (3) corresponds to the limit investigated in Section 2.4; and Section 2.6 aims to develop an approximation that is valid at (4), (2), and in the space between.

tionship that results from the chain model and its significance in the development of rubber elasticity will be discussed.

A common model of a polymer chain in classical rubber elasticity, and one that will be focused on in this work, is a linear chain (meaning monomers are bonded together, end-to-end, to its two neighboring monomers). The monomer length is defined as the distance between neighboring bonds and will be denoted by b, so that given the number of monomers in the chain, n, the length of the fully stretched chain is nb. In addition, the end-to-end vector, $\mathbf{r}$, is defined as the vector that connects the beginning of the chain to the end of the chain. Its length is denoted by $r = |\mathbf{r}|$. Last, we define the stretch as $\gamma = \frac{r}{nb}$.

In real polymers, the energy required to deform an individual monomer (bend, stretch, compress, etc.) is typically much greater than the energy required to rotate a monomer about either of its bonds. More precisely, let the energy of a monomer be written as

$$u = u_{\text{strain}} + u_{\text{bond}}$$

where u_{strain} is the energy associated with deforming the monomer and u_{bond} is the energy associated with rotating about neighboring bonds. Then we claim that the energies scale like

$$u_{\text{bond}} << kT << u_{\text{strain}}$$

so that, to a good approximation, u_{bond} can be neglected and degrees of freedom associated with monomer deformation are effectively "frozen out". For this reason, the polymer chain model considered in this work is idealized such that the monomers are modeled as rigid bodies and are free to rotate about their bonds. Monomer-monomer interactions, namely, excluded volume effects and van der Waals interactions between neighboring side groups, are also neglected for simplicity. Note, an important consequence of the model assumptions is that all chain configurations have the same potential energy.

We use equilibrium statistical mechanics, namely ensemble theory, to investigate the thermodynamics of a polymer chain. Ensemble theory is generally constructed by assuming, as one its fundamental postulates, that: in an ensemble representative of an isolated thermodynamic system (meaning the system does not interact with its surroundings or exchange energy, particles, etc. with its surroundings), the microstates of the ensemble are distributed uniformly, i.e. they are all equally likely [Hil86]. For the system that consists of a polymer chain, each microstate corresponds to a different chain configuration. Because each configuration has the same energy, one concludes that all chain configurations are equally likely.

We are ultimately interested in the elasticity of a polymer network, so we proceed by deriving the force-deformation relationship for a single polymer chain where the force-length relationship is described by a graph of the length of the chain end-to-end vector and the average force required to stretch the chain to that length. The thermodynamic analysis of a polymer chain results in the following expression

$$\mathfrak{f} = \left(\frac{\partial \mathcal{A}^*}{\partial r}\right)_T = \left(\frac{\partial \mathcal{U}}{\partial r}\right)_T - T\left(\frac{\partial \mathcal{S}}{\partial r}\right)_T \tag{2.1.0.1}$$

where $\mathcal{A}^*$ is the Helmholtz free energy, r is the chain length, $\mathcal{U}$ is the internal energy, T is the tem-

perature, and $\mathcal{S}$ is the entropy. It has already been pointed out that, as a consequence of the model assumptions, the internal energy of a polymer chain is the same for all configurations; thus, the $\left(\frac{\partial U}{\partial r}\right)_T$ term vanishes. To determine the force-length relation, it suffices to derive the entropy of a polymer chain as a function of its chain length, r. To determine the entropy-length relation, one considers the ensemble of microstates that correspond to a given chain length. It is a well-known result in statistical mechanics that the entropy of an ensemble of systems with constant internal energy is given by

$$\mathcal{S} = k \ln \Omega \tag{2.1.0.2}$$

where k is Boltzmann's constant and Ω is the number of microstates in the ensemble.

The space of all possible directions makes up the surface of the unit sphere. We parameterize the surface of the unit sphere in the usual way, so that a unit direction is expressed as $\hat{\mathbf{n}} = (\cos\phi \sin\theta, \sin\phi \sin\theta, \cos\theta)$ where ϕ is the azimuth angle and the coordinate system is chosen such that the polar angle, θ, is with respect to the direction of the end-to-end vector (i.e. in the $\mathbf{r}/r$ direction). Next, we partition the surface into $\mathcal{N}$ patches of area $\sin\theta_i \Delta\phi_i \Delta\theta_i$ and define the occupation numbers, m_i, as the number of monomers oriented such that their unit direction lies in the ith patch; i.e. their azimuth angle, ϕ, is between ϕ_i and $\phi_i + \Delta\phi_i$, and their polar angle, θ_i, is between θ_i and $\theta_i + \Delta\theta_i$. A polymer configuration is specified by prescribing the direction of each of the n monomers in the chain. There are $\frac{n!}{\Pi_{i=1}^{\mathcal{N}} m_i!}$ ways to assign the $\mathcal{N}$ directions to n monomers. Consequently,

$$\Omega = \sum_{\{m_i\}}{}' \frac{n!}{\Pi_{i=1}^{\mathcal{N}} m_i!} \tag{2.1.0.3}$$

where the prime in $\left\{ m_i \right\}'$ signifies that the sum is over all distributions that satisfy the constraints

$$n = \sum_{i=1}^{\mathcal{N}} m_i \tag{2.1.0.4}$$

$$\frac{\mathbf{r}}{b} = \sum_{i=1}^{\mathcal{N}} m_i \hat{\mathbf{n}}_i \tag{2.1.0.5}$$

In general, determining each collection of occupation numbers such that (2.1.0.4) and (2.1.0.5) are satisfied and evaluating the sum in (2.1.0.3) are both difficult. Additionally, recall from (2.1.0.2) that the quantity of interest is ultimately $\ln \Omega$. Recognize that the logarithm is a monotonically increasing function of its argument, and that its derivative goes as the inverse of its argument (i.e. when its argument is large, small changes in the argument result in small changes the function value). If the sum in (2.1.0.3) is dominated by one term, then $\ln \Omega$ can be accurately approximated by maximizing the logarithm of the combinatoric term in (2.1.0.3). This method of approximation is common in statistical mechanics and is referred to as the maximum-term method in [Hil86] (see Appendix II). It is valid in the present analysis as long as we restrict ourselves to cases in which the number of monomers in a chain is large enough (≥ 100). (Loosely speaking, this approximation is often justified in statistical mechanics–as it is in the current work–by the central limit theorem. For a more detailed discussion, see any statistical mechanics reference, such as [Hil86, Wei12, Kra06]) To perform the maximization, one can use the method of Lagrange multipliers. Thus, one searches for stationary points of

$$\ln \left(\frac{n!}{\prod_{i=1}^{\mathcal{N}} m_i!} \right) + \nu \left(n - \sum_{i=1}^{\mathcal{N}} m_i \right) + \boldsymbol{\tau} \cdot \left(\frac{\mathbf{r}}{b} - \sum_{i=1}^{\mathcal{N}} m_i \hat{\mathbf{n}}_i \right) \tag{2.1.0.6}$$

Employing Sterling's approximation, $\ln x! \approx x \ln x - x$, and setting partials with respect to m_j equal to zero, one obtains $m_j = \exp\left[\boldsymbol{\tau} \cdot \hat{\mathbf{n}}_j + \nu + 1\right]$. We proceed as follows: terms that do not depend on the unit direction are absorbed into an unknown constant C, and we take the limit as $\mathcal{N} \to \infty$, which results in the transition from a discrete collection of occupation numbers into a continuous density. The emphasize the distinction, we denote the density by ρ (as opposed to m). The last step is more subtle, but important: the unknown multipliers related to the kinematic constraint, (2.1.0.5),

are related, physically, to the force required to stretch the polymer chain to a length of r. Two of the multipliers vanish due to the following observation: in the absence of a kinematic constraint and at finite temperature, the free energy of the chain is minimized when $r = 0$ (because this corresponds to a maximum entropy). This means the force required to stretch the chain will be in the direction of stretch. As our coordinate system is such that the polar axis is taken to be the direction of stretch, the expression for the monomer density becomes

$$\rho(\phi, \theta) = C \exp\left[\lambda \cos\theta\right] \tag{2.1.0.7}$$

where λ is the component of $\boldsymbol{\tau}$ in the direction of the polar axis. The number of monomers with azimuth angle between ϕ and $\phi + \mathrm{d}\phi$ and polar angle between θ and $\theta + \mathrm{d}\theta$ is $\rho(\phi, \theta) \sin\theta \, \mathrm{d}\phi \, \mathrm{d}\theta$. Although technically the number of monomers in a given direction should be of integer value, and the previous expression is, in general, not of integer value, the distinction becomes less important when one considers that in the limit of large n the decimal contribution is a negligible difference. Alternatively, it is perhaps better to think of $\rho(\phi, \theta) \sin\theta \, \mathrm{d}\phi \, \mathrm{d}\theta$ as the expectation of the number of monomers with a given direction, where, by expectation, we mean in the ensemble average sense.

The next step is to determine the unknowns, C and λ. To do this, we consider the form of the constraints, (2.1.0.4) and (2.1.0.5), in the continuum limit (i.e. $\mathcal{N} \to \infty$). The summations over partitions of the unit sphere becomes integrals over the unit sphere

$$n = \int_0^{\pi} \mathrm{d}\theta \int_0^{2\pi} \mathrm{d}\phi \, \rho\left(\phi, \theta\right) \sin\theta = \frac{4\pi C}{\lambda} \sinh\lambda \tag{2.1.0.8}$$

$$\frac{r}{b} = \int_0^{\pi} \mathrm{d}\theta \int_0^{2\pi} \mathrm{d}\phi \, \rho\left(\phi, \theta\right) \cos\theta \sin\theta = \frac{\partial}{\partial\lambda}\left(\frac{4\pi C}{\lambda} \sinh\lambda\right) \tag{2.1.0.9}$$

$$= \frac{4\pi C}{\lambda}\left(\cosh\lambda - \frac{\sinh\lambda}{\lambda}\right) \tag{2.1.0.10}$$

Now the significance of choosing the coordinate system such that the polar axis is in the direction of the chain stretch becomes apparent. It allows for ease of evaluating the integrals in (3.0.0.3) and

(2.1.0.9). Dividing (2.1.0.10) by (3.0.0.3) results in the familiar relation

$$\coth \lambda - 1/\lambda = \gamma \tag{2.1.0.11}$$

The Langevin function appears in many physical problems and is defined as $\mathcal{L}(x) := \coth x - 1/x$. Hence, $C = \frac{n\lambda}{4\pi}$ csch λ, $\lambda = \mathcal{L}^{-1}(\gamma)$ and

$$\rho(\phi, \theta) = \frac{n\mathcal{L}^{-1}(\gamma)}{4\pi \sinh\left(\mathcal{L}^{-1}(\gamma)\right)} \exp\left[\mathcal{L}^{-1}(\gamma) \cos\theta\right]. \tag{2.1.0.12}$$

Although, a closed form expression of $\mathcal{L}^{-1}$ does not currently exist, many accurate approximations have been developed (see for example, [Kro15, Jed17]). Taking (2.1.0.2) to the continuum limit and again, using Stirling's approximation,

$$\mathcal{S} = k\left(n \ln n - \int_0^{\pi} \mathrm{d}\theta \int_0^{2\pi} \mathrm{d}\phi\, \rho \ln \rho \sin\theta\right) \tag{2.1.0.13}$$

Thus, remembering (2.1.0.11),

$$\mathcal{S} = -kn\left[\gamma\mathcal{L}^{-1}(\gamma) + \ln\left(\frac{\mathcal{L}^{-1}(\gamma)}{4\pi \sinh\left(\mathcal{L}^{-1}(\gamma)\right)}\right)\right] \tag{2.1.0.14}$$

Differentiating (2.1.0.14) with respect to r and recognizing

$$\coth\left(\mathcal{L}^{-1}(\gamma)\right) - 1/\left(\mathcal{L}^{-1}(\gamma)\right) = \gamma$$

results in

$$\mathfrak{f} = \frac{kT}{b}\mathcal{L}^{-1}(\gamma) \tag{2.1.0.15}$$

Notice that the force length relationship, that is, the stiffness of the chain, increases with increasing temperature. This is because, in the idealized chain model that was considered, the internal energy of the chain does not change when monomers rotate about their bonds (or, as a consequence, when the chain is stretched). Therefore, the stiffness of the chain is entirely an effect of thermal fluctuations and

entropy.

The chain statistics derived by Kuhn and Grun in [KG42] and revisited in the current section marked an important development in the modeling of rubber elasticity. Although the expression for the chain entropy, (2.1.0.14), was obtained by approximating the sum in (2.1.0.3) with its maximum-term, the approximation proves to be quite accurate up to the full extension of the chain (i.e. $\gamma \to 1$). In particular, as γ approaches unity, both the free energy and the force approach ∞; hence, unlike Gaussian chain statistics, (2.1.0.14) and (2.1.0.15) have the property that they capture the finite extensibility of the chain.

Two key steps in the procedure that was outlined in this section were choosing the coordinate system such that the polar axis was taken to be in the direction of chain stretch and recognizing that, as a result of this choice, $\boldsymbol{\tau} \cdot \hat{\mathbf{n}}$ simplified to $\lambda \cos\theta$. In the following sections, the procedure that was presented in this section will be generalized to deriving the monomer density function and free energy of DE chain subjected to an external electric field. The coordinate system and, in particular, the direction of the polar axis, will again be chosen carefully in order to facilitate evaluating integrals involving the density function.

2.2 DE chain model formulation

2.2.1 Energy scales and degrees of freedom in a DE chain

In this section, our thermodynamic system of interest consists of a dielectric elastomer chain which is contained in some volume Ω_c with boundary surface $\partial\Omega_c$ and is surrounded by a heat bath. The chain consists of n monomers, and for each microstate (i.e. chain configuration) of the ensemble the direction, $\hat{\mathbf{n}}_i$, and dipole vector, $\boldsymbol{\mu}_i$ is specified for each monomer. An example microstate is shown in Figure 2.2. Further, we assume the electric potential, φ, is specified for all $\mathbf{x} \in \partial\Omega_c$. Let $\mathbf{x}$ denote a position and $\mathbf{x}_i$ denote the position of the ith monomer. Then the potential energy of a microstate is

given by

$$U = \sum_{i=1}^{n} \left\{ u_{\text{strain}}^{(i)} + u_{\text{bond}}^{(i)} + u_{\text{dipole strain}}^{(i)} - \boldsymbol{\mu}^{(i)} \cdot \mathbf{E}\left(\mathbf{x}^{(i)}\right) \right\} + \frac{\epsilon_0}{2} \left(\int_{\Omega_c} E^2 \, \mathrm{d}V + \int_{\partial\Omega_c} \varphi \mathbf{E} \cdot \mathbf{n} \, \mathrm{d}A \right) \tag{2.2.1.1}$$

where in (2.2.1.1) we use the superscript, $\square^{(i)}$, to mean the same thing as $\square_i$; that is, to denote the index of a monomer quantity and $\mathbf{E} = -\operatorname{grad}\varphi$. The meaning of the terms in (2.2.1.1) are as follows: $u_{\text{strain}}^{(i)}$ represents the energy associated with deforming the ith monomer, $u_{\text{bond}}^{(i)}$ is the energy associated with the ith monomer rotating about its neighboring bonds, $u_{\text{dipole strain}}^{(i)}$ is the work required to take an electrically neutral monomer and separate charges in order to form its dipole, $-\boldsymbol{\mu}^{(i)} \cdot \mathbf{E}\left(\mathbf{x}^{(i)}\right)$ is the electrical potential energy of the ith monomer dipole, and the final term is the energy stored in the electric field. Although the boundary conditions (i.e. $\varphi\left(\mathbf{x}\right), \mathbf{x} \in \partial\Omega_c$ are assumed fixed, φ may vary independently of $\{\hat{\mathbf{n}}_i\}$ and $\{\boldsymbol{\mu}_i\}$ as long as it satisfies the boundary conditions. Therefore the partition function for this ensemble is given by

$$\mathcal{Z} = \int \exp\left\{-U\left[\varphi, \{\hat{\mathbf{n}}_i\}, \{\boldsymbol{\mu}_i\}\right]/kT\right\} \mathcal{D}\varphi \prod_{i=1}^{n} \left\{\mathrm{d}\boldsymbol{\mu}_i \, \mathrm{d}\hat{\mathbf{n}}_i\right\}$$

where by the above notation we mean a functional integral with respect to φ and integration with respect to all possible dipole vectors and monomer directions for each of the monomers in the chain. Such an approach would prove difficult for a number of reasons. Instead, we work toward simplifying the formulation.

Consider the potential energy given by (2.2.1.1) in the context of the theoretical framework of statistical mechanics. First, similar to Section 2.1, we postulate that the energies scale like

$$u_{\text{bond}}^{(i)} << kT << u_{\text{strain}}^{(i)} \text{ for } i = 1, 2, ..., n$$

so that, to a good approximation, u_{bond} can be neglected and degrees of freedom associated with monomer deformation are effectively frozen out. In addition, for simplicity, we assume the remaining

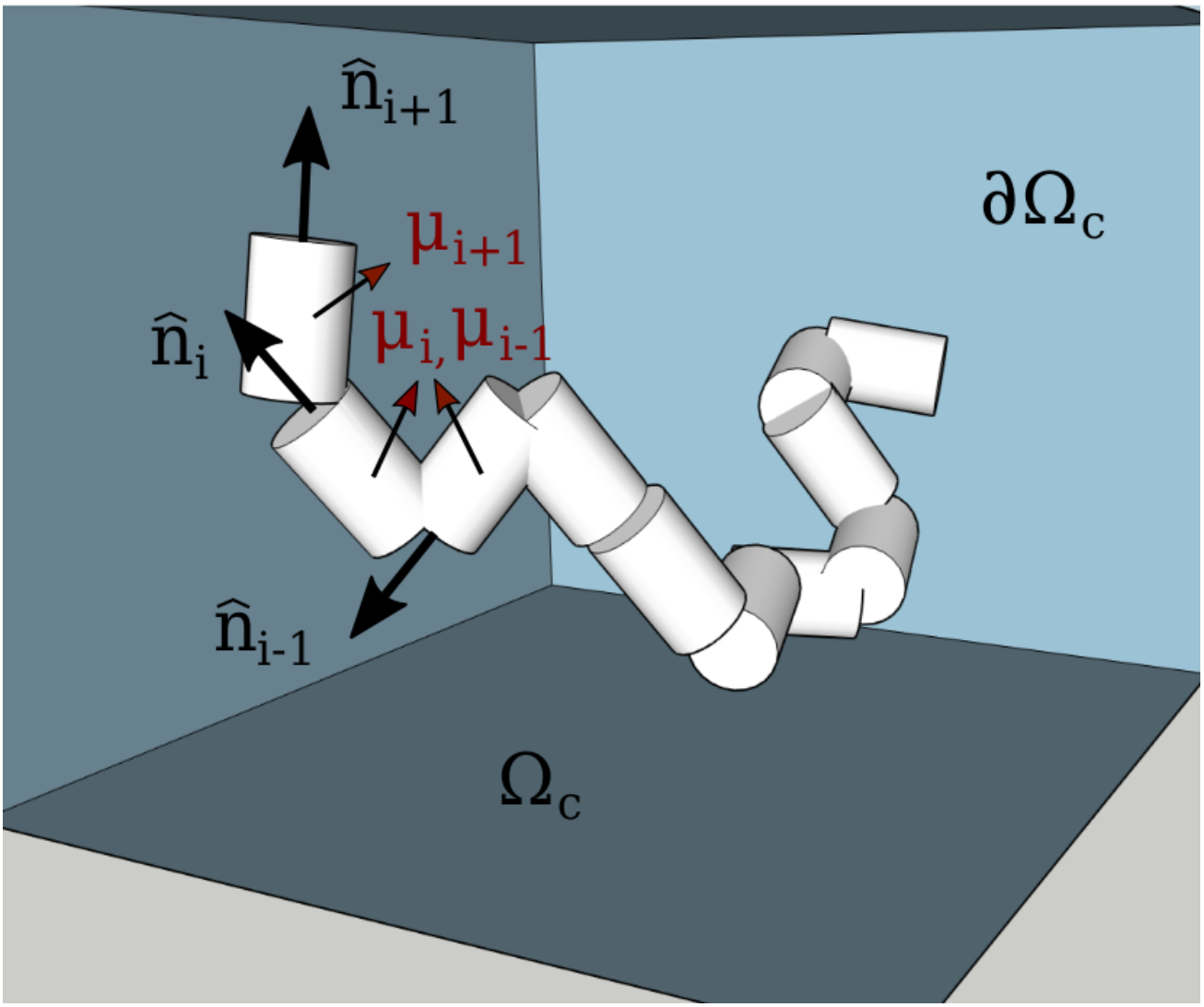

Figure 2.2: Schematic of a microstate of a dielectric elastomer chain. Monomers are depicted as cylinders. For each microstate, the monomer direction, $\hat{\mathbf{n}}_i$, and dipole vector, $\boldsymbol{\mu}_i$, are specified. (The direction and dipole are only shown for three monomers in the figure above in the interest of keeping the figure clear and readable.) The chain is contained in some volume, Ω_c, and associated boundary surface, $\partial\Omega_c$.

terms scale as follows: the monomer terms are an order of magnitude lesser than the energy of the electric field; in other words, we write this as

$$\begin{aligned} U = \beta \sum_{i=1}^{n} \left\{ u^{(i)}_{\text{dipole strain}} - \boldsymbol{\mu}^{(i)} \cdot \mathbf{E}\left(\mathbf{x}^{(i)}\right) \right\} + \\ \frac{\epsilon_0}{2} \left(\int_{\Omega_c} E^2 \, \mathrm{d}V + \int_{\partial \Omega_c} \varphi \mathbf{E} \cdot \mathbf{n} \, \mathrm{d}A \right) \end{aligned} \tag{2.2.1.2}$$

where $\beta << 1$. Then we make a saddlepoint-like approximation. The argument is as follows: in the canonical ensemble, the unnormalized probability of being in a microstate is given by the Boltzmann factor $\exp\left[-U/kT\right]$. Thus, the thermodynamic system will spend most of its time, loosely speaking, in those microstates which have the minimal potential energy. To find those microstates, we consider the solution of the optimization problem

$$\inf_{\varphi, \{\hat{\mathbf{n}}_i\}, \{\boldsymbol{\mu}_i\}} U\left[\varphi, \{\hat{\mathbf{n}}_i\}, \{\boldsymbol{\mu}_i\}\right]$$

subject to the boundary conditions on φ. Now, when optimizing a cost-function of the form given by (2.2.1.1) an approximate solution can be found by optimizing in a step-wise manner; that is, first optimizing over the $\mathcal{O}\left(1\right)$ terms and then plugging that solution into lower order terms and optimizing over the remaining unknowns:

$$\varphi^* = \arg \left\{ \inf_{\varphi} \frac{\epsilon_0}{2} \left(\int_{\Omega_c} E^2 \, \mathrm{d}V + \int_{\partial \Omega_c} \varphi \mathbf{E} \cdot \mathbf{n} \, \mathrm{d}A \right) \right\} \tag{2.2.1.3}$$

$$\{\hat{\mathbf{n}}_i\}^*, \{\boldsymbol{\mu}_i\}^* = \arg \left\{ \inf_{\{\hat{\mathbf{n}}_i\}, \{\boldsymbol{\mu}_i\}} \sum_{i=1}^{n} \left[u^{(i)}_{\text{dipole strain}} - \boldsymbol{\mu}^{(i)} \cdot \mathbf{E}^*\left(\mathbf{x}^{(i)}\right) \right] \right\} \tag{2.2.1.4}$$

where $\mathbf{E}^* = -\operatorname{grad}\varphi^*$ and, again, φ^* satisfies the given boundary conditions. This can be justified by noticing that, by assumption, the $\mathcal{O}\left(1\right)$ terms will dominate relative to the $\mathcal{O}\left(\beta\right)$ terms. By similar reasoning, the saddlepoint-like approximation is taken by fixing $\varphi = \varphi^*$ (whereby φ^* is determined by (2.2.1.3)) and considering the microstates with energy

$$U = \sum_{i=1}^{n} \left[u^{(i)}_{\text{dipole strain}} - \boldsymbol{\mu}^{(i)} \cdot \mathbf{E}^*\left(\mathbf{x}^{(i)}\right) \right]$$

Physically, this is equivalent to φ^* being determined by Gauss's law in the absence of the monomer dipoles (i.e. div grad$\varphi^* = 0$) and then being applied to the chain as a kind of external electric field. A consequence of this approximation is that $\mathbf{E}^* = \text{const}$ and the monomers are effectively noninteracting. Formally, this means we can simplify further

$$U = \sum_{i=1}^{n} \left[u^{(i)}_{\text{dipole strain}} - \boldsymbol{\mu}^{(i)} \cdot \mathbf{E}^* \right]$$

so that U is no longer a function of monomer positions. From here on, we use the notation $\mathbf{E}_0 = \mathbf{E}^*$ in order to emphasize that the electric field is constant and is something that is externally supplied.

It remains to develop a model for $u^{(i)}_{\text{dipole strain}}$. We desire that (1) each dipole will vanish on average in the absence of the external field (i.e. the DE is an electrically *responsive* material) and (2) the bulk material behaves as a linear dielectric. In general, an *ab initio* expression could be quite complex. Instead we can satisfy (1) and (2) through a simpler picture: imagine that the monomer dipole emerges as a consequence of an external electric field separating two equal and opposite point charges of magnitude q within the monomer; further, the charges are connected by two springs: one in the direction of $\hat{\mathbf{n}}$ with stiffness $k_{\parallel}$ and the other can rotate in the plane orthogonal to $\hat{\mathbf{n}}$ and has stiffness $k_{\perp}$. This is shown in Figure 2.3.

We now explore the consequences of this model. Let a local coordinate system be defined for a monomer with the origin attached to one point charge and basis vectors $\hat{\mathbf{n}}$ and $\mathbf{e}_3$, where $\mathbf{e}_3$ is orthogonal to $\hat{\mathbf{n}}$ and lies in the plane spanned by $\hat{\mathbf{n}}$ and $\hat{\mathbf{E}}_0$. Then, let (x, z) denote the location of the opposite charge so that

$$\boldsymbol{\mu} = q\left(x\hat{\mathbf{n}} + z\mathbf{e}_3\right)$$

and the associated spring energy is

$$u_{\text{dipole strain}} = \frac{1}{2}k_{\parallel}x^2 + \frac{1}{2}k_{\perp}z^2$$

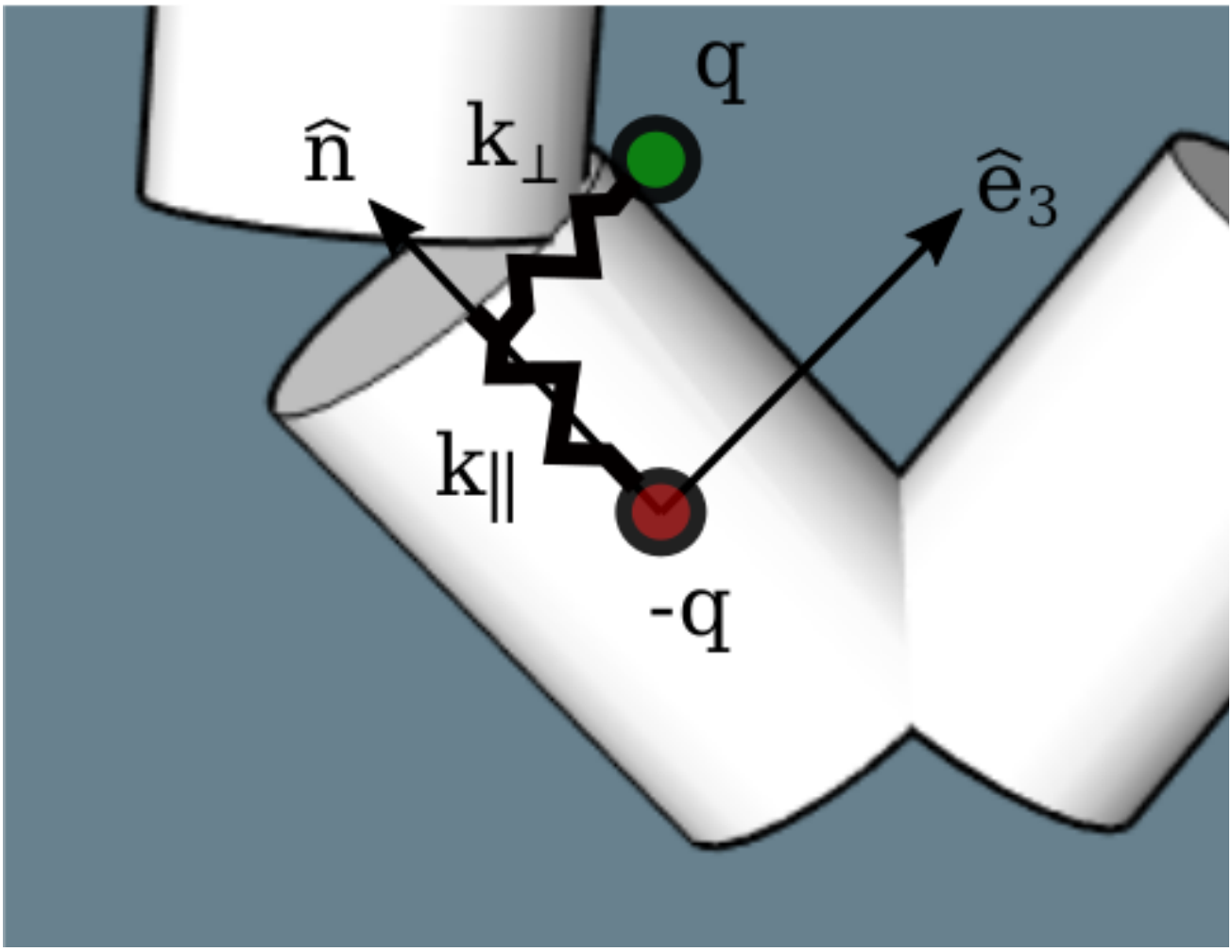

Figure 2.3: Model of dipole formation within a monomer; two equal and opposite point charges of magnitude q are connected by two springs: one in the direction of $\hat{\mathbf{n}}$ with stiffness $k_{\|}$ and the other can rotate in the plane orthogonal to $\hat{\mathbf{n}}$ and has stiffness $k_{\perp}$.

so that the total monomer energy is

$$u = \frac{1}{2}k_{\parallel}x^2 + \frac{1}{2}k_{\perp}z^2 - q\left(x\mathbf{E}_0 \cdot \hat{\mathbf{n}} + z\mathbf{E}_0 \cdot \mathbf{e}_3\right)$$

For a given $\hat{\mathbf{n}}$ and $\mathbf{E}_0$, the minimum energy, u^*, occurs when

$$x = q/k_{\parallel}\left(\mathbf{E}_0 \cdot \hat{\mathbf{n}}\right) := x^*$$

$$z = q/k_{\perp}\left(\mathbf{E}_0 \cdot \mathbf{e}_3\right) := z^*$$

and is given by

$$u^*\left(\hat{\mathbf{n}}, \mathbf{E}_0\right) = -\frac{1}{2}q^2\left(\mathbf{E}_0 \cdot \hat{\mathbf{n}}\right)^2 - \frac{1}{2}q^2\left(\mathbf{E}_0 \cdot \mathbf{e}_3\right)^2 = -\frac{1}{2}\boldsymbol{\mu}^* \cdot \mathbf{E}_0 \tag{2.2.1.5}$$

$$\boldsymbol{\mu}^*\left(\hat{\mathbf{n}}, \mathbf{E}_0\right) = q^2\left(\frac{\mathbf{E}_0 \cdot \hat{\mathbf{n}}}{k_{\parallel}}\hat{\mathbf{n}} + \frac{\mathbf{E}_0 \cdot \mathbf{e}_3}{k_{\perp}}\mathbf{e}_3\right) \tag{2.2.1.6}$$

In general for a given microstate, $\boldsymbol{\mu}_i$ are different than $\boldsymbol{\mu}_i^*$ for $i = 1, 2, ..., n$; that is, $\boldsymbol{\mu}_i$ can vary independently of $\hat{\mathbf{n}}_i$ because of thermal fluctuations in the system. However, we recognize that all energy is quantized and postulate that the first excited state of $u_{\text{dipole strain}}$ is much greater than kT. (We justify this by recalling that this model is meant to approximate polarization on the molecular scale that happens as a result of electron orbitals being displaced relative to nuclei. Since electrons are tightly bound to their nuclei, it is not unreasonable to believe that it would take a significant amount of energy for electron orbitals to be in an excited state which involves them vibrating about their ground state configuration.) As a result, the excited states are frozen out of the system and the point charges and springs are stuck in their ground state. In this case, $\boldsymbol{\mu}_i = \boldsymbol{\mu}_i^*$ and $\boldsymbol{\mu}_i$ is uniquely determined by $\hat{\mathbf{n}}_i$ and $\mathbf{E}_0$. Such an energy is considerably more tractable than the one outlined in (2.2.1.1).

Before proceeding, we take a moment to reformulate the monomer energy in more conventional terms. It is common to express a material's polarization response in terms of susceptibility, as opposed to spring stiffness. The dipole response given by (2.2.1.6) can be expressed in terms of susceptibility

by the following expressions:

$$\boldsymbol{\mu} = \boldsymbol{\chi}_{\mu}\left(\hat{\mathbf{n}}\right)\mathbf{E}_0 \tag{2.2.1.7}$$

$$\boldsymbol{\chi}_{\mu}\left(\hat{\mathbf{n}}\right) = \chi_{\parallel}\hat{\mathbf{n}}\otimes\hat{\mathbf{n}} + \chi_{\perp}\left(\mathbf{I} - \hat{\mathbf{n}}\otimes\hat{\mathbf{n}}\right) \tag{2.2.1.8}$$

where $\boldsymbol{\chi}_{\mu}$ is the dipole susceptibility tensor; and $\chi_{\parallel}$ and $\chi_{\perp}$ depend on the type of monomer and are a measure of the dipole susceptibility along the axis of the monomer direction and the dipole susceptibility in plane transverse to the monomer direction. Following [CDd16], we refer to monomers with $\chi_{\parallel} > \chi_{\perp}$ as uniaxial and monomers with $\chi_{\perp} > \chi_{\parallel}$ as transversely isotropic (TI). We will proceed to use this more common notion of susceptibility throughout the remainder of the work. The energy of a monomer in terms of susceptibility is

$$\begin{aligned} u\left(\hat{\mathbf{n}}\right) &= -\frac{1}{2}\boldsymbol{\mu}\left(\hat{\mathbf{n}}, \mathbf{E}_0\right)\cdot\mathbf{E}_0 \\ &= -\frac{\chi_{\parallel}}{2}\left(\mathbf{E}_0\cdot\hat{\mathbf{n}}\right)^2 - \frac{\chi_{\perp}}{2}\left[E_0^2 - \left(\mathbf{E}_0\cdot\hat{\mathbf{n}}\right)^2\right] \\ &= \frac{\Delta\chi}{2}\left(\mathbf{E}_0\cdot\hat{\mathbf{n}}\right)^2 - \frac{\chi_{\perp}}{2}E_0^2 \end{aligned} \tag{2.2.1.9}$$

where $\Delta\chi = \chi_{\perp} - \chi_{\parallel}$. Note that if $\chi_{\parallel} > \chi_{\perp}$ (or $\Delta\chi > 0$), that is, the monomer is of type uniaxial, then the monomer minimizes its energy by aligning or anti-aligning with the electric field. When the monomer direction is in the plane orthogonal to the electric field, then a uniaxial monomer's energy is maximized. When $\chi_{\perp} > \chi_{\parallel}$ (or $\Delta\chi < 0$), that is, the monomer is of type TI, the situation is reverse; namely, aligned or anti-aligned result in maximum energy and a direction in the plane orthogonal to the electric field result in minimum energy. This is shown graphically in Figure 2.4 where the potential energy of a monomer is plotted with respect to the angle between the electric field and the monomer direction, ψ_m.

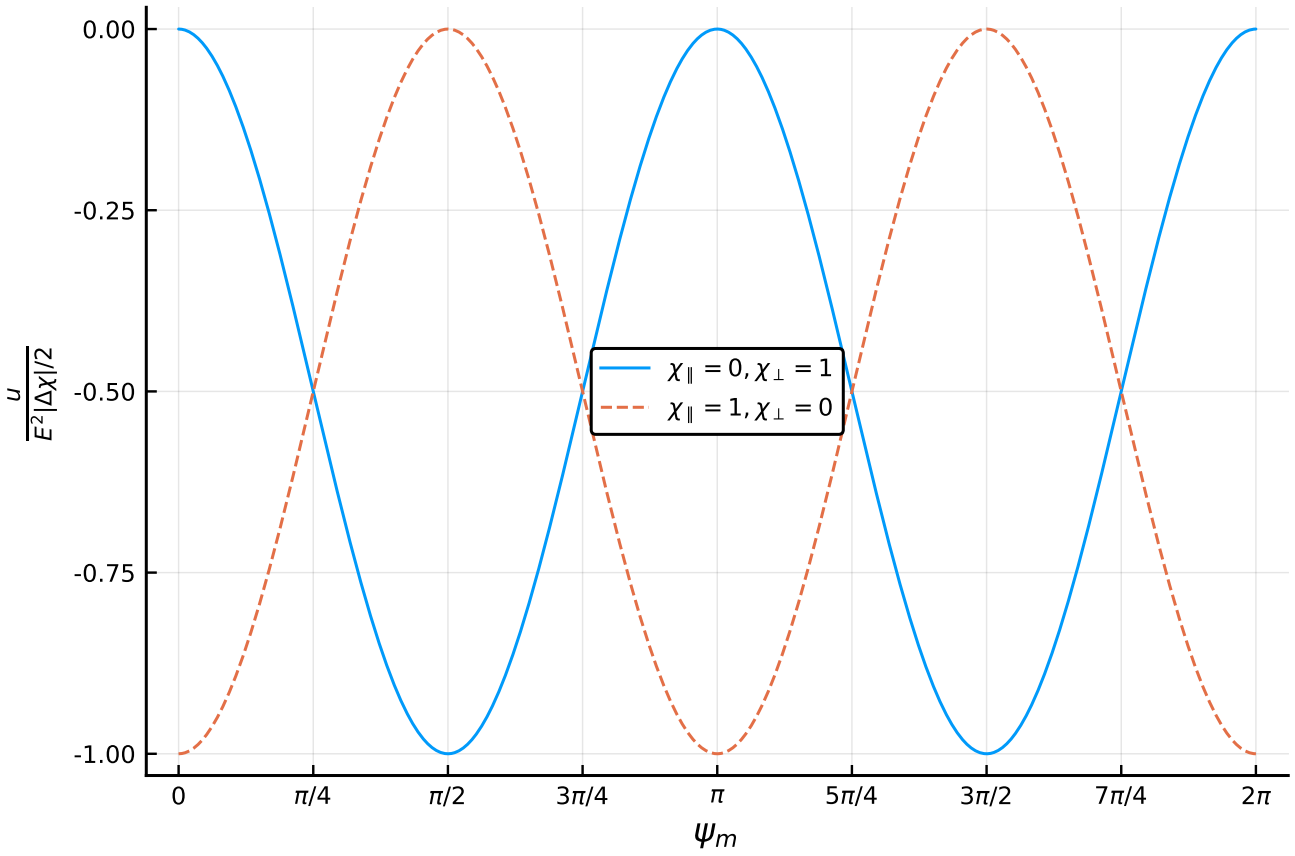

Figure 2.4: Potential energy of a monomer as a function of the angle between the direction of the electric field and the monomer direction. Note that when $\chi_\perp > \chi_\parallel$, the energy minimum is at $\psi_m = \frac{\pi}{2}, \frac{3\pi}{2}$. When $\chi_\perp < \chi_\parallel$, the energy minimum is at $\psi_m = 0, \pi$.

2.2.2 Free energy of a single DE chain

We are interested in deriving the free energy of an DE chain as a function of the applied electric field, its end-to-end vector, and its temperature. Note that, as a consequence of the dependence of a monomer's electrical potential energy on its orientation, not all chain configurations have the same energy. This means that, in contrast to Section 2.1, not all microstates in the ensemble are equally likely. Instead, we must weight each orientation by the Boltzmann factor, $\exp\left(-\beta U\right)$, where $\beta = 1/kT$ and U is the energy of the chain configuration. As in Section 2.1, we partition the surface of the unit sphere into $\mathcal{N}$ patches of area and define the occupation numbers, m_i, as the number of monomers oriented such that their unit direction, $\hat{\mathbf{n}}_i$, lies in the ith patch. The analog of (2.1.0.3) is

$$\mathcal{Z} = \sum_{\{m_i\}}{}' \exp\left[-\beta U\left(\{m_i\}\right)\right] \frac{n!}{\Pi_{i=1}^{\mathcal{N}} m_i!} \tag{2.2.2.1}$$

where $\mathcal{Z}$ is generally referred to as the partition function and the chain energy is taken as the sum of the individual monomer energies, i.e. $U\left(\{m_i\}\right) = \sum_{i=1}^{\mathcal{N}} m_i u\left(\hat{\mathbf{n}}_i\right)$. The significance of the partition function is that the free energy can be determined by taking its logarithm, $\mathcal{A}^* = -kT \ln \mathcal{Z}$. As in Section 2.1, we notice that enumerating each of the terms in (2.2.2.1) and evaluating the sum proves to be difficult, and that ultimately we are interested in $\ln \mathcal{Z}$. Thus, we approximate the sum by its maximum term. For ease of calculation, and since the logarithm is monotonic, we can maximize

$$\ln\left[\exp\left(-\beta \sum_{i=1}^{\mathcal{N}} m_i u\left(\hat{\mathbf{n}}_i\right)\right) \frac{n!}{\prod_{i=1}^{\mathcal{N}} m_i!}\right]$$

subject to the constraints (2.1.0.4) and (2.1.0.5). Using Stirling's approximation for the $\ln \square!$ terms and the method of Lagrange multipliers to enforce the constraints, the occupation numbers that result

in the maximum term are

$$\begin{aligned} m_j &= C \exp\left[-\beta u\left(\hat{\mathbf{n}}_j\right) + \boldsymbol{\tau} \cdot \hat{\mathbf{n}}_j\right] \\ &= C \exp\left[-\frac{\beta}{2} \Delta\chi \left(\mathbf{E}_0 \cdot \hat{\mathbf{n}}_j\right)^2 + \boldsymbol{\tau} \cdot \hat{\mathbf{n}}_j\right] \\ &= C \exp\left[-\kappa \left(\hat{\mathbf{E}}_0 \cdot \hat{\mathbf{n}}_j\right)^2 + \boldsymbol{\tau} \cdot \hat{\mathbf{n}}_j\right] \end{aligned} \tag{2.2.2.2}$$

where all of the terms in the argument of the exponential that did not have a directional dependence were absorbed into the unknown C and the unknown multipliers, $\boldsymbol{\tau}$, are related to the kinematic constraint. The second step is a result of plugging (3.0.0.1) in for the monomer energy (again, absorbing the constant term into C); and, in the last step we define the unit direction of the electric field, $\hat{\mathbf{E}}_0 = \mathbf{E}_0/E_0$, and define the dimensionless quantity $\kappa = \beta E_0^2 \Delta\chi/2$, which is a measure of monomer potential energy with respect to thermal energy. In the limit of $\mathcal{N} \to \infty$, (2.2.2.2) becomes the continuous monomer density function

$$\rho\left(\hat{\mathbf{n}}\right) = C \exp\left[-\kappa \left(\hat{\mathbf{E}}_0 \cdot \hat{\mathbf{n}}\right)^2 + \boldsymbol{\tau} \cdot \hat{\mathbf{n}}\right] \tag{2.2.2.3}$$

where the unknowns, C and $\boldsymbol{\tau}$, are determined by solving the system of equations that result from taking the discrete constraints, (2.1.0.4) and (2.1.0.5), to the continuum limit

$$n = \int_{\mathbb{S}^2} \mathrm{d}A \, \rho\left(\hat{\mathbf{n}}\right) \tag{2.2.2.4}$$

$$\frac{\mathbf{r}}{b} = \int_{\mathbb{S}^2} \mathrm{d}A \, \rho\left(\hat{\mathbf{n}}\right) \hat{\mathbf{n}} \tag{2.2.2.5}$$

and where $\mathbb{S}^2$ denotes the surface of the unit sphere. Once the monomer density function has been approximately determined, one can return to (2.2.2.1) to derive the free energy. Approximating the sum on the right-hand side by its maximum-term, taking the logarithm, and using Stirling's approximation

$$\ln \mathcal{Z} \approx -\beta \sum_{i=1}^{\mathcal{N}} m_i u\left(\hat{\mathbf{n}}_i\right) + n \ln n - \sum_{i=1}^{\mathcal{N}} m_i \ln m_i \tag{2.2.2.6}$$

Multiplying both sides by $-kT$ and taking the limit of $\mathcal{N} \to \infty$

$$\mathcal{A}^* \approx \int_{\mathbb{S}^2} \mathrm{d}A \ \{\rho(\hat{\mathbf{n}})\, u(\hat{\mathbf{n}}) + kT\rho(\hat{\mathbf{n}}) \ln(\rho(\hat{\mathbf{n}}))\} - nkT \ln n \tag{2.2.2.7}$$

we arrive at an expression for an approximation of the free energy.

However, there are a few difficulties related to (2.2.2.4), (2.2.2.5) and (2.2.2.7). First, the integrals in (2.2.2.4), (2.2.2.5) and (2.2.2.7) are difficult to evaluate. Second, the resulting system of equations will, in general, be nonlinear. Recall that in Section 2.1 the first difficulty was addressed by choosing the coordinate system such that the polar axis was in the direction of the chain end-to-end vector and recognizing that the symmetry of the problem allows one to simplify the $\boldsymbol{\tau} \cdot \hat{\mathbf{n}}$ term in (2.1.0.7) to $\lambda \cos\theta$. However, for an DE chain this simplification cannot be made. For example, given $\mathbf{r}$ and $\mathbf{E}_0$, the exact direction of $\boldsymbol{\tau}$ cannot be determined *a priori*. In addition, although there are now two directions, namely $\hat{\mathbf{r}} = \mathbf{r}/r$ and $\hat{\mathbf{E}}_0$, which have important physical and mathematical significance, only one of them can be taken as the direction of the polar axis. As a result, at least to the authors' knowledge, despite which coordinate system one chooses, (2.2.2.4) and (2.2.2.5) cannot be solved exactly. Instead, in Section 2.3 we will use numerical methods; and in Section 2.4 and Section 2.5 we will assume smallness of some parameters, expand in terms of the small parameters, and derive approximate solutions.

2.3 Numerical solution

2.3.1 Numerical methods

Both evaluating the integrals and solving the resulting nonlinear system of equations given by (2.2.2.4) and (2.2.2.5) is difficult to do (exactly) in a closed-form. In addition to closed-form approximations, another technique that one may use is that of numerical methods. There are certain advantages to numerical methods that we will find useful. For instance, a numerical solution does not, in general,

need to assume a physical parameter is small. Thus, we can obtain approximate solutions for instances where both the electrical energy and $\boldsymbol{\tau}$ are not small. Such solutions will provide us with a measure of accuracy for our closed-form approximations; and, may potentially allow us to investigate material responses over a broader range of environmental conditions (e.g. values of E_0, γ, etc.).

For numerical integration, we used the p-adaptive algorithm from the cubature package [Joha]. The p-adaptive algorithm is based on Clenshaw-Curtis quadrature rules [CC60] and is generally well-suited for smooth integrands and integration in low-dimensional space. Hence, it is well-suited for (2.2.2.4) and (2.2.2.5), as the integrands are infinitely differentiable and the space is two-dimensional. Newton's method was used to solve the nonlinear system of equations. The initial guess for Newton's method was the Kuhn and Grun solution from Section 2.1 (but in a rotated coordinate system where the polar axis is in the direction $\hat{\mathbf{E}}_0$), that is

$$\mathbf{x}_0 = \begin{Bmatrix} C_0 \\ \lambda_0 \\ \alpha_0 \end{Bmatrix} = \begin{Bmatrix} \frac{n\lambda}{4\pi} \operatorname{csch}\left[\mathcal{L}^{-1}(\gamma)\right] \\ \frac{r_3}{r}\mathcal{L}^{-1}(\gamma) \\ \frac{r_1}{r}\mathcal{L}^{-1}(\gamma) \end{Bmatrix}$$

when $|\kappa| = 0$, and

$$\mathbf{x}_0' = \begin{Bmatrix} \left(n\sqrt{\kappa}\right) / \left(2\pi^{3/2}\operatorname{erf}\left(\sqrt{\kappa}\right)\right) \\ \left(2\sqrt{\pi}\gamma_3\kappa e^{\kappa}\operatorname{erf}\left(\sqrt{\kappa}\right)\right) / \left(\sqrt{\pi}e^{\kappa}\operatorname{erf}\left(\sqrt{\kappa}\right) - 2\sqrt{\kappa}\right) \\ \left(4\sqrt{\pi}\gamma_1\kappa e^{\kappa}\operatorname{erf}\left(\sqrt{\kappa}\right)\right) / \left(\sqrt{\pi}\left(2\kappa - 1\right)e^{\kappa}\operatorname{erf}\left(\sqrt{\kappa}\right) + 2\sqrt{\kappa}\right) \end{Bmatrix}$$

when $|\kappa| > 1$. When $|\kappa| \in (0, 1)$ then the initial guess was taken as a linear relaxation between the two guesses, that is $|\kappa|\mathbf{x}_0' + (1 - |\kappa|)\mathbf{x}_0$. (The initial guess $\mathbf{x}_0'$ comes from the closed-form approximation derived in Section 2.5. We leave the details of the derivation until that section.) A residual tolerance of less than 10^{-10} was usually reached within 3-15 iterations. In instances when Newton's method did not convergence, a series of gradient-free, unconstrained optimization methods were used to approximate a solution. The SBPLX (based on the Subplex algorithm) [Row90] and Principle Axis (PRAXIS) [Bre72] algorithms from the NLopt package [Johb] were used, as was a simulated anneal-

ing implementation (the implementation was based on [Kra06]). The cost function was taken to be the square root of the sum of the squares of the residuals (equations (2.2.2.4) and (2.2.2.5)).

In Section 2.3.2, we present the numerical solution for different electric fields, monomer susceptibilities, and chain stretches and aim to explain some of the physical behavior that is observed.

2.3.2 Results and discussion of DE chain physics

Free energy

It is well known (and was pointed out in Section 2.1) that the stiffness of a classical polymer chain (and, eventually, a polymer network) is due to thermal fluctuations and the natural tendency of a (constant energy) thermodynamic system to maximize entropy. When investigating the free energy and stiffness of an DE chain, we expect both electrostatic energy and thermal fluctuations will play a role. We aim to determine how each affects the free energy and force-length relationship of an DE chain, and any possible trade-offs or interplay between their respective contributions. In order to probe these relationships, we generate numerical solutions for different electric fields, monomer susceptibilities, and chain stretches. Throughout this section the number of monomers, n, is taken to be 100 and the monomer length, b, is set to unity. In addition, when κ is positive the monomer susceptibilities are $\chi_{\parallel} = 0$ and $\chi_{\perp} = 1$; and when κ is negative the monomer susceptibilities are $\chi_{\parallel} = 1$ and $\chi_{\perp} = 0$ Consider the $\left(\hat{\mathbf{E}}_0 \cdot \hat{\mathbf{n}}\right)^2$ term in the monomer density function, (2.2.2.3). Clearly, it is not only the magnitude of the electric field that is important, but also its direction relative to the direction of stretch. Let ψ_r denote the angle between $\hat{\mathbf{E}}_0$ and $\hat{\mathbf{r}}$. In addition, for the present section, let λ and α be the components of $\boldsymbol{\tau}$ in the direction of $\hat{\mathbf{E}}_0$ and the direction orthogonal to $\hat{\mathbf{E}}_0$ (in the plane spanned by $\hat{\mathbf{E}}_0$ and $\hat{\mathbf{r}}$), respectively.

The residuals for (2.2.2.4) and (2.2.2.5) were calculated for all of the numerical results presented in the current section. The numerical solutions often converged to a maximum absolute residual of 10^{-10} or less; however, in some cases the numerical scheme could not achieve a reasonable level of accuracy. Those solution results that did not have a maximum absolute residual of most $n * 0.01$ (or 1.0) are not

included in the figures that follow. From here on, we shall refer to the polymer chain that behaves in accordance with the Kuhn and Grün model (as opposed to say, an electroactive chain) as a classical polymer chain. In regards to numerics, the numerical solutions are at times plotted along side the Kuhn and Grün solution presented in Section 2.1. When such calculations require the (approximate) evaluation of the inverse Langevin function, the following approximation is used [Kro15]:

$$\mathcal{L}^{-1}(x) \approx \frac{3x - \frac{x}{5}\left(6x^2 + x^4 - 2x^6\right)}{1 - x^2}$$

In Figure 2.5, we consider the free energy of chains as a function of stretch for increasing κ. The Kuhn and Grün solution for the free energy of a classical chain is also presented for comparison and is given by $-T\mathcal{S}_{KG}$ where $\mathcal{S}_{KG}$ denotes the entropy given by (2.1.0.14). Note that the $\kappa = 0$ and the classical chains agree exactly. One would expect this to be the case as $\kappa \to 0$ as $E_0 \to 0$. However, not only should the agreement lend confidence to the numerical solutions; but also it reinforces the fact that in the limit of $T \to \infty$, an DE chain behaves as a classical chain.

In Figure 2.5, note that the zero stretch free energy (per kT) decreases as κ increases. The free energy decreases because an increase in κ either corresponds to an increase in the magnitude of electrical energy or a decrease in thermal energy. In the former case, the potential well of each monomer increases its depth, decreasing the free energy; in the latter case, there is a reduction in thermal fluctuations and hence the effect of monomers aligning to the configuration that corresponds to the deepest part of their respective potential well. Note that in either case an important reason why there is a decrease in free energy is because, at zero stretch, the monomers in the chain have some freedom to their alignment (i.e. they are not kinematically constrained to align at or near a particular direction) so that as the well depth increases or the thermal fluctuations decrease, the monomers are able to attain their minimum energy configurations. Further, we can quantify these considerations. If $\kappa = \gamma = 0$ then one can expect $|\boldsymbol{\tau}| = 0$ and the monomers are uniformly distributed, that is $\rho = \frac{n}{4\pi}$. For uniformly distributed monomers, the entropy is $nk\ln(4\pi)$ and the free energy is $-nk\ln(4\pi)$, which agrees with the $\kappa = 0$ free energy at $\gamma = 0$. When $\kappa >> T$, the electrostatic contribution to the free energy

dominates the entropic one (i.e. the $k\int_{\mathbb{S}^2}\mathrm{d}A\,\rho\ln\rho$ term). One can argue that, since physically we know the equilibrium ρ (and hence, most-likely ρ) is the one which minimizes the free energy, that $\rho\left(\psi_m\right)\to\frac{n}{2\pi}\delta\left(\psi_m-\frac{\pi}{2}\right)$ as $\kappa\to\infty$. In this case the electrostatic contribution approaches $n\chi_\perp E_0^2$ ($=nkT\kappa$, in this case) and the entropy decreases to some small but finite value. Hence, for κ positive, the zero stretch free energy has a maximum of $-nk\ln\left(4\pi\right)$ and approaches $n\chi_\perp E_0^2$ when $T\to 0$.

Lastly, we consider the effect of chain stretch and, in particular, the effect of the direction of stretch relative to the electric field. In Figure 2.5 the direction of stretch, $\hat{\mathbf{r}}$, is taken as the same direction as the electric field, $\hat{\mathbf{E}}_0$ (i.e. $\psi_r=0$). Recall, that (1) κ is a measure of electrostatic energy with respect to thermal energy; and (2) $\kappa>0$ signifies monomers that have a higher susceptibility orthogonal to the axis of their unit direction than along their axis of unit direction, that is, it signifies TI monomers. Positive κ implies positive $\Delta\chi$. From (3.0.0.1) (or Figure 2.4), one can see that the electrostatic energy of a TI monomer increases as its directional axis (i.e. span of $\hat{\mathbf{n}}$) aligns with the electric field. The increase in free energy with respect to stretch is larger for chains with higher κ. The larger increase in free energy as a function of stretch can be explained by the fact that, since $\hat{\mathbf{r}}=\hat{\mathbf{E}}_0$, as the chain is stretched, monomers are forced by the kinematic constraint to align with the electric field. A larger κ corresponds to a larger increase in electrostatic energy as monomers are forced to align. Since the $\mathbf{E}_0\cdot\hat{\mathbf{n}}$ term in (3.0.0.1) is quadratic, the free energy curves in Figure 2.5 would look identical if $\hat{\mathbf{r}}=-\hat{\mathbf{E}}_0$. Notice that as $\gamma\to 1$, the curves converge. That is because at the fully stretched limit, the electrical potential energy of each of the monomers is zero. In general, with regard to the statistics of an DE chain, there are three competing factors: (1) electrical energy–which would induce monomer dipoles and have monomers rotate to align their respective dipoles with the electric field (2) thermal energy–which prefers monomers to be oriented in a uniform random manner and (3) the kinematic constraint. The quantity $|\kappa|$ is a measure of the influence of (1) versus (2). Whereas the quantity $|\boldsymbol{\tau}|$ (and, in a sense, γ) is a measure of the influence of (3). The fact that the free energy curves converge when the chains approach fully stretched shows that the effect of satisfying the kinematic constraint supersedes that of either (1) or (2), which should agree with intuition. That is, as the chain is fully stretched, the monomers are forced to align more densely in the direction of stretch regardless of the external electric

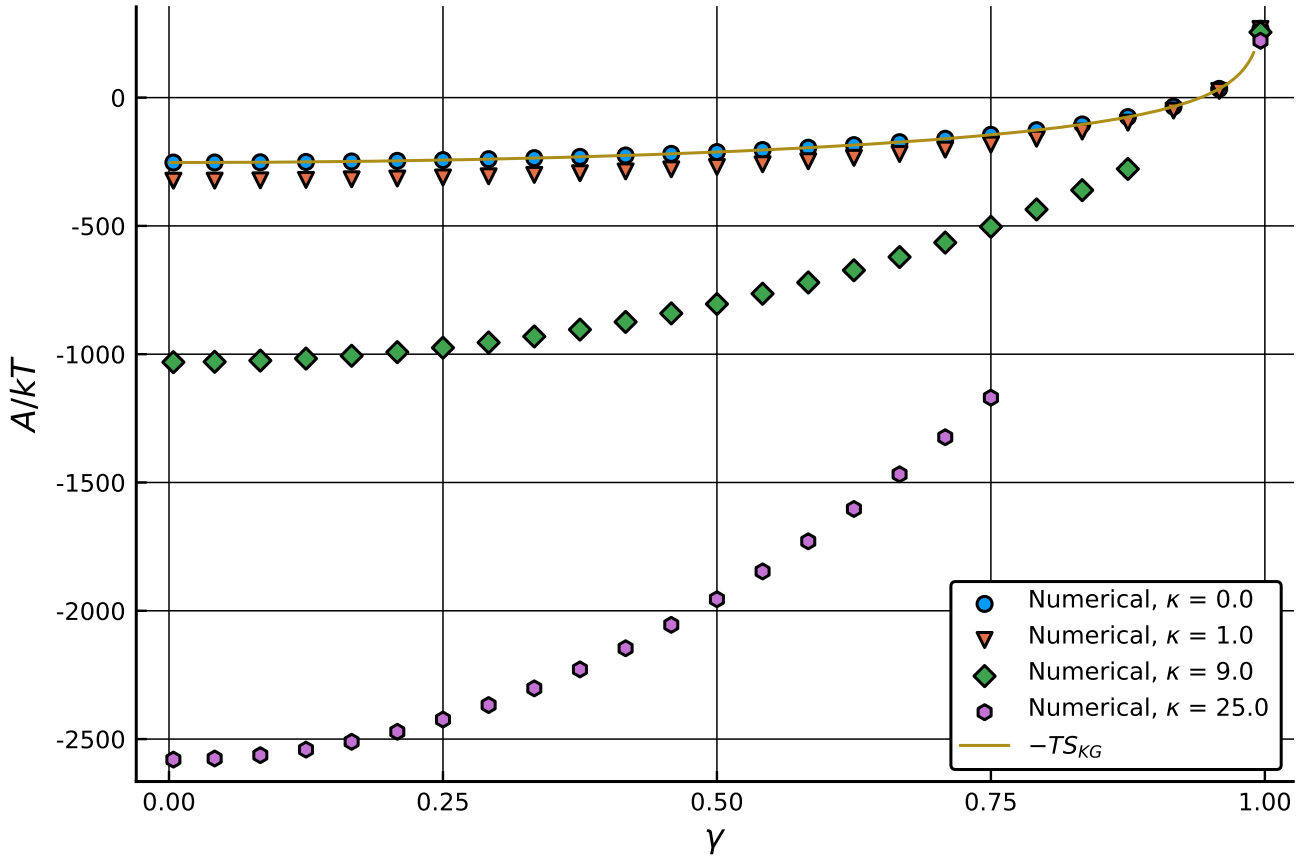

Figure 2.5: Chain free energy with respect to stretch for $\kappa = 0.0, 1.0, 9.0$ and 25.0; $\psi_r = 0$. The free energy increases more rapidly with stretch for chains with larger κ because chain stretch forces monomers to align with the electric field and the electrostatic energy increases more (when aligning with $\hat{\mathbf{E}}_0$) for monomers with larger κ.

field or temperature of the system because the constraint must be satisfied.

In Figure 2.6 and Figure 2.7, the free energy per kT with respect to stretch curves are shown for the same values of κ but with $\psi = \frac{\pi}{4}$ and $\psi = \frac{\pi}{2}$, respectively. The curves in Figure 2.6 are similar to that of Figure 2.5 and the free energy of the $\kappa = 9.0$ and $\kappa = 25.0$ chains, again, are shifted downward and increase more rapidly with stretch than the $\kappa = 1.0$ and classical chains. However, notice that in the case of $\psi_r = \frac{\pi}{4}$ (Figure 2.6), the increase in free energy for the larger κ chains is less rapid than when $\psi_r = 0$ (Figure 2.5). There is less of an increase in free energy with stretch for the $\psi_r = \frac{\pi}{4}$, DE chains than when $\psi_r = 0$ because as the chains stretch, the density of monomers with an orientation of or near to ψ_r must increase. Put differently: at $\psi_r = 0$ the monomers in the chain are being forced into an orientation in which they do not polarize and their electrical potential energy is zero; where as

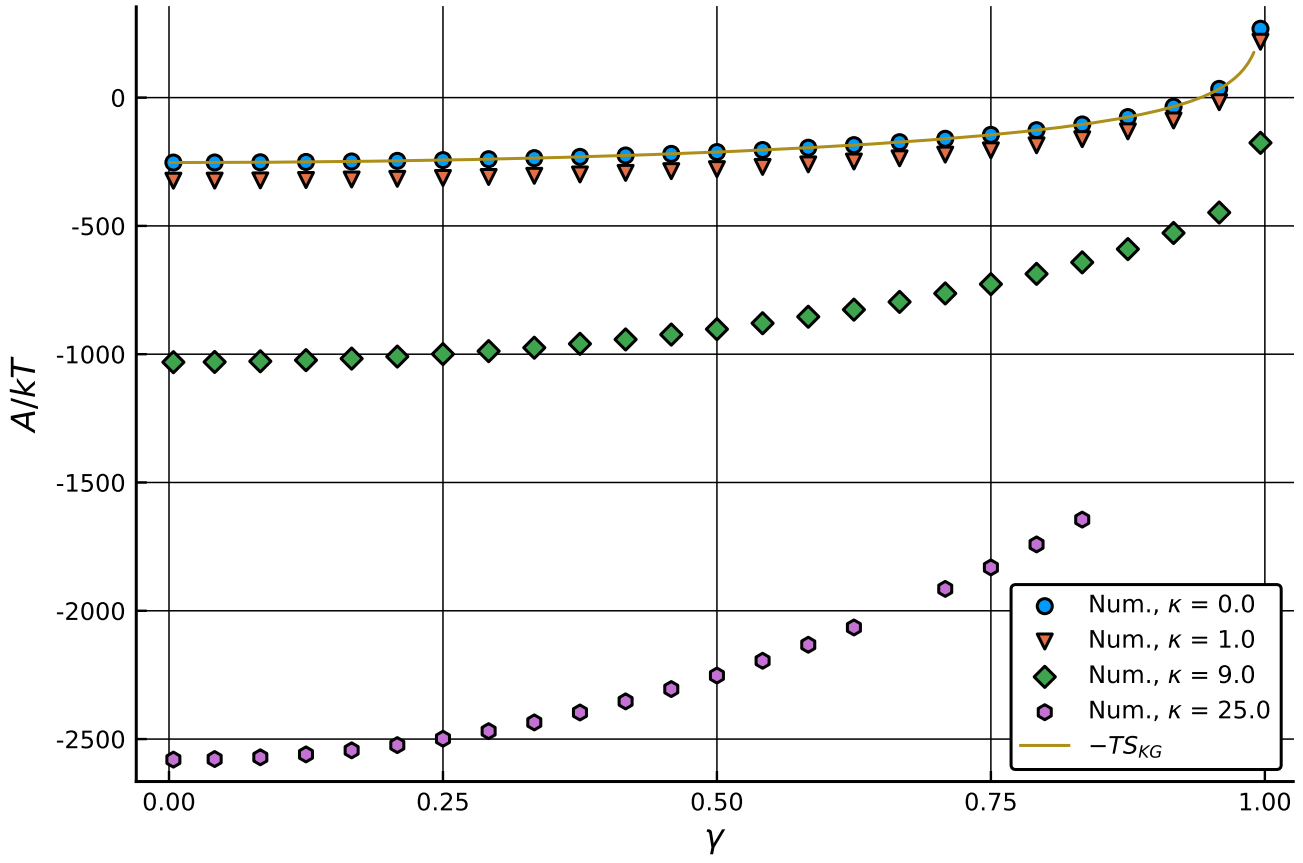

Figure 2.6: Chain free energy with respect to stretch for $\kappa = 0.0, 1.0, 9.0$ and 25.0; $\psi_r = \frac{\pi}{4}$. The free energy increases more rapidly with stretch for chains with larger κ because chain stretch forces monomers to align with the electric field and the electrostatic energy increases more (when aligning with $\hat{\mathbf{E}}_0$) for monomers with larger κ.

at $\psi_r = \frac{\pi}{4}$ the monomers are forced to oriented in a direction where their polarization is nonzero and the electrical potential energy is less than zero. The effect of the orientation of the chain stretch with respect to the electric field can also be seen in Figure 2.7 (and Figure 2.8), where $\psi_r = \frac{\pi}{2}$. Notice, in particular, that in Figure 2.7 and Figure 2.8 the shape of curves for each value of κ are similar. We can understand this as a consequence of the fact that DE monomers being forced into the direction of their minimum energy orientation as the chain is stretched, which is also the orientation that is exponentially favored due to electrostatics. Thus, the change in the potential energy term (i.e. $\int_{\mathbb{S}^2} \mathrm{d}A\ \rho u$) with respect to stretch is negligible. Instead the increase in free energy is primarily entropy driven and increasing κ merely has the effect of shifting the $\mathcal{A}^*/kT$ vs. γ curve downward.

Lastly, to further highlight the significance of ψ_r, we show (Figure 2.9) $\mathcal{A}^*/kT$ vs. γ for fixed κ

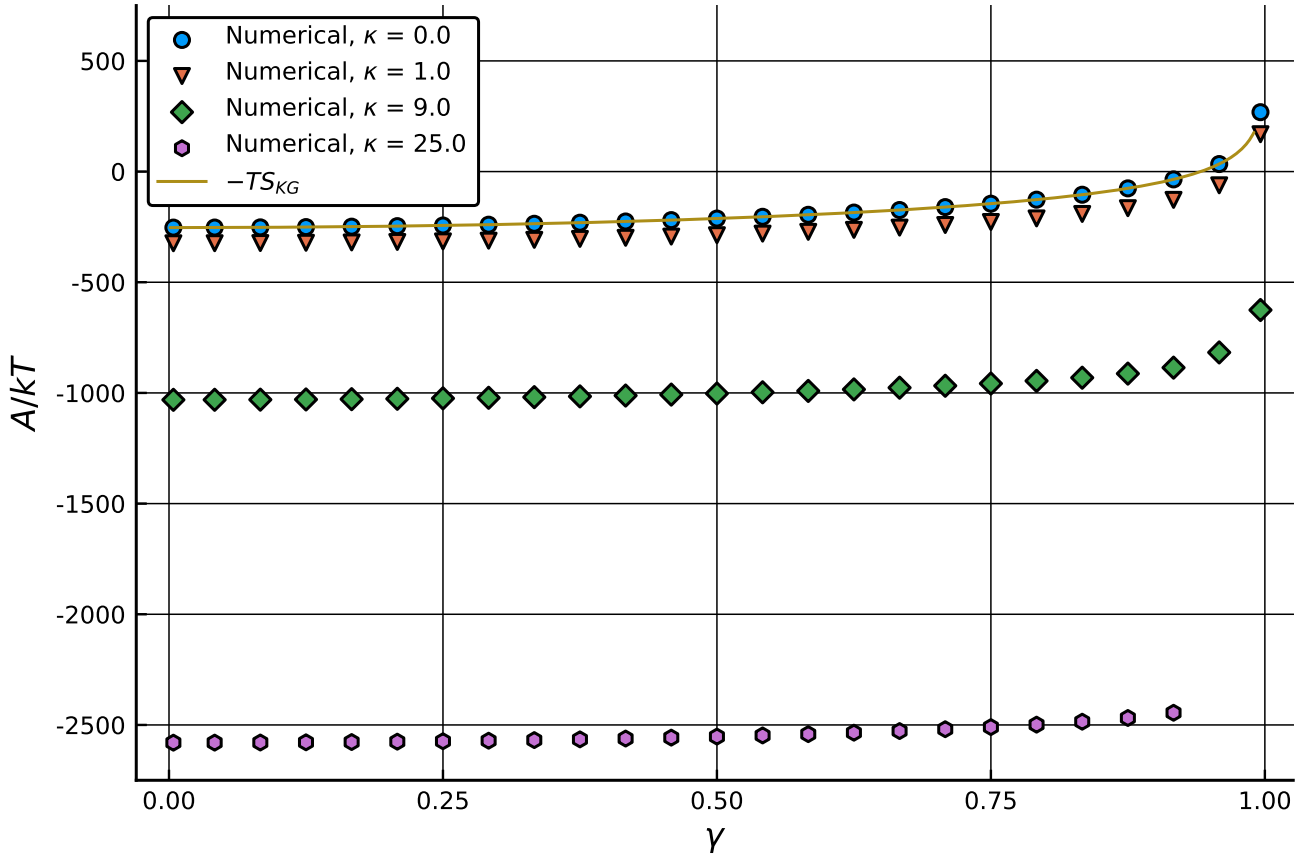

Figure 2.7: Chain free energy with respect to stretch for $\kappa = 0.0, 1.0, 9.0$ and 25.0; $\psi_r = \frac{\pi}{2}$. The change in $\mathcal{A}^*/kT$ vs γ curves are similar for all values of κ because the change is entropy driven.

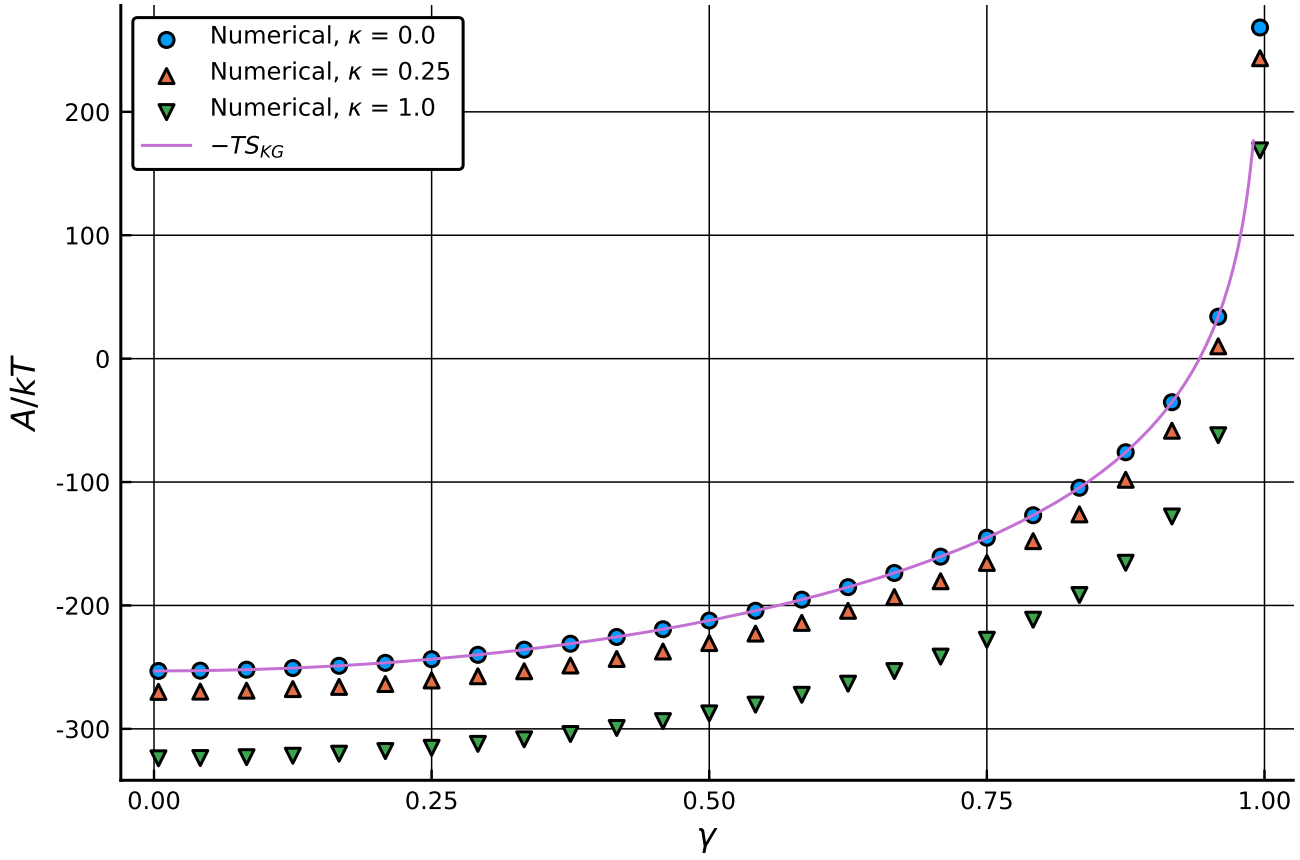

Figure 2.8: Chain free energy with respect to stretch for $\kappa = 0.0, 0.25$ and 1.0; $\psi_r = \frac{\pi}{2}$. The change in $\mathcal{A}^*/kT$ vs γ curves are similar for all values of κ because the change is entropy driven.

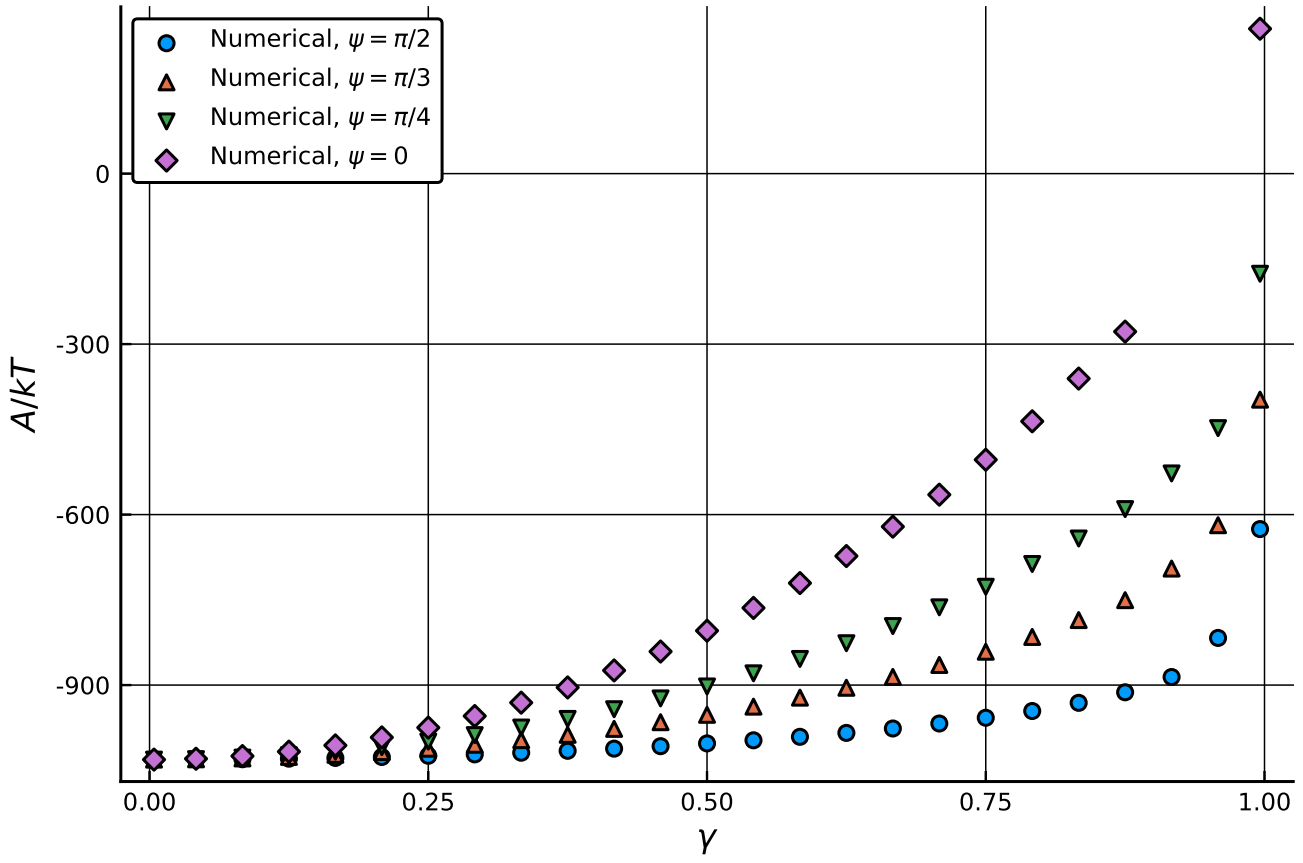

Figure 2.9: Chain free energy with respect to stretch for $\kappa = 0.0, 0.25$ and 1.0; $\psi_r = \frac{\pi}{2}$. The change in $\mathcal{A}^*/kT$ vs γ curves are similar for all values of κ because the change is entropy driven.

and $\psi_r = \frac{\pi}{2}, \frac{\pi}{3}, \frac{\pi}{4}$, and 0. As discussed previously, the increase in $\mathcal{A}^*/kT$ with respect to γ is greatest when the chain is stretched in the direction of the maximum electrical potential energy of a monomer ($\psi_r = 0$), and decreases as ψ_r transitions toward the direction of the minimum electrical potential energy of a monomer ($\psi_r = \frac{\pi}{2}$).

Next we present a similar analysis but for uniaxial monomers ($\kappa < 0$, for simplicity, $\chi_\perp = 0$). Figures 2.10-2.12 show $\mathcal{A}^*/kT$ vs γ for uniaxial monomers at $\psi_r = 0, \frac{\pi}{4}$ and $\frac{\pi}{2}$, respectively. In contrast to TI monomers, the increase in $\mathcal{A}^*/kT$ with respect to γ is greatest when the direction of chain stretch and the direction of the applied electric field are orthogonal (as opposed to aligned or $\psi_r = 0$). This is of course because the electrical potential energy of a uniaxial monomer attains its maximum when its orthogonal to the electric field and its minimum when aligned with the field.

Before closing the discussion of how κ, chain stretch, and chain orientation with respect to $\hat{\mathbf{E}}_0$ affect

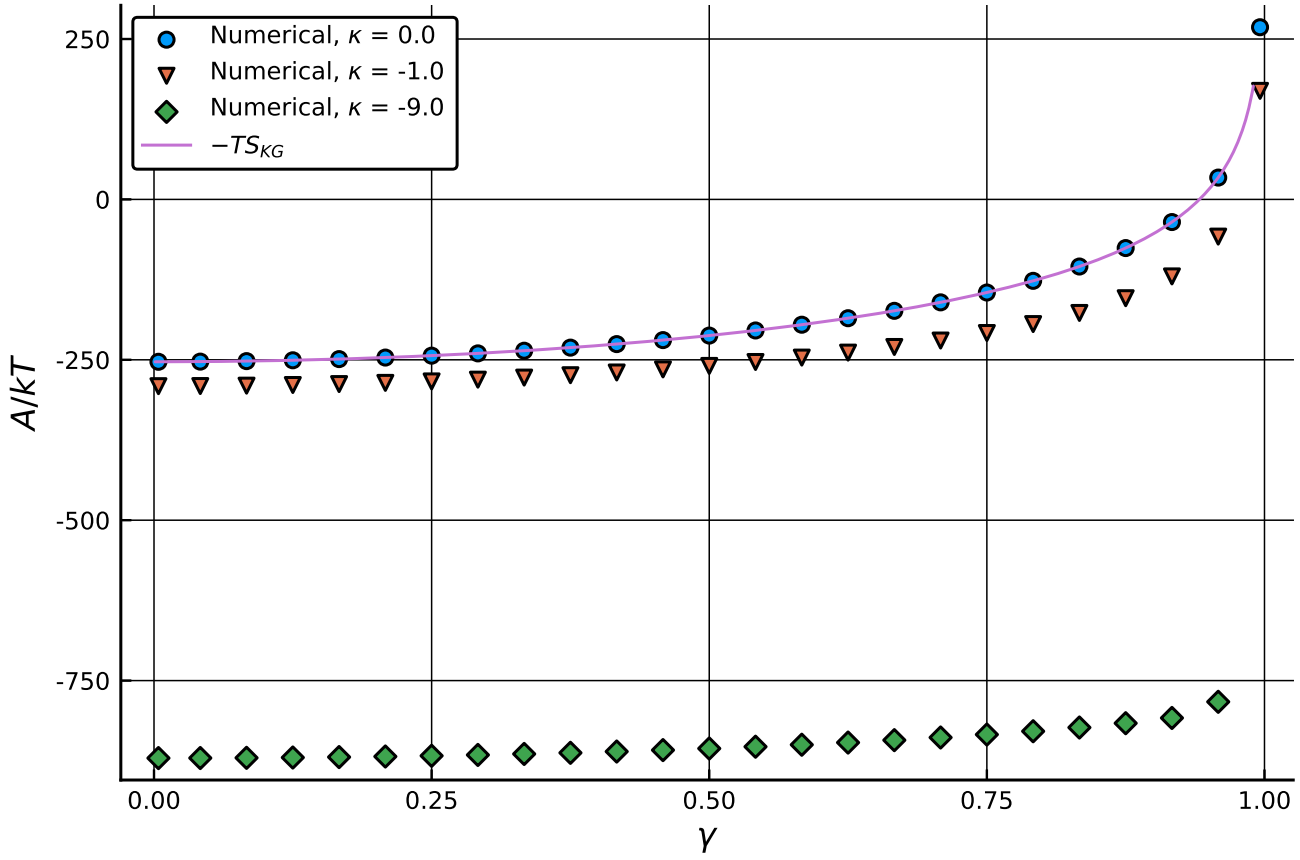

Figure 2.10: Chain free energy with respect to stretch for $\kappa = 0.0, -1.0$ and -9.0; $\psi_r = 0$. The change in $\mathcal{A}^*/kT$ vs γ curves are similar for all values of κ because the change is entropy driven. Increasing $|\kappa|$ shifts the curve downward.

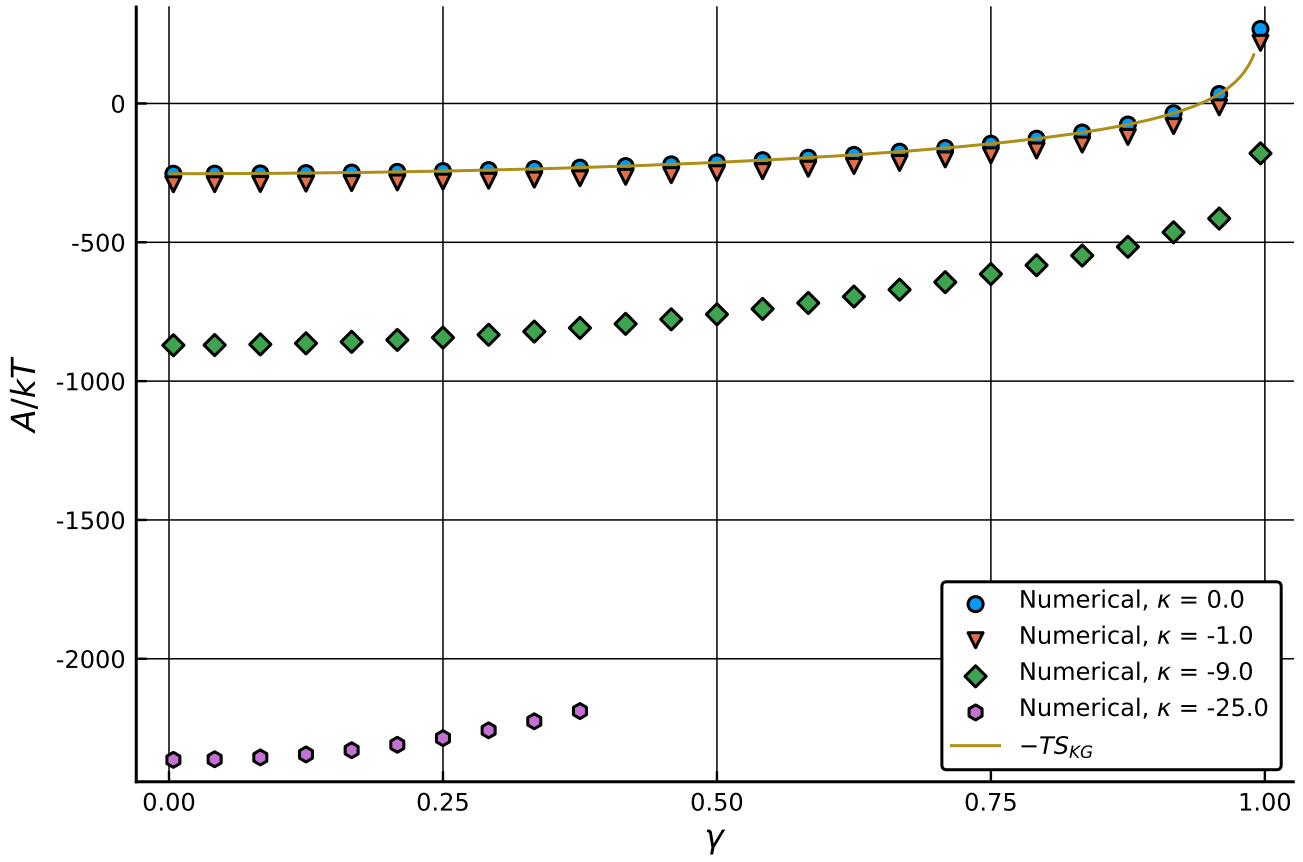

Figure 2.11: Chain free energy with respect to stretch for $\kappa = 0.0, -1.0, -9.0$ and -25.0; $\psi_r = \frac{\pi}{4}$. The free energy increases more rapidly with stretch for chains with larger $|\kappa|$ because chain stretch forces monomers to prefer an orientation of or near to $\psi_m = \frac{\pi}{4}$ and a larger $|\kappa|$ corresponds to a deeper potential well at $\psi_m = 0, \pi$ for uniaxial monomers.

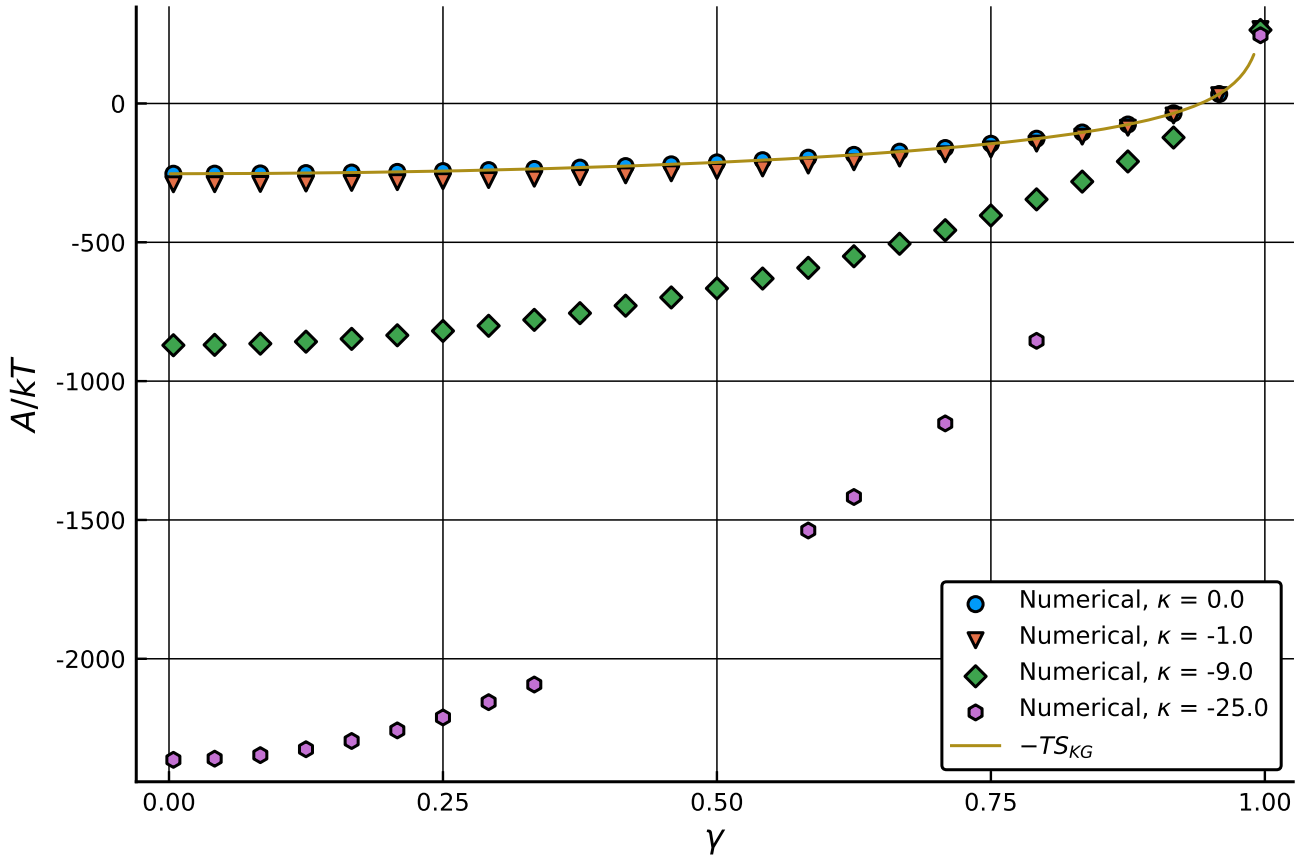

Figure 2.12: Chain free energy with respect to stretch for $\kappa = 0.0, -1.0, -9.0$ and -25.0; $\psi_r = 0$. The free energy increases more rapidly with stretch for chains with larger $|\kappa|$ because chain stretch forces monomers to prefer an orientation of or near to $\psi_m = \frac{\pi}{2}$ (which is a maximum of the electrical energy) and a larger $|\kappa|$ corresponds to a deeper potential well at $\psi_m = 0, \pi$ for uniaxial monomers.

the free energy of an DE chain, we point out a subtle but important detail. Upon inspection of the $\mathcal{A}^*/kT$ vs. γ curves (compare, for example, Figure 2.7 and Figure 2.10), one may be tempted to conclude that a symmetry exists such that changing the sign of κ and rotating ψ_r by $\frac{\pi}{2}$ results in the same DE chain statistics. However, the statistics are not the same. The $\mathcal{A}^*/kT$ - γ relation for TI and uniaxial chains oriented at $\psi_r = 0$ and $\psi_r = \frac{\pi}{2}$ are shown in Figure 2.13. Despite the fact that the depth of the electrical potential well is the same for TI and uniaxial monomers (Figure 2.4), the zero stretch free energy of the TI chains are lower. This can be explained by considering that the minimum energy orientation of a uniaxial monomer is when $\hat{\mathbf{n}} = \pm\hat{\mathbf{E}}_0$ where as the minimum energy orientation of a TI monomer occurs when $\hat{\mathbf{n}} \cdot E_0 = 0$. The uniaxial case is only two discrete directions but the TI case describes a plane in which $\hat{\mathbf{n}}$ can rotate and the TI monomer still be at an energy minimum. Thus, there is a larger space of directions in which TI monomers can be oriented which are also energetically favored (at or near a potential well), meaning the entropy is able to be larger and the entropic contribution to the free energy is able to more negative (compared with uniaxial monomers). Also, in particular, notice that as the TI, $\psi_r = 0$ and uniaxial, $\psi_r = \frac{\pi}{2}$ chains stretch (e.g. $\gamma \to 1$) the curves begin to meet. This is because (1) the kinematic constraint is forcing the monomers of each chain into or near their maximum energy state, which in this case is the same amount of energy, and (2) regardless of the direction of stretch or type of monomer, the entropic term approaches infinite as $\gamma \to 1$.

Force-length relations

Notice in (2.1.0.15) that the right hand side is the product of a characteristic force scale (i.e. $\frac{kT}{b}$) and the unknown multiplier λ (which in this case is also equivalent to $|\boldsymbol{\tau}|$). This is because the unknown multipliers, $\boldsymbol{\tau}$, represent a dimensionless measure of the force required to stretch the chain to its given end-to-end vector. Since we do not, as of yet, have a closed form expression for $\mathcal{A}^*$, we probe the force-length relationships of the DE chains by considering $\boldsymbol{\tau}$ (as opposed to $\frac{\partial \mathcal{A}^*}{\partial r}$). Figure 2.14 shows the component of $\boldsymbol{\tau}$ in the direction of stretch for DE chains with TI monomers oriented such that $\psi_r = 0$. Two important characteristics of the λ vs γ curves follow from the previous discussions

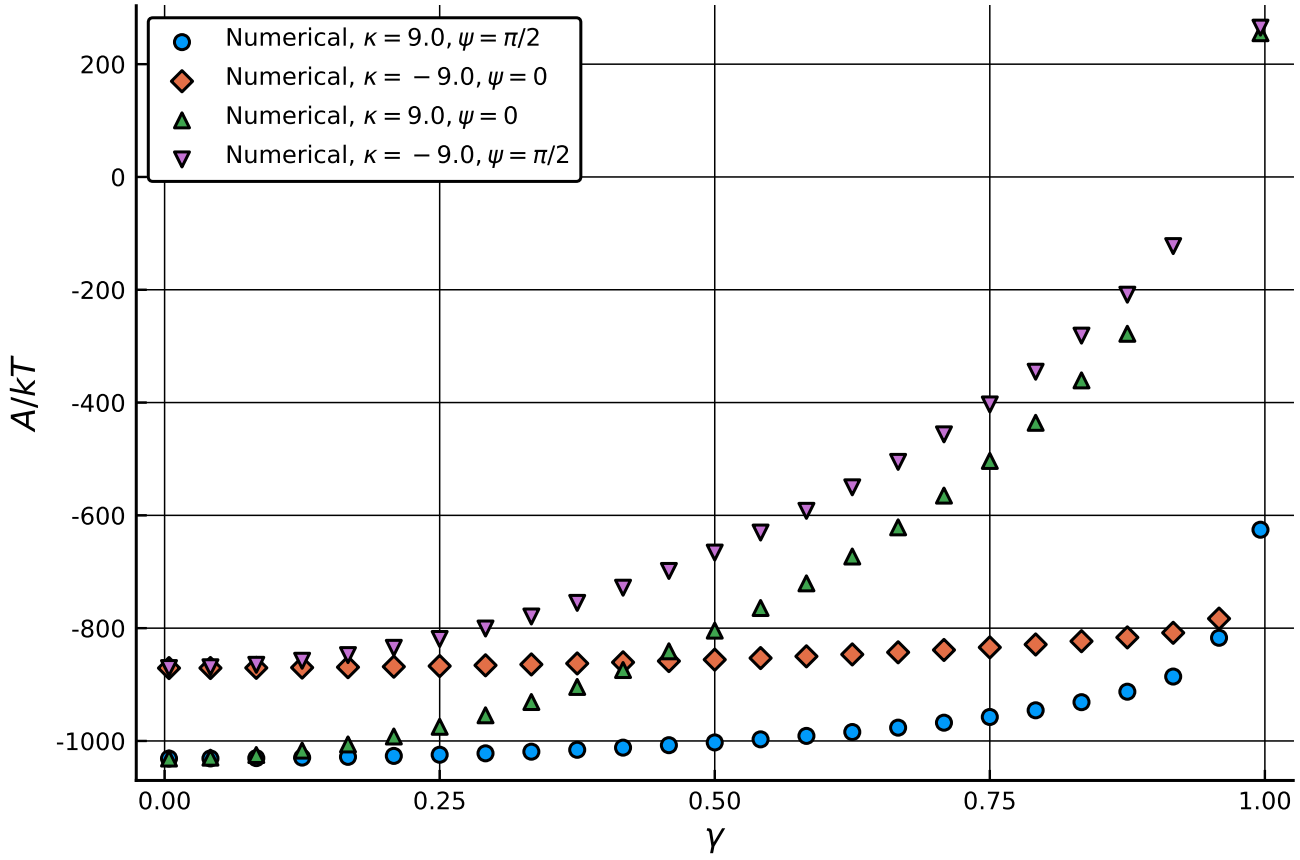

Figure 2.13: Comparison of TI and uniaxial DE chains being stretched in the direction of their respective energy maximum orientations, $\psi_r = \frac{\pi}{2}$ and 0, respectively; and TI and uniaxial DE chains being stretched in the direction of their respective energy minimum, $\psi_r = 0$ and $\frac{\pi}{2}$, respectively. Notice the subtle differences in behavior between the TI and uniaxial chains as a result of the fact that the minimum energy orientation of a uniaxial monomer is when $\hat{\mathbf{n}} = \pm\hat{\mathbf{E}}_0$, where as the minimum energy orientation of a TI monomer occurs when $\hat{\mathbf{n}} \cdot E_0 = 0$. The uniaxial minimum is only two discrete directions but the TI minimum orientation describes a plane in which $\hat{\mathbf{n}}$ can rotate and the TI monomer still be at an energy minimum. The differences in the electrostatic monomer responses lead to a difference in the overall chain behaviors.

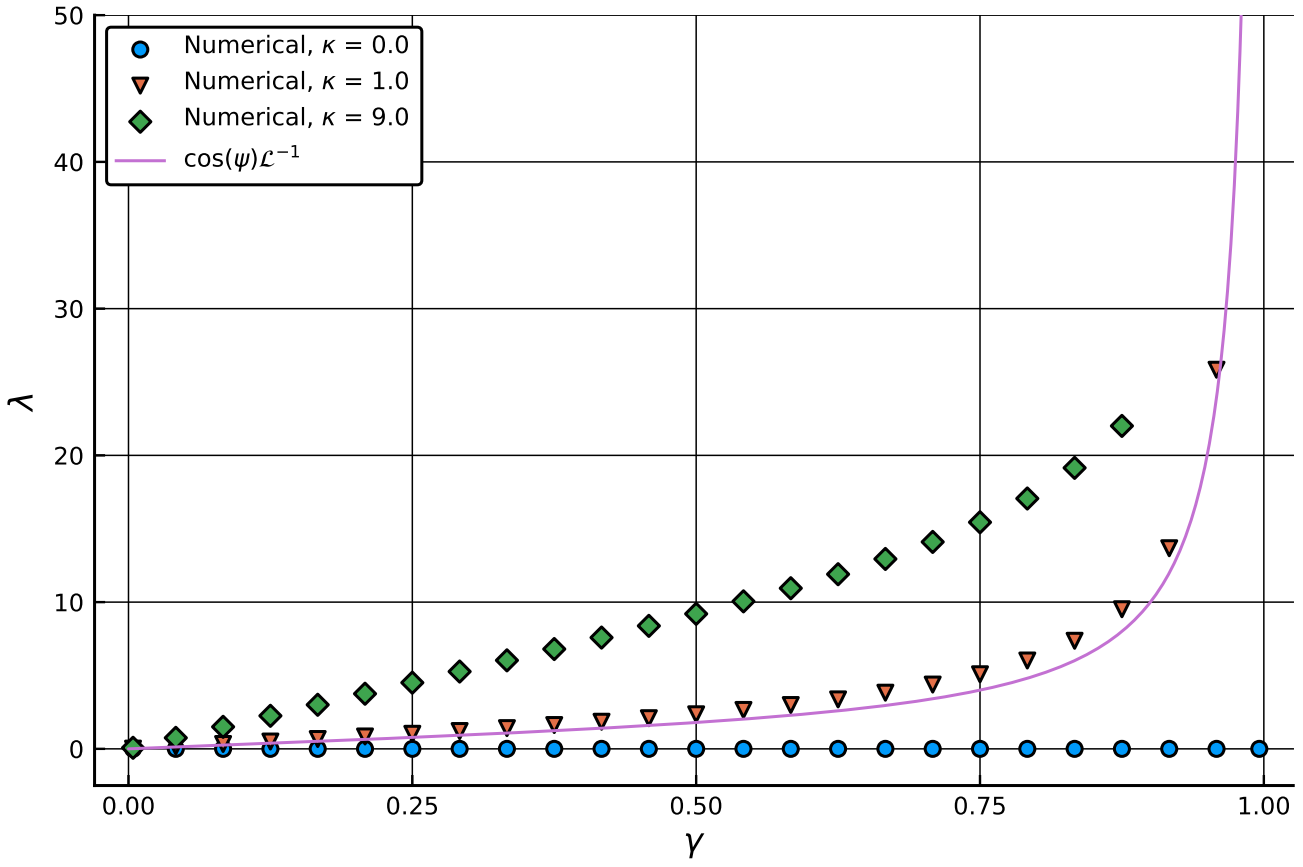

Figure 2.14: Component of $\boldsymbol{\tau}$ in the $\hat{\mathbf{r}}$ direction with respect to γ ($\psi_r = 0$). As κ increases, the change in $|\boldsymbol{\tau}|$ with respect to stretch increases because the TI monomers are being forced into or near their maximum energy orientation. Notice: the curves appear linear for moderate stretch ($\gamma \leq 0.5$) but are super linear as $\gamma \to 1$.

regarding the $\mathcal{A}^*/kT$ vs γ relationships. First, $\boldsymbol{\tau} = \mathbf{0}$ when $\gamma = 0$. This is a consequence of the fact that $\mathcal{A}^*/kT$ is a minimum when the chain is unstretched. Physically, $\gamma = 0$ is a stable equilibrium for all DE chains. Second, as κ increases, the force required to the stretch the chain increases. This is to be expected in this case because λ is a measure of the force in the direction of the polar axis, which in this case is also the direction of the electric field and a maximum energy orientation for TI monomers. Thus, for larger κ the monomers must climb out of a larger potential well to align in the direction of ψ_r; and consequently, a larger force. What is perhaps both more subtle and more interesting is that there appears to be two regimes to each of the λ vs γ curves: the curves appear linear for moderate stretch ($\gamma \leq 0.5$) but are super linear as $\gamma \to 1$.

Figure 2.15 shows α, that is, the component of $\boldsymbol{\tau}$ in the x-direction, with respect to stretch for TI

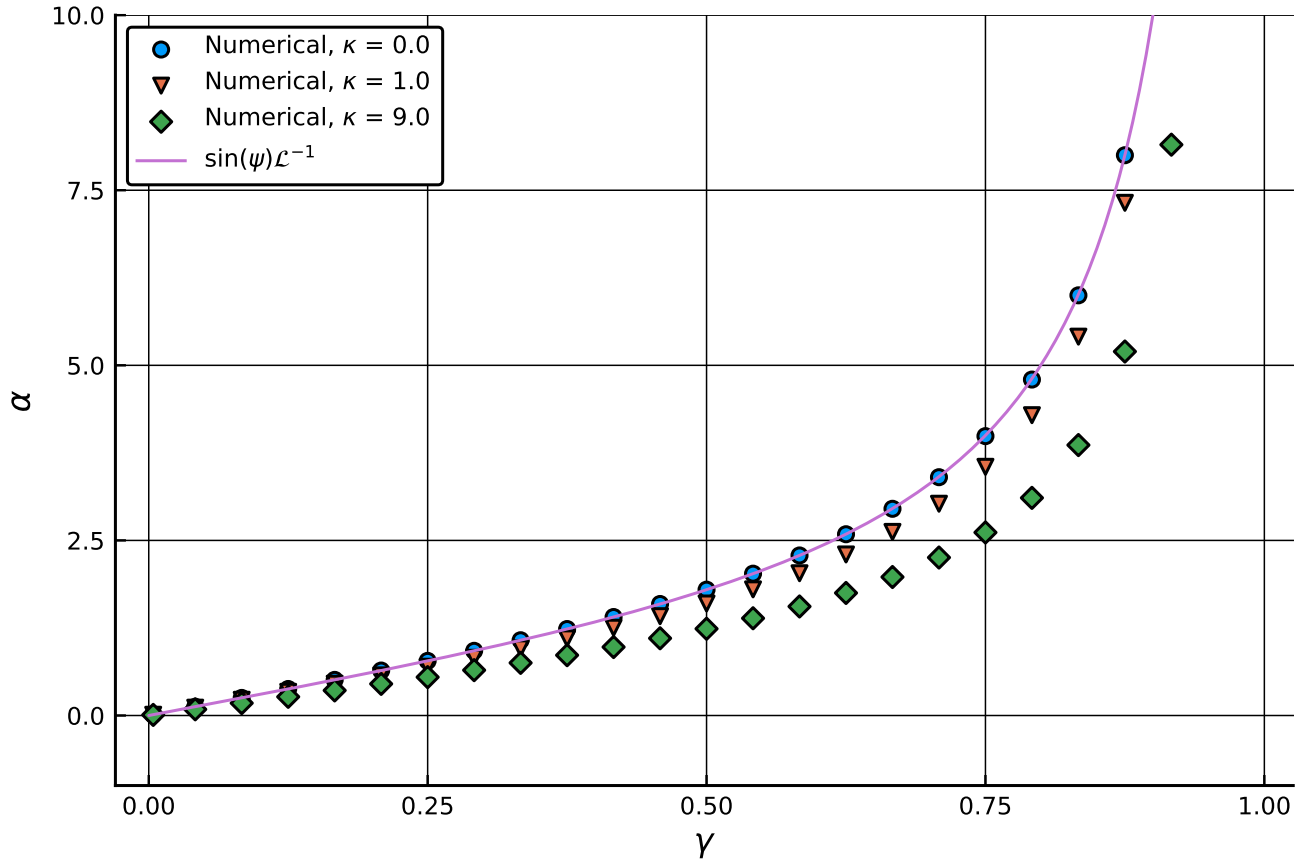

Figure 2.15: Component of $\boldsymbol{\tau}$ in the $\hat{\mathbf{r}}$ direction with respect to γ ($\psi_r = \frac{\pi}{2}$). As κ increases, the change in $|\boldsymbol{\tau}|$ with respect to stretch decreases because the TI monomers are being forced into or near their minimum energy orientation. Notice: the curves appear linear for moderate stretch ($\gamma \leq 0.5$) but are super linear as $\gamma \to 1$.

monomers. In contrast to Figure 2.14, the chains in Figure 2.15 are oriented such that $\psi_r = \pi/2$ so that, again, the ordinate represents the component of $\boldsymbol{\tau}$ in the direction of stretch. Notice that, again, α vanishes when $\gamma = 0$ and there appears to be a linear regime and super linear regime for each of the chains. In contrast, α decreases for increasing κ. This is because the monomers are being kinematically constrained into a minimum energy orientation as the chain stretches. The force is working against (increasing) entropy, however the zero stretch entropy is larger for larger κ (because monomers are more heavily concentrated at their minimum energy orientations as κ increases). Hence, the increase in entropy with stretch is more gradual when κ is larger and it requires less of a force to stretch the chain.

Figure 2.16 and Figure 2.17 show the component of $\boldsymbol{\tau}$ in the direction of stretch for uniaxial DE

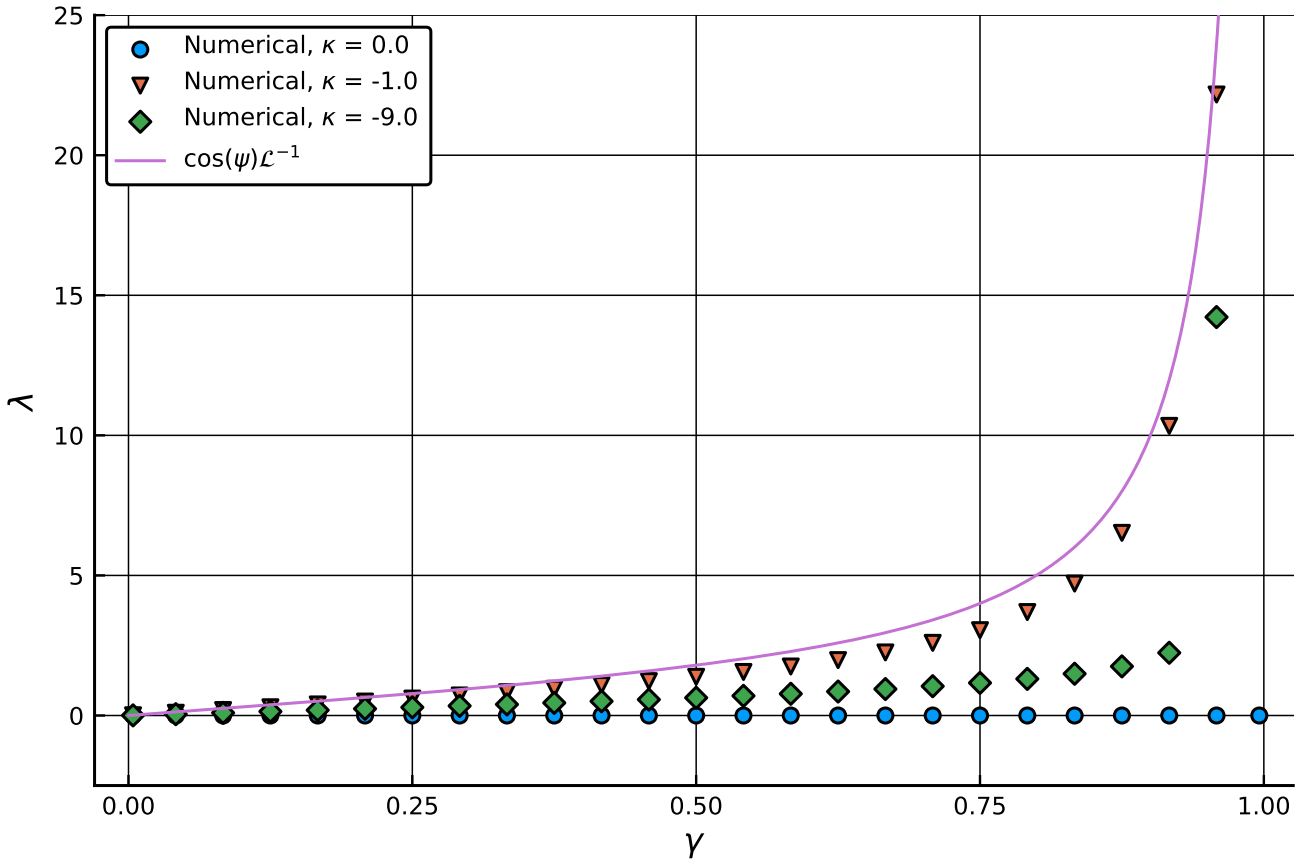

Figure 2.16: Component of $\boldsymbol{\tau}$ in the $\hat{\mathbf{r}}$ direction with respect to γ ($\psi_r = 0$). As κ increases, the change in $|\boldsymbol{\tau}|$ with respect to stretch decreases because the uniaxial monomers are being forced into or near their minimum energy orientation. Notice: the curves appear linear for moderate stretch ($\gamma \leq 0.5$) but are super linear as $\gamma \to 1$.

chains with $\psi_r = 0$ and $\psi_r = \pi/2$, respectively. The force-stretch relationships have a similar character; that is, the force vanishes at $\gamma = 0$ and there appears to be linear and super linear regimes. Also, the slope of the force-stretch relationship depends on κ. As expected, the slope is larger for larger κ when the chain is being stretched in a direction of maximum energy for uniaxial monomers; and the slope is smaller for larger κ when the chain is being stretched in a direction of minimum energy.

Dipole statistics and chain polarization

Dielectric elastomers have many desirable qualities for applications in sensors (e.g. flexible, compliant strain gauges) and power generation. As a result, the electrical properties of polymers, at the macromolecular scale, are of interest. Having obtained the monomer density function, one can approx-

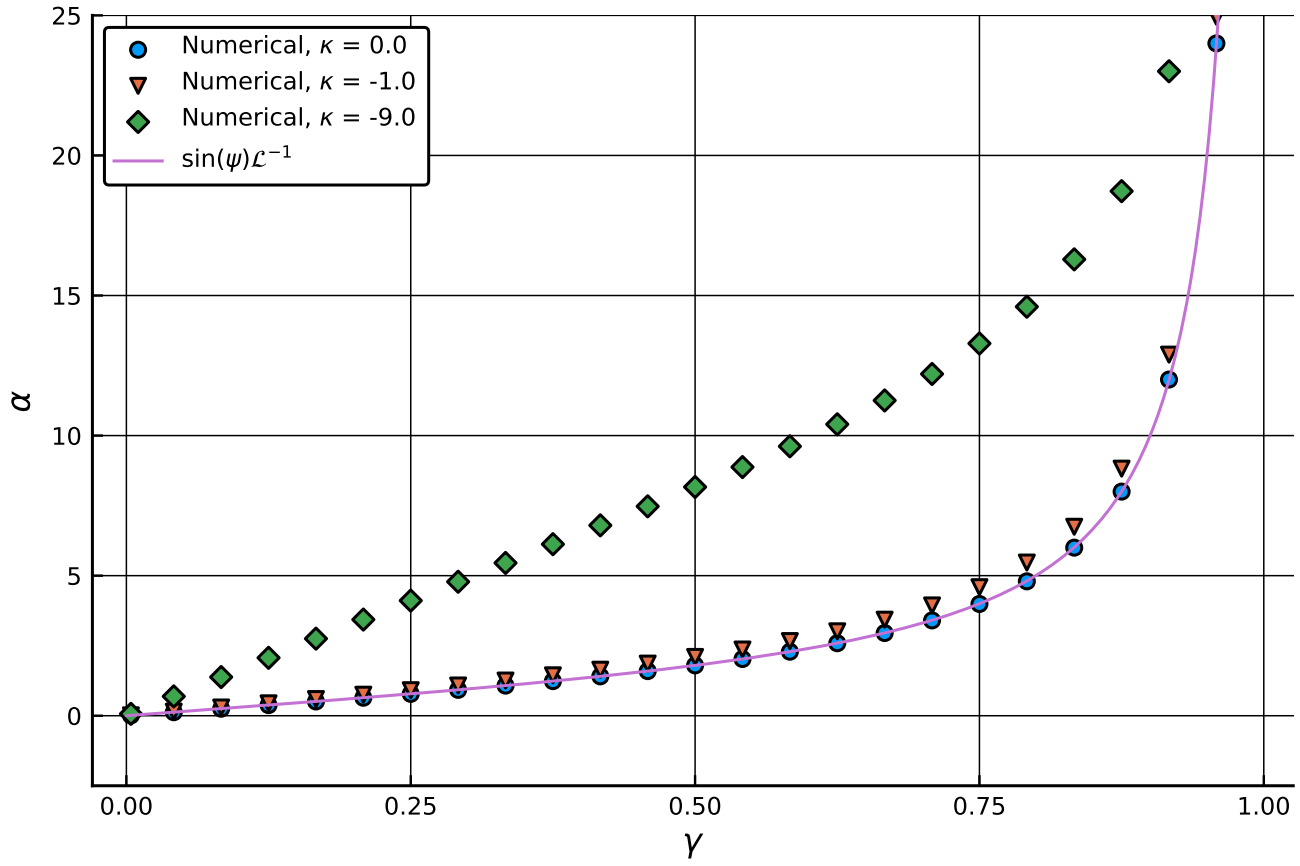

Figure 2.17: Component of $\boldsymbol{\tau}$ in the $\hat{\mathbf{r}}$ direction with respect to γ ($\psi_r = \frac{\pi}{2}$). As κ increases, the change in $|\boldsymbol{\tau}|$ with respect to stretch increases because the uniaxial monomers are being forced into or near their maximum energy orientation. Notice: the curves appear linear for moderate stretch ($\gamma \leq 0.5$) but are super linear as $\gamma \to 1$.

imate the expected chain polarization, $\mathbf{p}$, by integrating the dipole moment over the monomer density function; i.e.

$$\mathbf{p} \approx \int_{\mathbb{S}^2} \mathrm{d}A \, \boldsymbol{\mu}(\hat{\mathbf{n}}) \, \rho(\hat{\mathbf{n}}) \tag{2.3.2.1}$$

where $\boldsymbol{\mu}$ is given by (2.2.1.7) and (2.2.1.8). The expression given by (2.3.2.1) is merely an approximation because in order to properly account for the contribution of each monomer dipole to the overall chain polarization, it would be necessary to consider the positions of each of the dipoles as well.

Figure 2.18 shows the chain polarization for $\kappa = 1.0$ at different stretches and orientations. The x and y coordinates of (the base of) each polarization vector represents the chain stretch in the direction orthogonal to the electric field (i.e. $\gamma_\perp$) and aligned with the electric field (i.e. $\gamma_\parallel$), respectively; and the chain polarization vectors are scaled such that each vector is given by $\mathbf{p}/\left(10n\sqrt{|\kappa|kT}\right)$ (where the factor of 10 is included purely for the convenience of not having vectors overlap each other). At small stretches (0.0 to 0.25) the polarization is in the direction of the electric field, as expected. As the stretch increases toward its limit, monomers are forced to oriented in the direction of chain stretch which influences the direction of magnitude of the chain polarization. Because $\chi_\parallel < \chi_\perp$, the magnitude of the polarization decreases with increasing $\gamma_\parallel$ and increases with $\gamma_\perp$.

Figure 2.19 shows the chain polarization for a chain of uniaxial monomers ($\kappa = -1.0$) at different stretches and orientations. Similar to Figure 2.18: the chain polarization is in the direction of the electric field at small stretches and is influenced by the chain end-to-end vector orientation at larger stretches. Because $\chi_\parallel > \chi_\perp$, the magnitude of the polarization increases with $\gamma_\parallel$ and decreases with increasing $\gamma_\perp$. Lastly, note, comparing Figure 2.18 to Figure 2.19, the small stretch chain polarization is (approximately) two times greater for $\kappa = 1.0$ than $\kappa = -1.0$. This difference can again be explained by considering the fact that a TI monomer has a plane of directions in which it attains its maximum $|\boldsymbol{\mu}|$, whereas a uniaxial monomer only has two discrete directions in which it attains its maximum $|\boldsymbol{\mu}|$. Hence, in the balance between the internal energy and entropy terms in the chain free energy, TI monomers are able attain a larger polarization because a chain with a larger density of monomers oriented nearly orthogonal to the electric field will have a larger entropy. And since the difference in $|\mathbf{p}|$ between $\kappa = 1.0$ and $\kappa = -1.0$ is due to entropy, one can see that it vanishes as the chain is nears

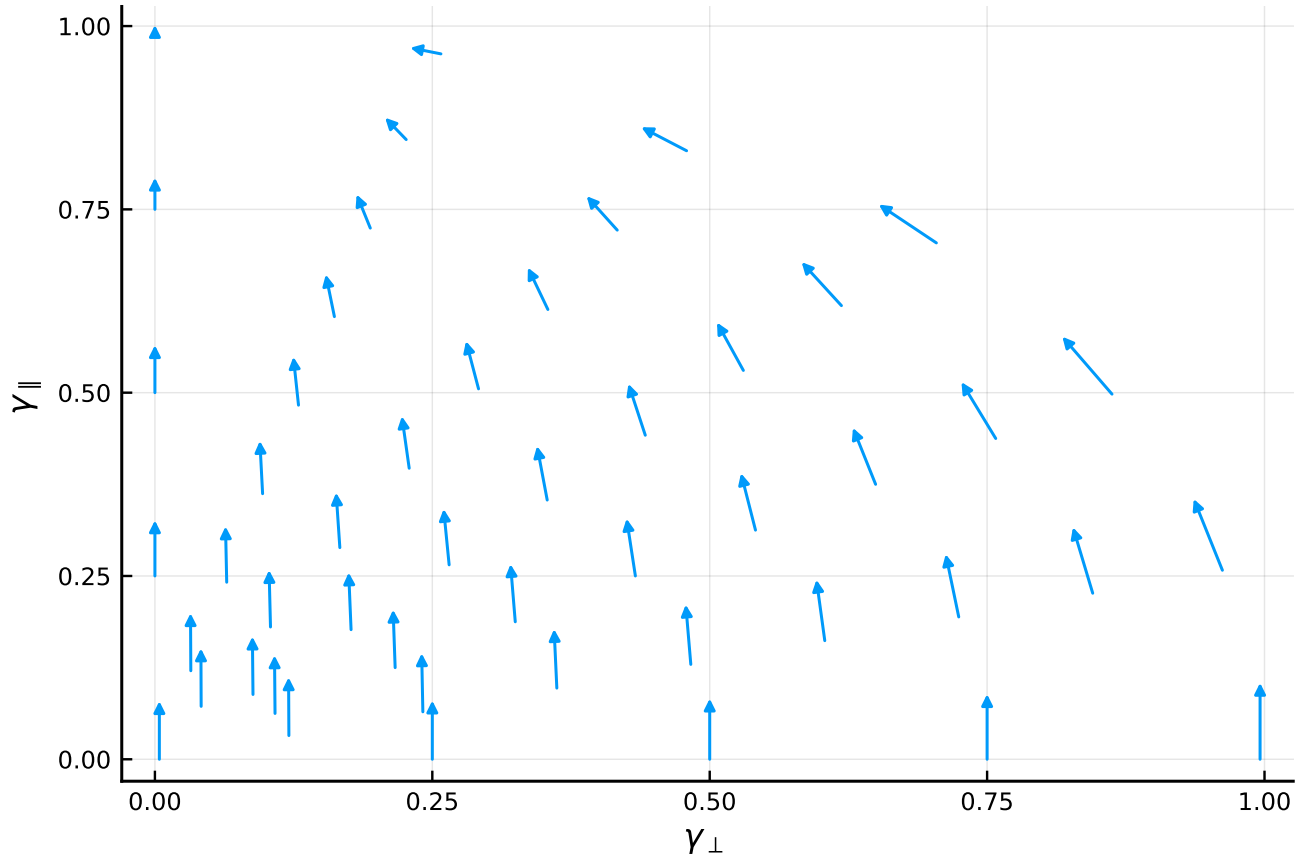

Figure 2.18: Chain polarization for $\kappa = 1.0$ at different stretches and orientations. The x and y coordinates of (the base of) each polarization vector represents the chain stretch in the direction orthogonal to the electric field (i.e. $\gamma_\perp$) and aligned with the electric field (i.e. $\gamma_\parallel$), respectively. The chain polarization vectors are scaled such that each vector is given by $\mathbf{p}/\left(10n\sqrt{|\kappa|kT}\right)$. At small stretches (0.0 to 0.25) the polarization is in the direction of the electric field, as expected. As the stretch increases toward its limit, monomers are forced to oriented in the direction of chain stretch which influences the direction of magnitude of the chain polarization.

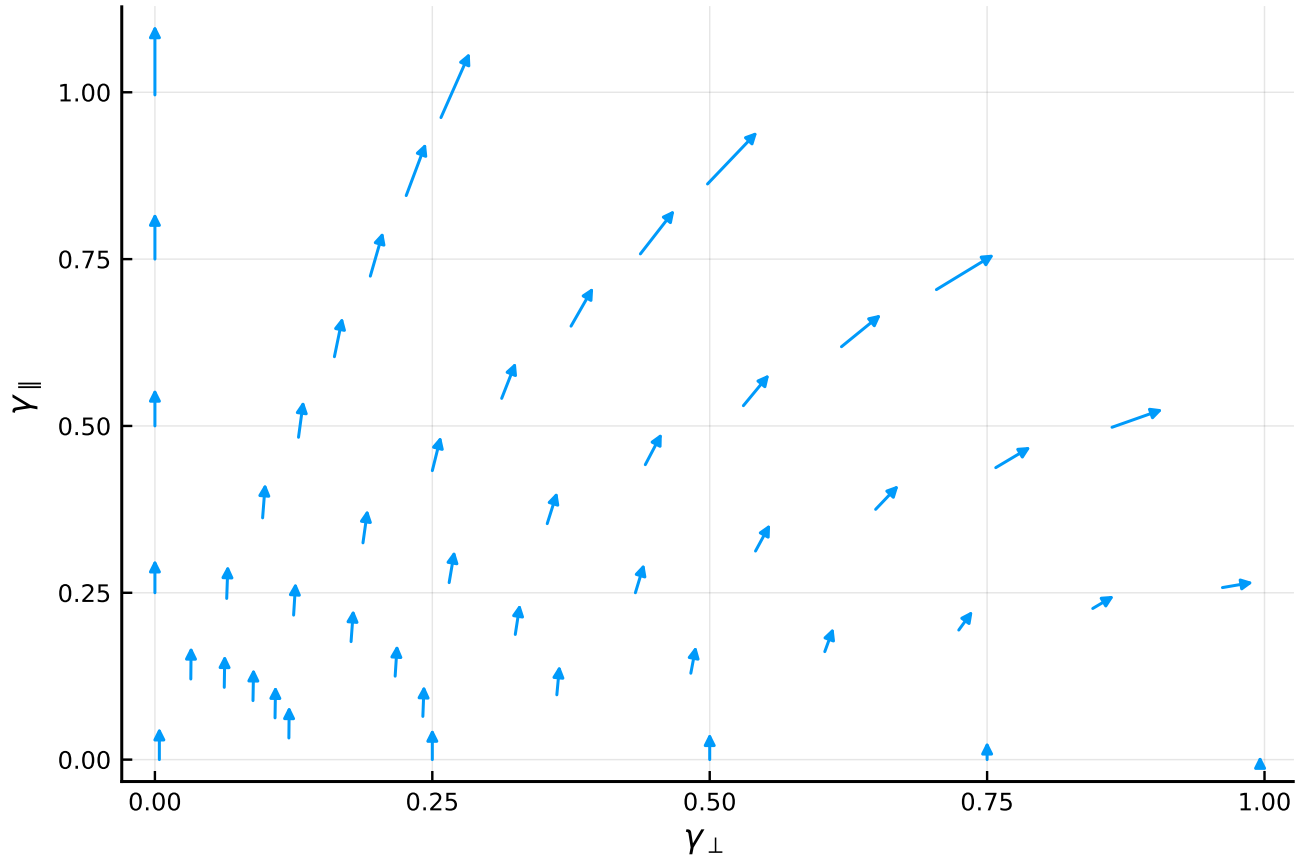

Figure 2.19: Chain polarization for $\kappa = -1.0$ at different stretches and orientations. The x and y coordinates of (the base of) each polarization vector represents the chain stretch in the direction orthogonal to the electric field (i.e. $\gamma_\perp$) and aligned with the electric field (i.e. $\gamma_\parallel$), respectively. The chain polarization vectors are scaled such that each vector is given by $\mathbf{p}/\left(10n\sqrt{|\kappa|kT}\right)$.

its fully stretched limit.

Before moving on, we consider the effect of $|\kappa|$ on the chain polarization. Figure 2.20 shows the chain polarization vector fields for $\kappa = 0.25$ (top left), $\kappa = -0.25$ (top right), $\kappa = 9.0$ (bottom left), and $\kappa = -9.0$ (bottom right). Recall that the vectors are scaled by $1/\sqrt{|\kappa|kT}$; as a result the polarization vectors appear identical when $\sqrt{\gamma_\parallel^2 + \gamma_\perp^2}$ nears unity. However, in comparing $\kappa = 0.25$ and $\kappa = 9.0$ (or alternatively, $\kappa = -0.25$ and $\kappa = -9.0$) one can see that as $|\kappa|$ increases the small stretch magnitude of $|\mathbf{p}|/\left(10n\sqrt{|\kappa|kT}\right)$ increases. This effect can be explained by considering the fact that equilibrium corresponds to a minimization of free energy. When $\gamma \to 0$, the influence of chain orientation (with respect to the electric field) vanishes and instead the density of monomer orientations is determined by a balance between the electrostatic energy and entropy terms in the free energy; that

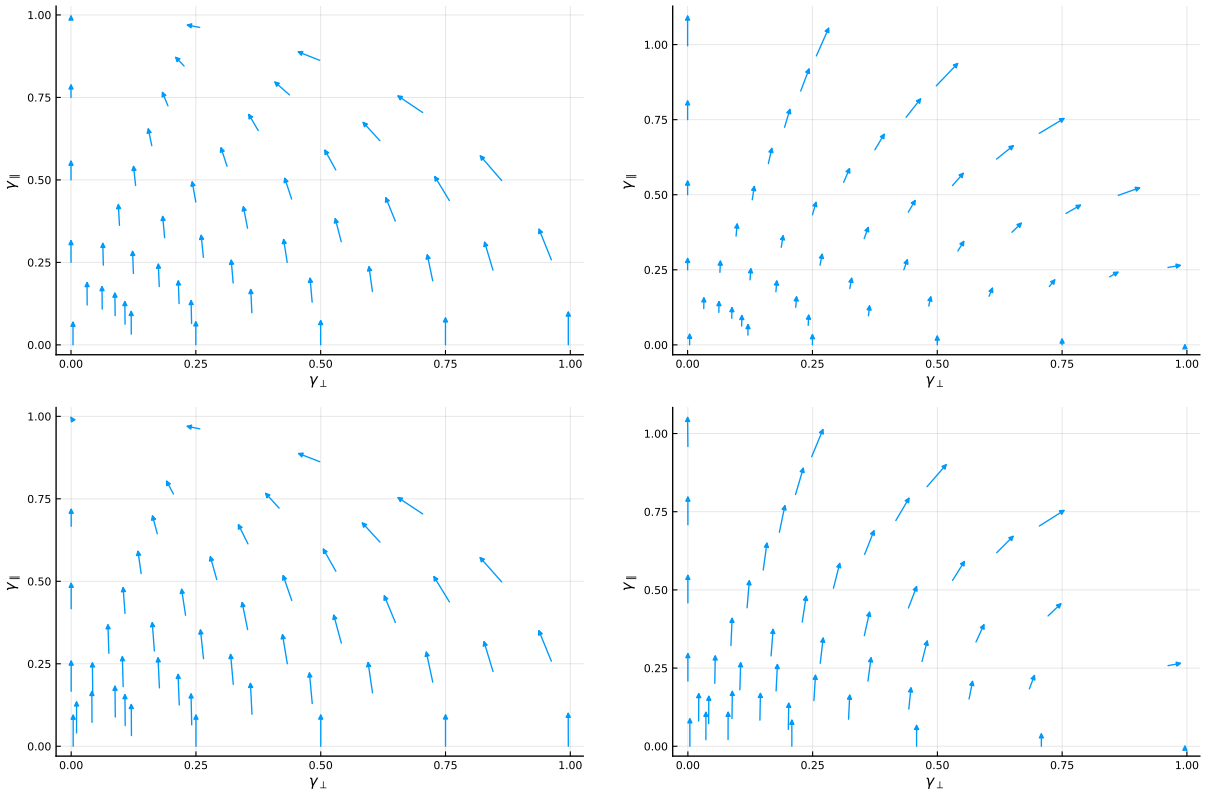

Figure 2.20: Chain polarization for $\kappa = 0.25$ (top left), $\kappa = -0.25$ (top right), $\kappa = 9.0$ (bottom left), and $\kappa = -9.0$ (bottom right) at different stretches and orientations. The chain polarization vectors are scaled such that each vector is given by $\mathbf{p}/\left(10n\sqrt{|\kappa|kT}\right)$.

is, the first and second terms in the integral of (2.2.2.7), respectively. The entropy term is minimal when the monomer density function is uniform in all directions. The electrostatic energy term is minimal when all the monomers are oriented such that the component of their dipoles in the direction of the electric field are maximized. As $|\kappa|$ increases, the influence of the electrostatic energy term increases relative to the entropic term such that $|\mathbf{p}|/\left(10n\sqrt{|\kappa|kT}\right)$ increases.

2.3.3 Summary

In general, with regard to the statistics of an DE chain, there are three competing factors: (1) electrical energy–which would induce monomer dipoles and have monomers rotate to align their respective dipoles with the electric field (2) thermal energy–which prefers monomers to be oriented in a uniform random manner and (3) the kinematic constraint. The quantity $|\kappa|$ is a measure of the influence of (1)

versus (2). Whereas the quantity $|\boldsymbol{\tau}|$ (and, in a sense, γ) is a measure of the influence of (3). The stiffness of a polymer chain is related to the slope of the free energy with respect to stretch curve. For an DE chain, its stiffness depends on κ, the current stretch, and its orientation with respect to the electric field. More specifically, TI chains exhibit a larger stiffness when stretched in or near the direction of the electric field, or opposite the direction of the electric field, than when stretched in or near a direction orthogonal to the electric field. This is because the electrostatic energy minimum of a TI monomer is in the plane orthogonal to the electric field. For a chain of uniaxial monomers, the larger stiffness occurs when stretched in or near a direction orthogonal to $\hat{\mathbf{E}}_0$ as opposed to in the direction $\hat{\mathbf{E}}_0$. The effect of orientation on chain stiffness increases with respect to $|\kappa|$ and vanishes when $\kappa \to 0$.

There are two regimes to the chain polarization. When the chain stretch is small (< 0.25), the chain polarization is in the direction of the electric field and its magnitude increases with n and E_0. In addition, all other parameters equal, the small stretch polarization for $\chi_{\parallel} = 0, \chi_{\perp} = 1$ (TI monomers) is twice that of $\chi_{\parallel} = 1, \chi_{\perp} = 0$ (uniaxial monomers). As the stretch increases, the chain polarization approaches $\boldsymbol{\chi}_{\mu}(\hat{\mathbf{r}})\,\mathbf{E}_0$ where $\boldsymbol{\chi}_{\mu}$ is defined in (2.2.1.7) and depends on the monomer dipole susceptibilities, $\chi_{\parallel}$ and $\chi_{\perp}$.

2.4 Closed-form approximation, high temperature limit

Let the coordinate system be defined such that

- the polar axis is taken to be in the direction of $\hat{\mathbf{r}}$,
- $\hat{\mathbf{E}}_0$ lies in the plane spanned by $\mathbf{e}_1$ and $\mathbf{e}_3$ (i.e. $\mathbf{E}_0 = (E_1, 0, E_3)$).

Because $\mathbf{r}$ and $\mathbf{E}_0$ both lie in the $\mathbf{e}_1$, $\mathbf{e}_3$-plane, $\boldsymbol{\tau}$ is also in the $\mathbf{e}_1$, $\mathbf{e}_3$-plane. Thus, let $\boldsymbol{\tau} = (\alpha, 0, \lambda)$. Plugging (3.0.0.1) into (2.1.0.7) and expressing the result in terms of ϕ and θ, one obtains

$$\rho(\phi, \theta) = C \exp\left[-f_{s\kappa}(\phi, \theta) + \alpha \cos\phi \sin\theta + \lambda \cos\theta\right] \tag{2.4.0.1}$$

where we let $\Delta\chi = \chi_\perp - \chi_\parallel$ and define the dimensionless parameters

$$\kappa_3 = \beta E_3^2 (\Delta\chi)/2$$
$$\kappa_1 = \beta E_1^2 (\Delta\chi)/2$$
$$\kappa_{13} = \beta E_1 E_3 (\Delta\chi)/2 = \sqrt{\kappa_3 \kappa_1}$$

that are a measure of the electrical energy per monomer with respect to thermal energy per monomer (related to the $\mathbf{e}_3$ direction, $\mathbf{e}_1$ direction, and interaction of the E_3 and E_1 components of the electric field, respectively), $f_{s\kappa}(\phi,\theta) = \kappa_3 \cos^2\theta + 2\kappa_{13}\cos\phi\cos\theta\sin\theta + \kappa_1 \cos^2\phi \sin^2\theta$, and where terms in the argument of the exponential that were independent of ϕ and θ were absorbed into the unknown C.

We proceed by assuming that $E_0^2(\Delta\chi) << kT$; and, we note that as a result of this assumption and the choice of coordinate system that α should also be small (regardless of the amount of chain stretch because α is a component of the force orthogonal to the direction of stretch). Rewrite the exponential as $\exp[-f_{s\kappa} + \alpha\cos\phi\sin\theta] \times \exp[\lambda\cos\theta]$, then Taylor expand the first exponential in the product up to first order to obtain the approximate density function

$$\rho(\phi,\theta) \approx C[1 - f_{s\kappa}(\phi,\theta) + \alpha\cos\phi\sin\theta]\exp(\lambda\cos\theta). \tag{2.4.0.2}$$

Plugging the approximate density function into (2.2.2.4) and (2.2.2.5) and integrating results in the system of equations

$$n = \frac{4\pi C}{\lambda^3}\left[\Delta\lambda\cosh\lambda - \left(\Delta - \zeta\lambda^2\right)\sinh\lambda\right] \tag{2.4.0.3}$$
$$\frac{r}{b} = -\frac{4\pi C}{\lambda^4}\left[\left(3\Delta - \zeta\lambda^2\right)\lambda\cosh\lambda + \left(-3\Delta - (\Delta - \zeta)\lambda^2\right)\sinh\lambda\right] \tag{2.4.0.4}$$
$$0 = -\frac{4\pi C}{\lambda^4}\left[-(\alpha\lambda + 6\kappa_{13})\lambda\cosh\lambda + \left(\alpha\lambda + 2\left(3 + \lambda^2\right)\kappa_{13}\right)\sinh\lambda\right] \tag{2.4.0.5}$$

where we define $\Delta = 2\kappa_3 - \kappa_1$ and $\zeta = 1 - \kappa_3$ for brevity. Also, let I_1, I_2, and I_3 be defined as the right hand side of (2.4.0.3), (2.4.0.4), and (2.4.0.5), respectively. The system (2.4.0.3)–(2.4.0.5) is clearly nonlinear. In principle, one could approximate a solution to (2.4.0.3)–(2.4.0.5) by perturbation methods

(see for example, [BO13] Ch. 7 or [Hin91] Ch. 1). However, there are some concerns related to such an approach. Power series expansions sometimes suffer from a slow rate of convergence and a limited radius of convergence. In addition, for the case of the system (2.4.0.3)–(2.4.0.5), it is not immediately obvious what one should take as a small parameter. The dimensionless parameters κ_1, κ_3, and κ_{13} are all assumed small; however, they are not totally dependent (i.e. one cannot take $\kappa_1 = \kappa_3 = \kappa_{13} = \epsilon$ because κ_1 and κ_3 can be varied independently of each other) nor are they totally independent. As a result, how one chooses a small parameter and how that choice relates to κ_1, κ_3, and κ_{13} is not trivial.

Instead, we look to iterative methods that, while are typically used in numerical analysis, are well-suited for the current problem. As in [DB81] (Section 2.6), we use Newton's method to obtain an approximate solution to (2.4.0.3)–(2.4.0.5). Recall that in Section 2.1 we effectively derived a solution for C and λ in the absence of an electric field. Since we are interested in the limit $E_0^2 \Delta\chi << kT$, we can use the result of Section 2.1 as an initial guess and calculate a correction using a Newton iteration. Two advantages of Newton's method are that its rate of convergence is quadratic and that the resulting approximation is rational instead of a power series. Although rational approximations can be obtained by other means, such as Padé approximations (see [BO13] Ch. 8), they generally converge faster than power series and better capture behavior near singularities (for example, in the context of a polymer chain, a fully stretched chain).

Let $\mathbf{x} = (C, \lambda, \alpha)$ be the vector of unknowns, $\mathbf{f} = \left(n - I_1, \frac{r}{b} - I_2, I_3\right)$ be the vector of residuals, and $J_{ij} = \partial f_i / \partial \mathbf{x}_j$ be the Jacobian matrix. The initial guess will be denoted by $\mathbf{x}_0 = (C_0, \lambda_0, \alpha_0)$ so that $\mathbf{f}_0 = \mathbf{f}(\mathbf{x}_0)$ and $J_0 = J(\mathbf{x}_0)$ are the vector of residuals and Jacobian matrix evaluated at the initial guess. Then

$$\mathbf{x} \approx \mathbf{x}_0 - J_0^{-1} \mathbf{f}_0 \tag{2.4.0.6}$$

As mentioned previously, because we are interested in an approximation that is accurate in the limit $E_0^2 \chi << kT$, we take the exact solution for $E_0^2 \chi = 0$ as the initial guess. Thus, $\lambda_0 = \mathcal{L}^{-1}(\gamma)$ and C_0 is set as the right-hand side of (2.1.0.8). To determine α_0, we substitute C_0 and λ_0 into (2.4.0.5) and,

remembering $(\coth \mathcal{L}^{-1}(\gamma) - 1/\mathcal{L}^{-1}(\gamma)) = \gamma$, solve for α to obtain

$$\alpha_0 = -2\kappa_{13}\left(\frac{3}{\mathcal{L}^{-1}(\gamma)} - \frac{1}{\gamma}\right) \tag{2.4.0.7}$$

Evaluating J and $\mathbf{f}$ at $\mathbf{x}_0$ and simplifying results in

$$J_0 = \lambda_0^{-3}\begin{bmatrix} 4\pi\lambda_0 a_4 \sinh\lambda_0 & n\lambda_0(a_2 - a_1) & 0 \\ 4\pi(a_2 - a_1)\sinh\lambda_0 & n(a_4\lambda_0^2 + 4a_1 - 2a_2)\,0 & \\ 0 & 2na_3\kappa_{13}/\gamma & n\lambda_0^2\gamma \end{bmatrix} \tag{2.4.0.8}$$

and

$$\mathbf{f}_0 = n\begin{Bmatrix} a_4/\lambda_0 - 1 \\ \gamma(\zeta - 1) - a_1/\lambda_0^2 \\ 0 \end{Bmatrix} \tag{2.4.0.9}$$

respectively, where

$$\begin{aligned} a_1 &= (3\gamma\Delta - \Delta\lambda_0) \\ a_2 &= \gamma\lambda_0^2\zeta \\ a_3 &= \gamma^2\left(\lambda_0^2 + 3\right) + 2\gamma\lambda_0 - \lambda_0^2 \\ a_4 &= \lambda_0\zeta + \gamma\Delta \end{aligned}$$

have been defined, as they are terms that repeated throughout the derivation. Their exact physical significance is not obvious; however, one should pause to notice that: a_1, a_2, and a_4 consist of terms involving products of dimensionless energy (e.g. Δ, ζ, etc.) and stretch terms (e.g. γ, λ_0), and a_3 is a parameter that depends entirely on stretch. Substituting $\mathbf{x}_0$, J_0, and $\mathbf{f}_0$ into (2.4.0.6) results in the

approximation

$$C \approx \frac{nb_3 \operatorname{csch} \lambda_0}{4\pi b_1} \tag{2.4.0.10}$$

$$\lambda \approx \lambda_0 \left(1 - b_2/b_1\right) \tag{2.4.0.11}$$

$$\alpha \approx -\frac{2\left(a_1 b_1 \gamma + a_3 b_2 \Delta\right)\kappa_{13}}{b_1 \gamma^2 \Delta \lambda_0} \tag{2.4.0.12}$$

where

$$b_1 = a_1^2 + a_2^2 + 2a_2a_4 - 2a_1\left(a_2 + 2a_4\right) - a_4^2\lambda_0^2 = \frac{\lambda_0^6 \operatorname{csch} \lambda_0}{4\pi n^2 \gamma}|J_0|$$

$$b_2 = a_2\left(a_4 - \lambda_0\right) + \lambda_0\left(a_1 + a_4\gamma\lambda_0\kappa_3\right)$$

$$b_3 = a_4\lambda_0^3 - a_2^2 - a_2\lambda_0\left(\gamma\lambda_0\kappa_3 + 2\right) + a_1\left[a_2\lambda_0\left(4 + \gamma\lambda_0\kappa_3\right)\right]$$

Having obtained an approximate solution for the unknowns C and $\boldsymbol{\tau}$, we turn our attention to the free energy. Plugging the approximate density function (2.4.0.2) into (2.2.2.6), using the Taylor expansion

$$\ln\left(1 + f_{s\kappa} + \alpha \sin\theta\cos\phi\right) \approx f_{s\kappa} + \alpha\sin\theta\cos\phi$$

and integrating results in

$$\begin{aligned}\mathcal{A}^* = \frac{kT}{\lambda^4}\big[&-4\pi C\sinh(\lambda)\left(\alpha^2\lambda + 2\alpha\left(\lambda^2+3\right)\kappa_{13} + \lambda\ln(C)\left(\Delta - \lambda^2\zeta\right) - \right.\\ &\left.\Delta\lambda(\kappa_\perp + 3) + \lambda^3(-(\kappa_\perp+3)\kappa_3 + \kappa_\perp + \kappa_1 + 1)\right) + \\ &4\pi C\lambda\cosh(\lambda)\left(6\alpha\kappa_{13} + \lambda\left(\alpha^2 + 2\kappa_3\ln(C) - \kappa_3\left(\lambda^2 + 2\kappa_\perp + 6\right) + \lambda^2\right) + \right.\\ &\left.\lambda\kappa_1(-\ln(C) + \kappa_\perp + 3)) - \lambda^4 n\ln(n)\big]\end{aligned} \tag{2.4.0.13}$$

where $\kappa_\perp = \chi_\perp E_0^2/2kT$ is the non-dimensional analog of the constant energy term in (3.0.0.1).

Next, we compare the closed-form approximate solution derived in this section to the numerical solutions obtained in Section 2.3. Figure 2.21 shows such a comparison in approximating $\mathcal{A}^*/kT$ with respect to stretch. The left plots in Figure 2.21 show TI DE chains while uniaxial chains are

shown on the right. The parameter $|\kappa_3|$ is increasing from the top of the figure to bottom ($|\kappa_3| = 0.0625, 0.25, 1.0, 9.0$, respectively; $\kappa_1 = \kappa_{13} = 0.0$). Recall that $|\kappa|, |\kappa_3|, |\kappa_1|$, etc. are measures of electrical energy with respect to thermal energy; that is, increasing $|\kappa_3|$ corresponds to an increase in the electric field and/or a decrease in temperature. One can see that the approximation is accurate for smaller values of $|\kappa_3|$ (e.g. $0.0625, 0.25$), but that it can be very inaccurate for $|\kappa_3| = 1.0$ (and larger). In addition, even for moderate $|\kappa_3|$ (i.e. $|\kappa_3| \geq 0.25$), the small κ approximation for TI monomers predicts phase transition(s) (i.e. the $\mathcal{A}^*/kT$ vs γ curve is not convex) that the numerical solution does not. As discussed in Section 2.3, one would not expect such phase transitions to be physical since (1) stretch can only cause an increase in entropy and (2) a decrease in the electrical energy term cannot be greater than the increase in the entropy term since otherwise, before the stretch, the monomers would have taken such a configuration (equilibrium corresponds to a minimization of free energy).

Figure 2.22 and Figure 2.23 show the $\mathcal{A}^*/kT$-γ relationship–comparing the small κ approximation to the numerical solutions–for increasing $|\kappa_1|$ ($|\kappa_1| = 0.0625, 0.25, 1.0$) and $|\kappa_{13}|$ ($|\kappa_{13}| = |\kappa_1| = |\kappa_3| = 0.0625, 0.25, 1.0$), respectively. Similar to what was shown in Figure 2.21, the small κ agrees well with the numerical solutions over the entire domain of stretch (i.e. $\gamma \in [0, 1)$) when $|\kappa_1| \leq 0.25$ and $|\kappa_{13}| \leq 0.25$. However, the small κ does not agree with the numerical solutions when $|\kappa_1| \geq 1.0$ and $|\kappa_{13}| \geq 1.0$ and often appear nonphysical.

In regards to electro-elasticity, we are also interested in predicting the correct force-length relationship of DE chains. As a result, it is important to consider the accuracy of the small κ approximate solution with respect to the numerical solutions in reproducing $\boldsymbol{\tau}$. In general, we find a similar relationship between accuracy of the small κ approximation in reproducing λ obtained from the numerical solution (i.e. the component of $\boldsymbol{\tau}$ in the direction of stretch) as was found in the closed-form approximation's accuracy of reproducing $\mathcal{A}^*/kT$; that is, the small κ approximation agrees well for $|\kappa_3|, |\kappa_1|, |\kappa_{13}| \leq 0.25$ but not for $|\kappa_3|, |\kappa_1|, |\kappa_{13}| \geq 1.0$. An example of this is shown in Figure 2.24, where λ is plotted with respect to γ for TI (left) and uniaxial (right) chains with $|\kappa_3| = 0.625$ (top), 0.25 (middle), and 1.0 (bottom). Lastly, note that, even when it is inaccurate, the small κ approximation reproduces the qualitative behavior of the numerical solutions. Specifically, the small κ approximation

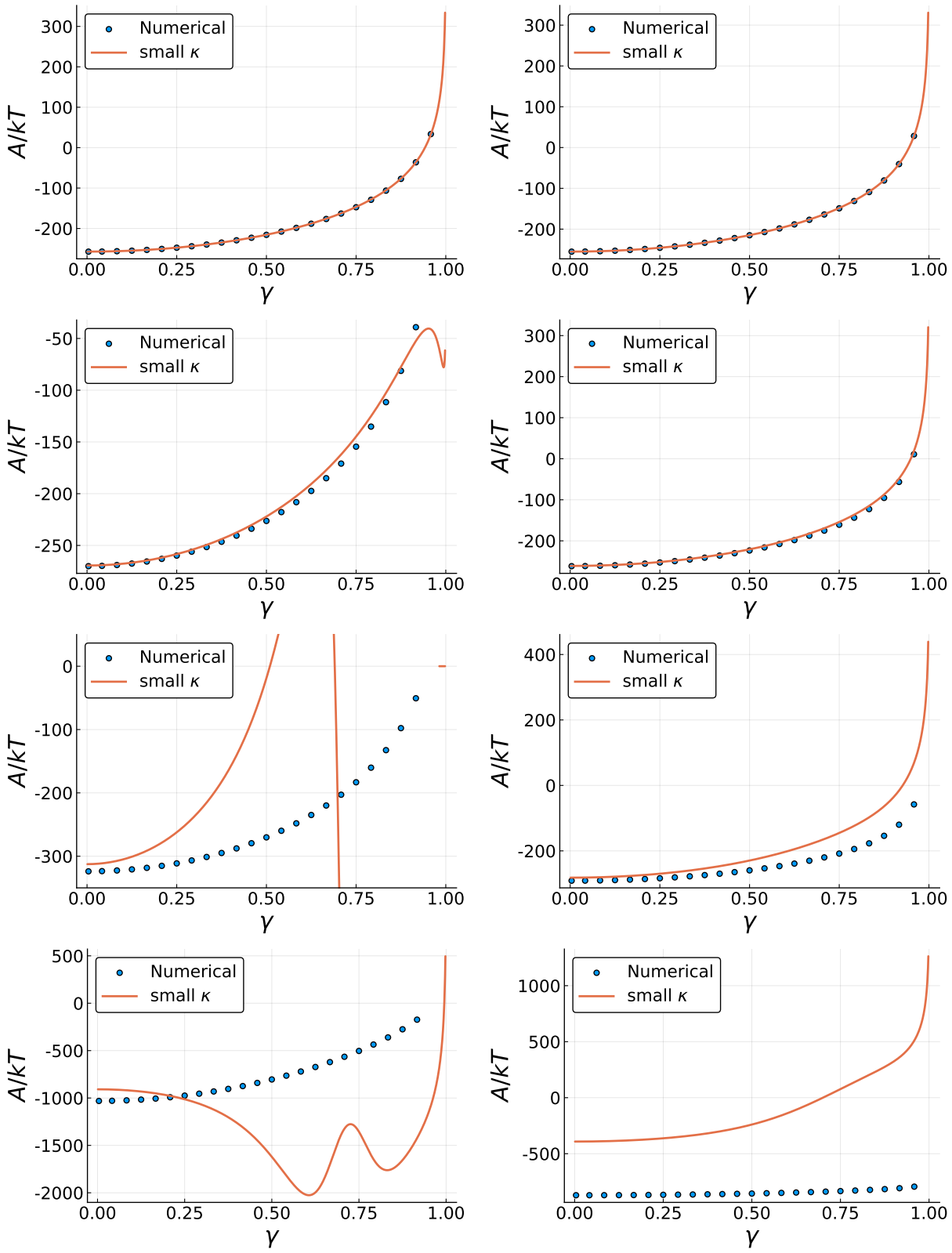

Figure 2.21: Comparison of the predicted $\mathcal{A}^*/kT$ with γ relationship using the small κ approximation and the numerical solutions. TI chains appear on the right and uniaxial chains on the left; $|\kappa_3| = 0.0625, 0.25, 1.0, 9.0$ (top row, middle-top, middle-bottom, bottom); $\kappa_1 = \kappa_{13} = 0.0$

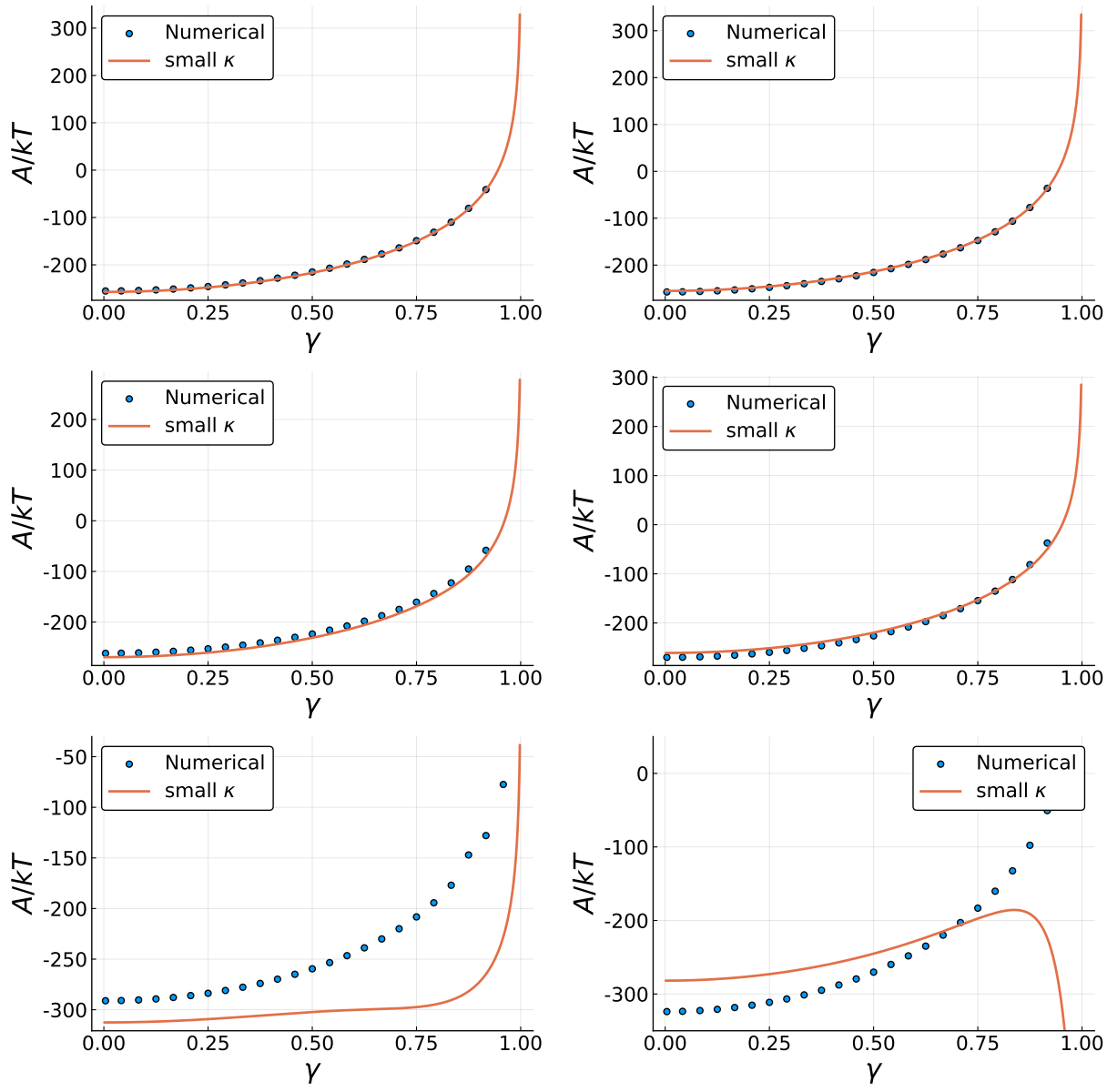

Figure 2.22: Comparison of the predicted $\mathcal{A}^*/kT$ with γ relationship using the small κ approximation and the numerical solutions. TI chains appear on the right and uniaxial chains on the left; $|\kappa_1| = 0.0625, 0.25, 1.0$ (top row, middle, bottom); $\kappa_3 = \kappa_{13} = 0.0$

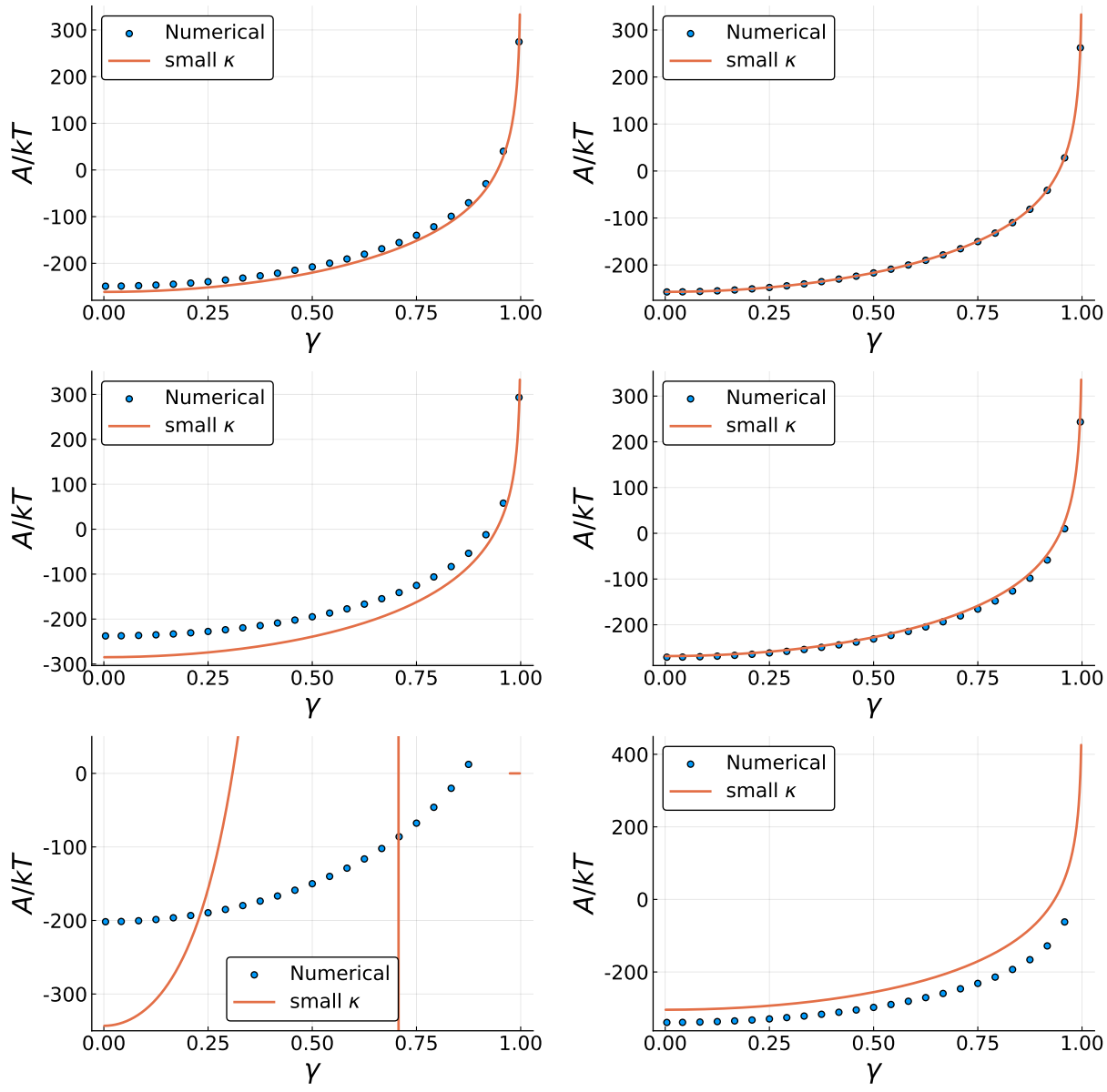

Figure 2.23: Comparison of the predicted $\mathcal{A}^*/kT$ with γ relationship using the small κ approximation and the numerical solutions. TI chains appear on the right and uniaxial chains on the left; $|\kappa_1| = |\kappa_3| = |\kappa_{13}| = 0.0625, 0.25, 1.0$ (top row, middle, bottom)

also predicts a linear regime followed by a super linear regime.

2.4.1 Summary

In summary, the closed-form approximation derived in this section assumed that $|\kappa|$ and $|\alpha|$ were small. Physically, the small $|\kappa|$ assumption corresponds to the magnitude of the electrical energy of the system being less than the thermal energy; and the small $|\alpha|$ is likely justified since α is the component of $\boldsymbol{\tau}$ orthogonal to the direction of stretch. By assuming $|\kappa|$ and $|\alpha|$ small, it allowed us to Taylor expand the monomer density function such that κ and α were no longer in the argument of the exponential and, hence, obtain an approximation of the monomer density function that allowed for a straight forward evaluation of the integrals given by (2.2.2.4) and (2.2.2.5). However, the system of equations that resulted from this approximate form were nonlinear in the unknowns C and $\boldsymbol{\tau}$. To obtain an approximate solution to the nonlinear system of equations, we used the $\kappa = 0$ solution (derived in Section 2.1) as an initial guess and performed a Newton iteration. The closed-form approximation proved to accurately reproduce numerical solutions for $|\kappa_3|, |\kappa_1|, |\kappa_{13}| \leq 0.25$. However, the closed-form approximation was not accurate for $|\kappa_3|, |\kappa_1|, |\kappa_{13}| \geq 1.0$ and, in fact, predicted nonphysical phenomena such as phase transitions at different amounts of stretch. The inaccuracy of the approximation for $|\kappa_3|, |\kappa_1|, |\kappa_{13}| \geq 1.0$ was likely due to the a number of reasons. First: physically, we require that ρ be strictly nonnegative (as it does not make sense to have a negative density of monomers in a particular direction). However, there is no guarantee that, when $\kappa_3, \kappa_1, \kappa_{13} \geq 1.0$, the approximate density given by (2.4.0.2) is strictly nonnegative. Second, the error of the Taylor series approximation in (2.4.0.2) grows with $|\kappa|$. And third, a Newton-Raphson iteration was used to approximate a solution to the nonlinear system of equations given by (2.4.0.3)-(2.4.0.5). The convergence of Newton-Raphson depends on how close the initial guess is to the exact solution. Since the initial guess was taken to be the $\kappa = 0$ solution, the error of the Newton-Raphson iteration necessarily increases with $|\kappa_3|, |\kappa_1|$, and $|\kappa_{13}|$. The limitations of the approach taken in this section motivate the need for the asymptotic matching approach taken in Section 2.6.

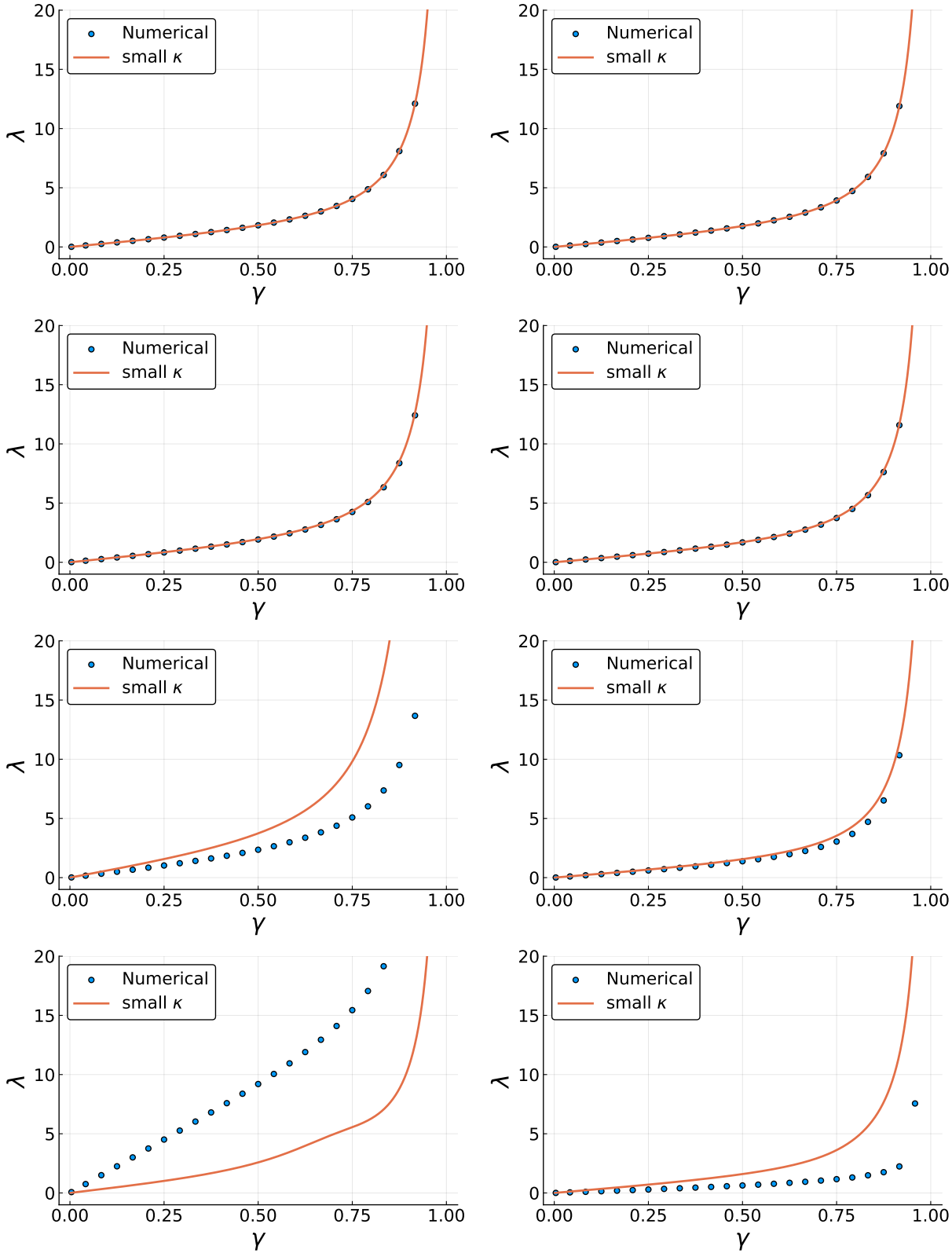

Figure 2.24: Comparison of the predicted λ with γ relationship using the small κ approximation and the numerical solutions. TI chains appear on the right and uniaxial chains on the left; $|\kappa_3| = 0.0625, 0.25, 1.0, 9.0$ (top row, middle-top, middle-bottom, bottom); $\kappa_1 = \kappa_{13} = 0.0$. Note that the small κ approximation, like the numerical solutions, also predicts a linear regime followed by a super linear regime

2.5 Closed-form approximation, small stretch limit

To investigate the limit of $|\boldsymbol{\tau}| << 1$, we use a similar process to Section 2.4; that is, we (1) choose the coordinate system such that the polar axis is in a direction of physical important and mathematical convenience, (2) we Taylor expand about the small quantity ($|\boldsymbol{\tau}|$ in the present case) and (3) we solve the approximate system of equations (for the unknowns C and $\boldsymbol{\tau}$) that result from enforcing the normalization and kinematic constraints.

We choose the coordinate system such that the polar axis is in the direction of the electric field, that is $\mathbf{e}_3 = \mathbf{E}_0/|\mathbf{E}_0|$ and $\mathbf{r}$ lies in the $\mathbf{e}_1, \mathbf{e}_3$-plane. This choice allows one to leave the dimensionless energy term, $\kappa \cos^2\theta$, inside the argument of the exponential while integrating. Next, we write $\exp\left[-\kappa\cos^2\theta + \boldsymbol{\tau}\cdot\hat{\mathbf{n}}\right]$ as $\exp\left[-\kappa\cos^2\theta\right] \times \exp\left[\boldsymbol{\tau}\cdot\hat{\mathbf{n}}\right]$, then Taylor expand the second exponential in the product up to first order to obtain the approximate density function

$$\rho(\phi,\theta) = C\left(1 + \lambda\cos\theta + \alpha\sin\theta\cos\phi\right)\exp\left[\kappa\cos^2\theta\right] \tag{2.5.0.1}$$

Plugging (2.5.0.1) into the constraint equations, namely (2.2.2.4) and (2.2.2.5), and integrating

$$n = 2\pi^{3/2} C \operatorname{erf}\left(\sqrt{\kappa}\right)/\sqrt{\kappa} \tag{2.5.0.2}$$

$$\frac{r_3}{b} = \pi C\lambda\left(\frac{\sqrt{\pi}\operatorname{erf}\left(\sqrt{\kappa}\right)}{\kappa^{3/2}} - \frac{2e^{-\kappa}}{\kappa}\right) \tag{2.5.0.3}$$

$$\frac{r_1}{b} = \pi C\alpha\left(\frac{\sqrt{\pi}\left(2\kappa-1\right)\operatorname{erf}\left(\sqrt{\kappa}\right)}{2\kappa^{3/2}} + \frac{e^{-\kappa}}{\kappa}\right) \tag{2.5.0.4}$$

(With the understanding that κ can be negative, and in such cases

$$\begin{aligned}\operatorname{erf}\left(\sqrt{\kappa}\right)/\sqrt{\kappa} &= \operatorname{erf}\left(i\sqrt{|\kappa|}\right)/i\sqrt{|\kappa|} \\ &= -\operatorname{erfi}\left(\sqrt{|\kappa|}\right)/i^2\sqrt{|\kappa|} \\ &= \operatorname{erfi}\left(\sqrt{|\kappa|}\right)/\sqrt{|\kappa|}\end{aligned}$$

where erfi is the imaginary error function. Hence, all the quantities on the left-hand side of (2.5.0.2)–

(2.5.0.4) are real, as desired.) Notice that (2.5.0.2)–(2.5.0.4) are linear in the unknowns. Thus, we can solve the system directly to obtain

$$C = \left(n\sqrt{\kappa}\right) / \left(2\pi^{3/2}\,\mathrm{erf}\left(\sqrt{\kappa}\right)\right) \tag{2.5.0.5}$$

$$\lambda = \left(2\sqrt{\pi}\gamma_3\kappa e^{\kappa}\,\mathrm{erf}\left(\sqrt{\kappa}\right)\right) / \left(\sqrt{\pi}e^{\kappa}\,\mathrm{erf}\left(\sqrt{\kappa}\right) - 2\sqrt{\kappa}\right) \tag{2.5.0.6}$$

$$\alpha = \left(4\sqrt{\pi}\gamma_1\kappa e^{\kappa}\,\mathrm{erf}\left(\sqrt{\kappa}\right)\right) / \left(\sqrt{\pi}\,(2\kappa-1)\,e^{\kappa}\,\mathrm{erf}\left(\sqrt{\kappa}\right) + 2\sqrt{\kappa}\right) \tag{2.5.0.7}$$

where $\gamma_3 = \frac{r_3}{nb}$ and $\gamma_1 = \frac{r_1}{nb}$.

2.5.1 Free energy

Having obtained an approximate solution for the unknowns C and $\boldsymbol{\tau}$, we turn our attention to the free energy. Plugging the approximate density function (2.5.0.1) into (2.2.2.6), using the Taylor expansion

$$\ln\left(1 + \lambda\cos\theta + \alpha\sin\theta\cos\phi\right) \approx \lambda\cos\theta + \alpha\sin\theta\cos\phi$$

and integrating results in

$$A = kT\left[\frac{\pi^{3/2}C\,\mathrm{erf}\left(\sqrt{\kappa}\right)}{2\kappa^{3/2}}\left(\alpha^2\left(2\kappa-1\right) + 2\left(\lambda^2 - 2\kappa_\perp\kappa\right) + 4\kappa\ln C\right) + \frac{\pi C\exp\left(-\kappa\right)\left(\alpha^2 - 2\lambda^2\right)}{\kappa} - n\ln n\right] \tag{2.5.1.1}$$

Again, as in Section 2.4, having obtained an approximate solution for the unknowns C and $\boldsymbol{\tau}$ and an approximate expression for the free energy, we wish to test its accuracy by comparing it with numerical solutions obtained in Section 2.3. Figure 2.25 shows the $\mathcal{A}^*/kT$–γ relationship as approximated by both the small $|\boldsymbol{\tau}|$ approximate solution and the numerical solutions. The plots are shown for TI (right) and uniaxial (left) DE chains, oriented at $\psi_r = 0$ (top), $\psi_r = \frac{\pi}{4}$ (middle) and $\psi_r = \frac{\pi}{2}$ (bottom). In all cases, the zero and small stretch ($\gamma \leq 0.1$) agree nearly exactly. In addition, in contrast to the small $|\kappa|$ closed-form approximation (derived in Section 2.4), all of the curves are convex–meaning there

is no phase transition–as is desired, for physical reasons (discussed in more detail in Section 2.3 and Section 2.4). However, none of the small $|\boldsymbol{\tau}|$ curves have finite extensibility. In other words, $\mathcal{A}^*/kT$ does not approach infinity as $\gamma \to 1$. Lastly, note that the accuracy of the approximation in the regime of moderate to large stretch ($\gamma > 0.25$) depends on $|\kappa|$, the type of monomers (TI or uniaxial) the chain is composed of, and the orientation of the chain end-to-end vector with respect to the electric field (i.e. ψ_r). More specifically, the TI chains with $\psi_r = 0$ and $\psi_r = \frac{\pi}{4}$ and the uniaxial chains with $\psi_r = \frac{\pi}{4}$ and $\psi_r = \frac{\pi}{2}$ over predict $\mathcal{A}^*/kT$ (and hence, would result in predicting overly stiff chains) for γ in about the interval $(0.25, 0.99)$. Recall that these chain end-to-end vector orientations are such that monomers are being kinematically constrained to high energy states as γ increases.

2.5.2 Force-length relation

In addition to investigating the accuracy of the $\mathcal{A}^*/kT$ approximation, we also consider the $|\boldsymbol{\tau}|$–γ relationship. Figure 2.26 shows the component of $\boldsymbol{\tau}$ in the direction of stretch for TI (left) and uniaxial (right) chains oriented at $\psi_r = 0$ (top) and $\psi_r = \frac{\pi}{2}$. As mentioned in Section 2.3, there are two regimes in the force–stretch relationship: a linear regime (generally $\gamma \in (0, 0.5)$) and a super linear regime. From (2.5.0.6) and (2.5.0.7), it can be seen that the small $|\boldsymbol{\tau}|$ closed-form approximation predicts a linear relationship and in Figure 2.26 we see that, with respect to the numerical solutions, the small $|\boldsymbol{\tau}|$ captures the linear regime almost exactly. The error with respect to the numerical solutions does not occur until the super linear regime $\gamma > 0.5$. Thus, the error of the small $|\boldsymbol{\tau}|$ approximation in the $\mathcal{A}^*/kT$ curves over $\gamma \in (0.25, 0.5)$ is likely due to error in the normalization constant, C. Indeed, (2.5.0.5) shows that this approximation predicts a normalization constant that does not change with stretch. Consequently, the normalization condition is only satisfied at $\gamma = 0$.

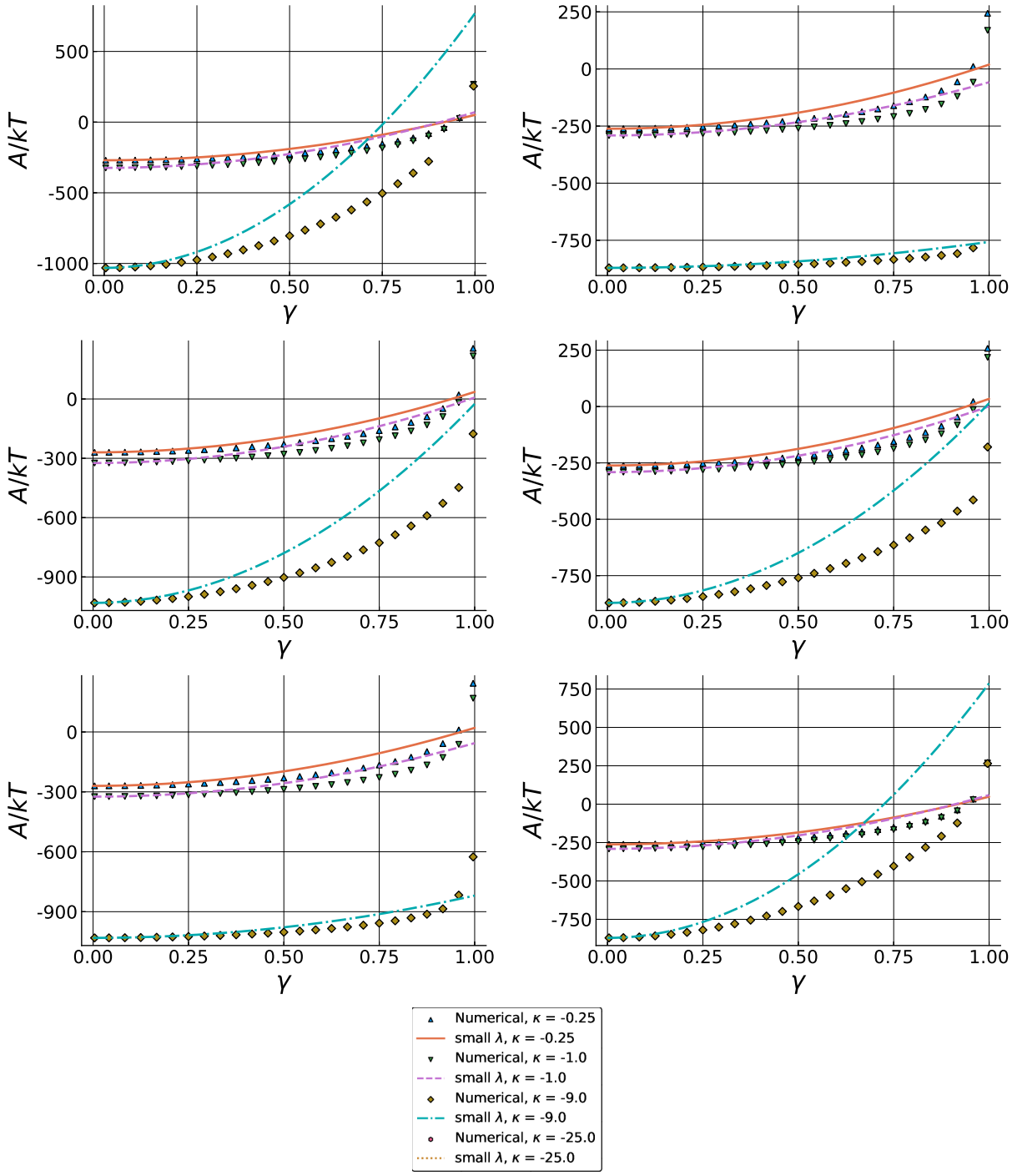

Figure 2.25: Comparison of the predicted $\mathcal{A}^*/kT$ with γ relationship using the small $|\boldsymbol{\tau}|$ approximation and the numerical solutions. TI chains appear on the right and uniaxial chains on the left; $\psi_r = 0, \frac{\pi}{4}, \frac{\pi}{2}$ (top row, middle, bottom).

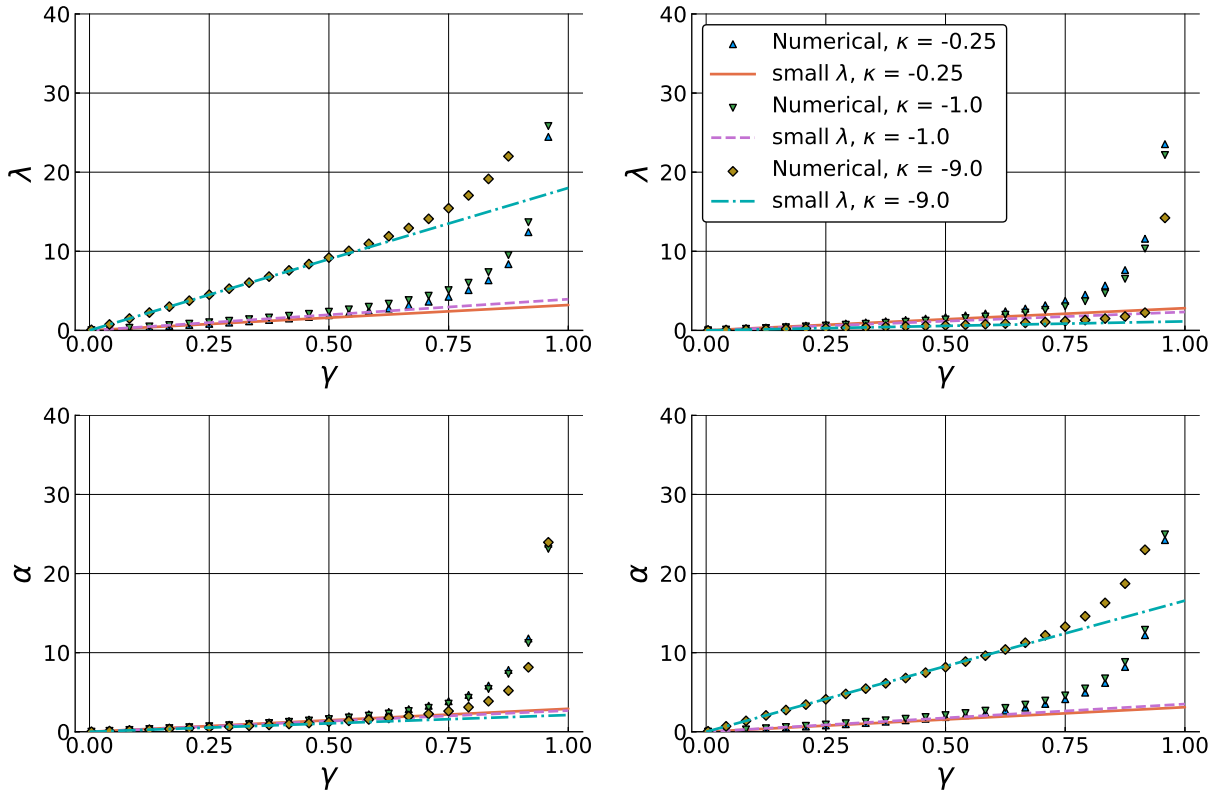

Figure 2.26: Comparison of the predicted component of $\boldsymbol{\tau}$ in the direction of stretch with γ relationship using the small $|\boldsymbol{\tau}|$ approximation and the numerical solutions. TI chains appear on the right and uniaxial chains on the left; $\psi_r = 0, \frac{\pi}{4}, \frac{\pi}{2}$ (top row, middle, bottom). The small $|\boldsymbol{\tau}|$ approximation matches the linear regime almost exactly, but does not capture the super linear regime.

2.5.3 Chain polarization

Lastly, we consider the accuracy of the approximation of the chain polarization. Using (2.5.0.5)-(2.5.0.6) in (2.3.2.1), we obtain $p_x = p_y = 0$ and

$$p_z = \frac{E_0 n}{2\kappa}\left[\chi_{\parallel} + \chi_{\perp}\left(2\kappa - 1\right)\right] + \frac{e^{-\kappa} E_0 n \Delta\chi}{\sqrt{\pi\kappa}\,\mathrm{erf}\left(\sqrt{\kappa}\right)} \tag{2.5.3.1}$$

Note that the above expressions for the chain polarization do not have a dependence on the chain end-to-end vector which, from Section 2.3.2, we know is incorrect. However, the above expressions are exact when $\mathbf{r} = \mathbf{0}$.

2.6 Asymptotic matching

Obtaining an approximate, closed-form solution that is both accurate for $|\kappa| > 1$ and moderate stretches ($\gamma > 0.25$) has proved difficult. However, we can take a different approach. Instead of assuming some parameter is small *a priori*, we can use what we have learned thus far to guide our thinking in developing a new solution. For instance: although determining the monomer density function is difficult for general γ, we do know the exact function at $\gamma = 0$ (which is obtained by recognizing that at $\gamma = 0$, $\boldsymbol{\tau} = \mathbf{0}$; and is $\rho = C\exp\left(\kappa\left(\hat{\mathbf{E}}_0 \cdot \hat{\mathbf{n}}\right)^2\right)$ where C is given by (2.5.0.5)). In addition, we know that at $\gamma = 1$, the kinematic constraint dictates that $\rho = n\delta\left(\hat{\mathbf{r}} - \hat{\mathbf{n}}\right)$. In principle, we expect the actual density to transition from the $\gamma = 0$ density to the $\gamma = 1$ density as the chain is stretched. In addition, we can extend this idea to consider densities that have the correct limiting behavior and are accurate in the neighborhood of their respective limits. The small $|\boldsymbol{\tau}|$ closed-form approximation (see Section 2.5) is accurate in the neighborhood of $\gamma = 0$ and recovers the exact solution as $\gamma \to 0$. Also, we know a solution that, not only recovers the dirac delta density in the limit of $\gamma \to 1$, but also is near exact in the neighborhood of $\gamma = 1$–namely, the Kuhn and Grün solution (see Section 2.1). Although the Kuhn and Grün solution is derived under the assumption that all chains have the same potential energy, as $\gamma \to 1$ all of the possible chain configurations have approximately the same energy since the

individual monomers in each chain must be oriented near to $\hat{\mathbf{r}}$. A viable strategy then, is to synthesize these two solutions to generate an approximation that is reasonably accurate for $|\kappa| \geq 1$, over the entire range of stretch. Ideally we would take this approach with the monomer density function; however, this leads to a difficult in calculating the entropy term of (2.2.2.7) (i.e. $\int_{\mathbb{S}^2} \mathrm{d}A\, \rho \ln \rho$). Indeed, let $\rho_{s\tau}$ and ρ_{KG} denote the small $|\boldsymbol{\tau}|$ density and Kuhn and Grün density, respectively. Then ideally we would make an approximation of the form

$$\rho \approx w_{s\tau}\rho_{s\tau} + w_{KG}\rho_{KG}$$

where $w_{s\tau}$ and w_{KG} are the weights of each respective monomer density; and in general, the weights of each density are functions of the macroscopic parameters (i.e. $w_{s\tau} = w_{s\tau}\left(\kappa, \gamma, \hat{\mathbf{E}}_0, \hat{\mathbf{r}}\right)$, $w_{KG} = w_{KG}\left(\kappa, \gamma, \hat{\mathbf{E}}_0, \hat{\mathbf{r}}\right)$). Since $w_{s\tau}$ and w_{KG} are weights, we require

$$\begin{aligned} w_{s\tau} + w_{KG} &= 1.0 \\ 0.0 \leq w_{s\tau} &\leq 1.0 \\ 0.0 \leq w_{KG} &\leq 1.0 \end{aligned}$$

However, the integral in (2.2.2.7) would have a term that would be the logarithm of a sum of two exponentials. Such a term would be difficult to evaluate or approximately evaluate.

2.6.1 Free energy

In this section we take a different approach and look to approximate $\mathcal{A}^*$ directly. Let $\mathcal{A}^*_{s\tau}$ denote the free energy approximation derived in Section 2.5, namely, (2.5.1.1). As mentioned previously, the approximation is exact in the neighborhood of $\gamma = 0$. Additionally, plugging ρ_{KG} into (2.2.2.7) results

in a free energy approximation that is exact in the limit $\gamma \to 1$:

$$\mathcal{A}^*_{KG} = \mathcal{U}_{KG} - T\mathcal{S}_{KG} \tag{2.6.1.1}$$

$$\mathcal{U}_{KG} = \int_{\mathbb{S}^2} \mathrm{d}A\, \rho_{KG} u \tag{2.6.1.2}$$

$$= nkT\left[\kappa_3 - \kappa_\perp + \frac{\gamma}{\mathcal{L}^{-1}(\gamma)}(\kappa_1 - 2\kappa_3)\right] \tag{2.6.1.3}$$

and $\mathcal{S}_{KG}$ was derived in Section 2.1 (see (2.1.0.14)). Finally, we make the approximation

$$\begin{aligned}
\mathcal{A}^* &\approx \mathcal{A}^*_{as} \\
&= \mathcal{A}^*_{KG} + \left(1-\gamma^2\right)\left(\lim_{\gamma\to 0}\mathcal{A}^*_{s\tau} - \lim_{\gamma\to 0}\mathcal{A}^*_{KG}\right) \\
&= nkT\left\{-\kappa_\perp + \gamma\mathcal{L}^{-1}(\gamma) + \ln\left(\frac{\mathcal{L}^{-1}(\gamma)\ \mathrm{csch}\ \left[\mathcal{L}^{-1}(\gamma)\right]}{4\pi}\right) + \right. \\
&\qquad \frac{\gamma\kappa}{\mathcal{L}^{-1}(\gamma)} + \left(1-\gamma^2\right)\left[-\frac{\kappa}{3} + \ln\left(\frac{2\sqrt{\kappa}}{\sqrt{\pi}\,\mathrm{erf}\left(\sqrt{\kappa}\right)}\right)\right] + \\
&\qquad \left.\left(\kappa - 3\frac{\gamma\kappa}{\mathcal{L}^{-1}(\gamma)}\right)\left(\hat{\mathbf{E}}\cdot\hat{\mathbf{r}}\right)^2\right\}
\end{aligned} \tag{2.6.1.4}$$

Notice that (2.6.1.4) (1) recovers the exact solution when $\kappa = 0$ and (2) is exact in the limits of zero stretch and full stretch. In principle, the (stretch) limiting behavior would be recovered with any choice of exponent on γ; however, the stretch term was chosen to be quadratic because of additional physical considerations. It was discovered in Section 2.3 that there are generally two regimes to the force-length relation of an DE chain: a linear regime at small to moderate stretches followed by a super linear regime. By choosing the stretch term to be quadratic, we reproduce the linear regime while the $\mathcal{A}^*_{KG}$ term recovers the super linear regime. Figure 2.27 shows the predicted free energy-stretch relation of the $\mathcal{A}^*_{as}$ approximation compared to the numerical solution for $\kappa = 1.0, -1.0, 9.0, -9.0, 25.0$, and -25.0, (top left to bottom right, respectively). The comparison is shown for chain orientations with respect to the electric field of $\psi_r = 0, \pi/6, \pi/4, \pi/3$, and $\pi/2$. It can be seen from Figure 2.27 that the approximation developed using asymptotic matching and physical intuition, $\mathcal{A}^*_{as}$, agrees well with the numerical solutions for a wide range of chain stretch, chain orientation, and κ.

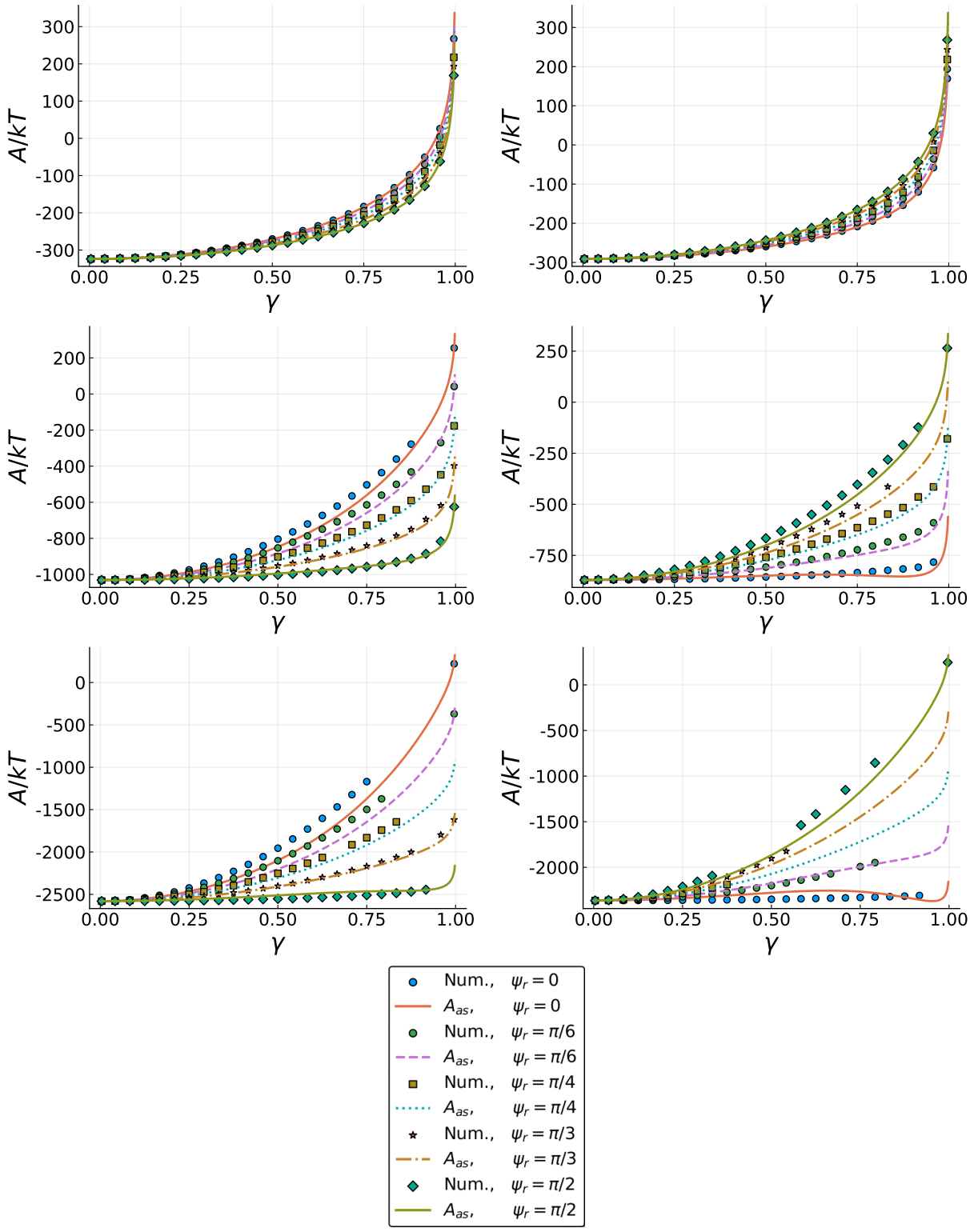

Figure 2.27: Comparison of the predicted $\mathcal{A}^*/kT$ with γ relationship using the asymptotic matching approximation and the numerical solutions. TI chains appear on the right and uniaxial chains on the left; $\kappa = 1.0, -1.0, 9.0, -9.0, 25.0$, and -25.0, (top left to bottom right, respectively).

2.6.2 Chain polarization

We now make a similar approximation to the chain polarization. Let $\mathbf{p}_{s\tau}$ be the polarization derived in Section 2.5.3 (see (2.5.3.1)). Next, let the coordinate system be such that the polar axis (i.e. $\mathbf{e}_3$) is taken in the direction of chain stretch. The approximate chain polarization using ρ_{KG} is

$$\mathbf{p}_{kg} = n \begin{Bmatrix} E_{01}\left[\chi_{\perp} - \Delta\chi\gamma/\mathcal{L}^{-1}(\gamma)\right] \\ 0 \\ E_{03}\left[\chi_{\parallel} + 2\Delta\chi\gamma/\mathcal{L}^{-1}(\gamma)\right] \end{Bmatrix} \tag{2.6.2.1}$$

Lastly, the asymptotic approximation is taken to be

$$\mathbf{p}_{as} = \mathbf{p}_{kg} + \left(1-\gamma^2\right)\left(\mathbf{R}\mathbf{p}_{s\tau} - \lim_{\gamma\to 0}\mathbf{p}_{kg}\right) \tag{2.6.2.2}$$

where $\mathbf{R}$ is a proper orthogonal matrix that rotates the coordinate system used to derived $\mathbf{p}_{s\tau}$ (i.e. polar axis taken in the direction of the electric field) to the coordinate system in which $\mathbf{p}_{kg}$ was derived. Figure 2.28 shows the predicted magnitude of the chain polarization of the $\mathbf{p}_{as}$ approximation compared to the numerical solution for $\kappa = 1.0, -1.0, 9.0$, and -9.0, (top left to bottom right, respectively). The comparison is shown for chain orientations with respect to the electric field of $\psi_r = 0, \pi/6, \pi/4, \pi/3$, and $\pi/2$. It can be seen from Figure 2.28 that, once again, the approximation developed using asymptotic matching and physical intuition agrees well with the numerical solutions for a wide range of chain stretch, chain orientation, and κ.

2.7 Conclusion

The aim of this chapter was to investigate the electro-elasticity of DE chains using statistical mechanics. In Section 2.1, we revisited the work of Kuhn and Grün in regards to classical rubber elasticity. Following a similar approach, we derived equations for the most-likely monomer density function of an DE chain. However, the equations proved difficult to solve exactly. In Section 2.3, we used nu-

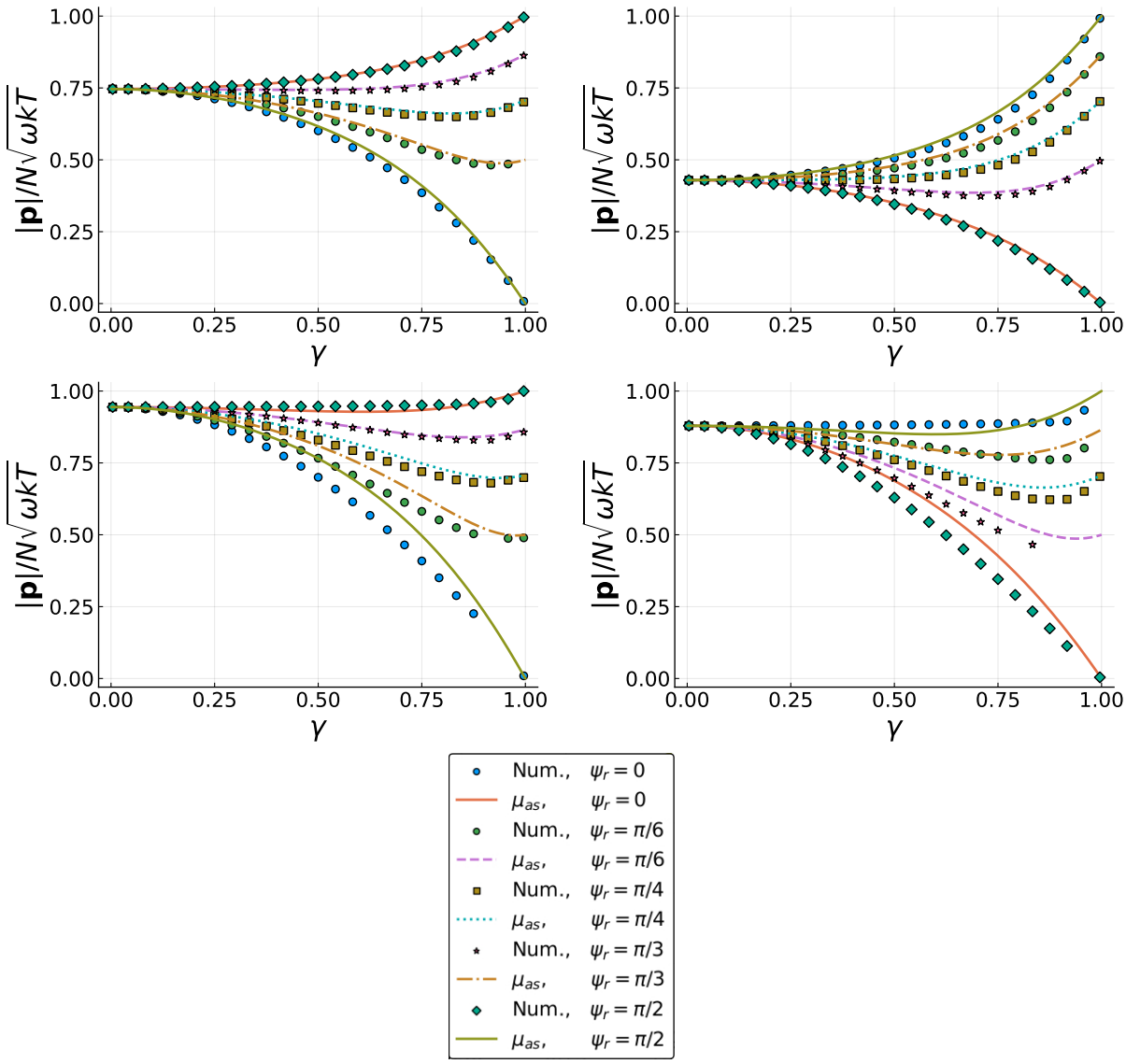

Figure 2.28: Comparison of the predicted $|\mathbf{p}|/\sqrt{|\kappa|kT}$ with γ relationship using the asymptotic matching approximation and the numerical solutions. TI chains appear on the right and uniaxial chains on the left; $\kappa = 1.0, -1.0, 9.0$, and -9.0, (top left to bottom right, respectively).

merical integration, the Newton-Raphson method and, when necessary, gradient-free optimization to approximate solutions to C, $\boldsymbol{\tau}$, ρ, $\mathcal{A}^*$, and $\mathbf{p}$ of DE chains. We considered the physical implications of the resulting solutions–emphasizing the interplay between the electrostatic energy, the thermal energy, and the kinematic constraints of the chain. In Section 2.4 and Section 2.5, we derived closed-form approximations by assuming $|\kappa|$ and $|\boldsymbol{\tau}|$ were small, respectively. These closed-form approximations proved accurate when $|\kappa| \leq 0.25$ and $\gamma \leq 0.25$, respectively, but did not generalize well for larger $|\kappa|$ or γ. Finally in Section 2.6, we used knowledge about the exact monomer density function in certain limits, such as $\gamma \to 0$, $\gamma \to 1$, and $|\kappa| \to 0$, and knowledge gained previously in the paper to form a closed-form approximation using asymptotic matching and physical intuition. The approximations for the free energy and chain polarization that were developed using the asymptotic matching approach agreed well with numerical solutions for various values of κ, γ, $\hat{\mathbf{E}}_0$, and $\hat{\mathbf{r}}$.

In the context of the bigger picture of predicting the electromechanical constitutive response of DEs, the next logical step is to take what has been learned and derived regarding the statistics of a single DE chain and, in conjunction with polymer network theory (for example, [AB93, MGL04]), predict the macroscopic response of an DE network. This will be examined in the next chapter.

Chapter 3

Interaction between broken symmetries: chain torque contributes to electromechanical coupling in polarizable polymer chains

Dielectric elastomers (DEs) are soft materials that can be used to convert electrical energy into mechanical energy, or vice versa. For this reason, DEs are promising for applications in biomedical devices and biologically inspired robotics. The quintessential example of a DE actuator (DEA) is a thin DE film sandwiched between two compliant electrodes–a soft parallel plate capacitor, in a sense. When a voltage difference is applied across the electrodes, a positive charge density accumulates on one of the electrodes and an equal and opposite charge density accumulates on the other. The DE film polarizes and compresses across its thickness and, because DEs are incompressible, the DE film expands in the plane of the electrodes.

Often this deformation has been explained as occurring because the electrodes are attracted to each other and, as a result of that attraction, apply a pressure–called the Maxwell stress–to the top and bottom of the DE film [PKK00, WM07, Kof08, KZSK12]. Although the Maxwell stress is obviously a factor, it has been pointed out (both theoretically and experimentally) that if the permittivity of the DE film is a function of deformation, then an additional stress develops in the DE film [ZS08,

Suo10, Cd16]. In this work, we explain the cause of this stress at the macromolecular level. We then proceed to show by example that this model predicts that the *direction* of polarization in DEs is not only dependent on the electric field, but also the deformation of the material. This is more general than having a permittivity that is deformation dependent and leads to new types of electromechanical coupling. This is again explained through the lens of the electroelasticity of macromolecules and their interaction with the surrounding network.

We review the core details of the DE model before proceeding to show the role of chain orientation and torque in the electromechanical coupling of DEs. We start by considering the mechanics of DEs at the monomer scale. Following [Tre75, KG42], we idealize the mechanics of a polymer chain such that (1.) monomers are rigid, (2.) monomers are free to rotate about their neighboring bonds, and (3.) we neglect excluded volume effects for simplicity. This means the maximum length of the chain end-to-end vector, $\mathbf{r}$, is nb, where n is the number of monomers in the chain and b is the monomer length. Note that, in the absence of electrostatic energy, the elasticity of a polymer chain solely due to entropy.

In the presence of an electric field, bound charges on an individual monomer can separate and an electric dipole, $\boldsymbol{\mu}$, forms. Following [Sto67, CDd16], we make the assumption that the separation of charges depends on the magnitude of the electric field and the orientation of the monomer with respect to the direction of the electric field, $\hat{\mathbf{E}}$. Because, empirically speaking, we expect the DE to be a linear dielectric, we assume the form

$$\boldsymbol{\mu}\left(\hat{\mathbf{n}}, \mathbf{E}\right) = \left[\chi_{\parallel}\hat{\mathbf{n}} \otimes \hat{\mathbf{n}} + \chi_{\perp}\left(\mathbf{I} - \hat{\mathbf{n}} \otimes \hat{\mathbf{n}}\right)\right] \mathbf{E}$$

where $\hat{\mathbf{n}}$ is a unit vector describing the monomer orientation, $\chi_{\parallel}$ and $\chi_{\perp}$ are the dipole susceptibility along $\hat{\mathbf{n}}$ and the susceptibility in plane orthogonal to $\hat{\mathbf{n}}$, respectively, and $\mathbf{E}$ is the local electric field. Following [CDd16], we refer to monomers with $\chi_{\parallel} > \chi_{\perp}$ as uniaxial and monomers with $\chi_{\perp} > \chi_{\parallel}$ as transversely isotropic (TI).

We continue to use the analogy of the dipole being like two point charges separated by the electric

field. We expect that the polarization vanishes when the electric field vanishes. We can model this behavior by connecting the two point charges by springs: one with a stiffness in the $\hat{\mathbf{n}}$ direction and the other with a stiffness in the plane orthogonal to the $\hat{\mathbf{n}}$ direction. Then the potential energy of the monomer is a sum of its dipole spring energy and the electrostatic potential energy of the dipole. This potential energy is given by

$$u\left(\hat{\mathbf{n}}\right) = \frac{1}{2}\boldsymbol{\mu}\cdot\boldsymbol{\chi}_{\mu}^{-1}\boldsymbol{\mu} - \boldsymbol{\mu}\cdot\mathbf{E} = \frac{\Delta\chi}{2}\left(\mathbf{E}\cdot\hat{\mathbf{n}}\right)^2 - \frac{\chi_{\perp}}{2}E^2 \tag{3.0.0.1}$$

where u denotes the energy, $E = |\mathbf{E}|$, and $\Delta\chi = \chi_{\perp} - \chi_{\parallel}$. Lastly, in general, dipoles interact with each other. However, for simplicity, we assume that monomer-monomer interactions are negligible as compared to the electric field, $\mathbf{E}$. Thus, in the remainder of this work, we assume that the potential energy of a DE chain is a summation of terms of the form (2.2.1.9) for each of the monomers in the chain.

Having described the energy of a monomer, we wish to derive the free energy of a DE chain. To this end, we derive a mean-field theory and determine that the density of monomers oriented in the direction $\hat{\mathbf{n}}$ is given by

$$\rho\left(\hat{\mathbf{n}}\right) = C\exp\left[-\kappa\left(\hat{\mathbf{E}}\cdot\hat{\mathbf{n}}\right)^2 + \boldsymbol{\tau}\cdot\hat{\mathbf{n}}\right] \tag{3.0.0.2}$$

where $\kappa = E^2\Delta\chi/2kT$, and the unknowns, C and $\boldsymbol{\tau}$, are determined by enforcing the constraints

$$n = \int_{\mathbb{S}^2}\mathrm{d}A\,\rho\left(\hat{\mathbf{n}}\right), \quad \frac{\mathbf{r}}{b} = \int_{\mathbb{S}^2}\mathrm{d}A\,\rho\left(\hat{\mathbf{n}}\right)\hat{\mathbf{n}} \tag{3.0.0.3}$$

where $\mathbb{S}^2$ denotes the surface of the unit sphere. In terms of the monomer density function, one can show that the free energy is approximately:

$$\mathcal{A}^* \approx \int_{\mathbb{S}^2}\mathrm{d}A\,\left\{\rho u + kT\rho\ln\rho\right\} - nkT\ln n \tag{3.0.0.4}$$

There are still two remaining difficulties in solving for C and $\boldsymbol{\tau}$: (1.) the integrals in (3.0.0.3) are difficult to evaluate and (2.) the resulting systems of equations are nonlinear. However, there are two

limits in which a solution is tenable. Let $\gamma = r/nb$ denote the absolute chain stretch. Then, by Taylor expanding in small parameters, we derive approximate solutions in the limit of small stretch, $\mathcal{A}^*_{s\tau}$, and near the fully stretched limit, $\mathcal{A}^*_{KG}$ (i.e. $\rho \approx C\left(1+\boldsymbol{\tau}\cdot\hat{\mathbf{n}}\right)\exp\left[-u/kT\right]$ and $\rho \approx C\exp\left[\boldsymbol{\tau}\cdot\hat{\mathbf{n}}\right]$, respectively). Then, using what is known about the limiting behavior, we construct a free energy approximation:

$$\begin{aligned}\mathcal{A}^* &= \mathcal{A}^*_{KG} + \left(1-\gamma^2\right)\left(\lim_{\gamma\to 0}\mathcal{A}^*_{s\tau} - \lim_{\gamma\to 0}\mathcal{A}^*_{KG}\right) \\ &= nkT\left\{f\left(\gamma,\kappa\right) + \kappa\left(1-\frac{3\gamma}{\mathcal{L}^{-1}\left(\gamma\right)}\right)\left(\hat{\mathbf{E}}\cdot\hat{\mathbf{r}}\right)^2\right\}\end{aligned} \tag{3.0.0.5}$$

where $\kappa_\perp = E^2\chi_\perp/2kT$, $\mathcal{L}^{-1}$ is the inverse Langevin function, and terms which do not depend on $\hat{\mathbf{E}}\cdot\hat{\mathbf{r}}$ have been grouped into $f\left(\gamma,\kappa\right)$. Notice that (3.0.0.5) recovers the exact solution when $\kappa = 0$ and is exact in the limits of zero stretch and full stretch. This approximation has been shown to agree well with numerical experiments for a large variety of general chain conditions (e.g. stretches, orientations with respect to the electric field, $|\kappa|$, etc.).

Having obtained an approximation of the free energy, one can obtain the chain polarization, $\mathbf{p}$, by differentiating the free energy with respect to the electric field, which is equivalent to integrating the dipole moment over the monomer density function; i.e.

$$\mathbf{p} = -\frac{\partial\mathcal{A}^*}{\partial\mathbf{E}} = \int_{\mathbb{S}^2}\mathrm{d}A\,\boldsymbol{\mu}\left(\hat{\mathbf{n}}\right)\rho\left(\hat{\mathbf{n}}\right)$$

Before moving on, we note an important feature of the free energy-stretch relationship of DE chains: numerical experiments suggest that the $\mathcal{A}^*/kT$ vs γ curve is convex and its minimum is at zero stretch. This means that an individual chain will not spontaneously stretch under electrical excitation. Therefore, the additional electrostriction that occurs in DEAs when the permittivity is deformation dependent cannot be explained by the notion that chains spontaneously stretch or contract within the network due the applied field (whereby additional electrostriction, we mean the contribution to electromechanical coupling in DEAs that is not due to the Coulomb attraction between the electrodes). Physically, this feature of the $\mathcal{A}^*/kT$-γ relationship can be understood as a consequence of: (1.) the electrostatic

energy of the monomers are quadratic in $\mathbf{E}\cdot\hat{\mathbf{n}}$ (see (2.2.1.9)) and (2.) the assumption that monomer-monomer interactions are negligible. This means that if a monomer's orientation is reversed (i.e. $\hat{\mathbf{n}}\rightarrow-\hat{\mathbf{n}}$), its energy, and hence, its contribution to the Boltzmann factor is the same. And since there is no energy penalty associated with large or small bond angles between neighboring monomers, the chain is free to fold back on itself. So in terms of the Boltzmann factor, a longer end-to-end vector is never any more favorable than a shorter end-to-end vector. However, in terms of entropy, the shorter end-to-end vector is more favorable. For these reasons, the free energy versus stretch relationship for a DE chain should be convex with its minimum at zero stretch. The correct explanation for the additional stress will become clear shortly.

Now, in order to relate the continuum scale deformation to the electroelasticity of individual chains in the network, we use the 8-chain model developed in [AB93]. The 8-chain model assumes a representative volume element (RVE) at each material point in the reference configuration consists of 8-chains emanating from the center of a cube to each of the cube's vertices, each with length $|\tilde{\mathbf{r}}|=\sqrt{n}b$ where by $\tilde{\mathbf{r}}$ we mean a chain end-to-end vector in the reference configuration. The RVE is assumed to rotate such that it is stretched in the principal frame: let $\mathbf{c_i}, i=1,2,3$ denote the principal directions of the right stretch tensor (chosen and normalized such that $\mathbf{c_i}\cdot\mathbf{c_j}=\delta_{ij}$), $\boldsymbol{\Phi}=\begin{pmatrix}\mathbf{c_1} & \mathbf{c_2} & \mathbf{c_3}\end{pmatrix}$, and $\boldsymbol{\Lambda}=\operatorname{diag}(\lambda_1,\lambda_2,\lambda_3)$. Then the free energy density is given by

$$\mathcal{W}^*(\mathbf{F},\mathbf{E})=N\left\langle\mathcal{A}^*\left(\boldsymbol{\Phi}^T\boldsymbol{\Lambda}\tilde{\mathbf{r}},\mathbf{E}\right)\right\rangle_{\tilde{\mathbf{r}}} \tag{3.0.0.6}$$

where N is the number of chains per unit volume and $\langle\cdot\rangle_{\tilde{\mathbf{r}}}$ denotes an average over the distribution of chains. For a detailed discussion of the 8-chain model, see [AB93, BA00].

Having touched upon the DE model, we now turn our attention to the electrostriction of DEAs. In order to isolate the phenomena of interest, we consider a typical DEA, but with the pressure from the electrodes removed. This could be done by applying a traction, $\mathbf{t_0}$, to the outside surfaces of the electrodes that are equal and opposite to the Coulomb attraction and by ensuring the voltage difference is adjusted to keep the electric field constant when the distance between the electrodes changes. This

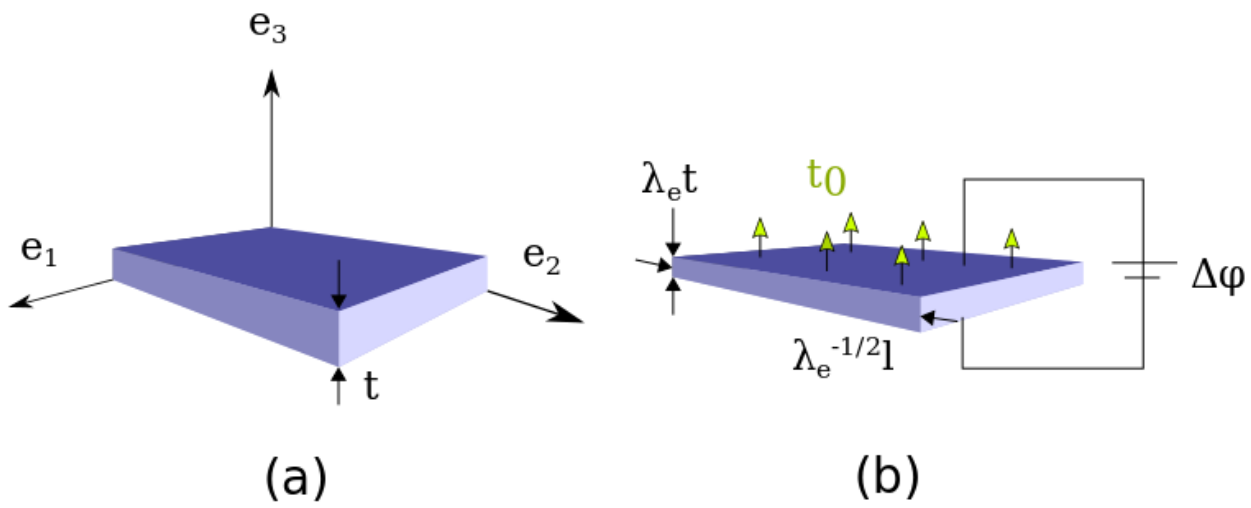

Figure 3.1: Thin film DEA but with a fixed bottom surface and an applied traction, $\mathbf{t_0}$, to the top surface of the actuator that is equal and opposite to the Coulomb attraction: (a) undeformed reference configuration; (b) a voltage difference is applied across the electrodes and by symmetry we assume a biaxial homogeneous deformation.

is shown in Figure 3.1.

In this case, the change in energy stored in the electric field and the work of the applied traction will cancel each other out; as a result, the equilibrium configuration will be the one that minimizes the free energy of the DE film. By symmetry, we assume the DE body undergoes homogeneous deformation, with deformation gradient, $\mathbf{F}$, of the form: $\mathbf{F} = \text{diag}\left(1/\sqrt{\lambda_e}, 1/\sqrt{\lambda_e}, \lambda_e\right)$ Employing the 8-chain model, we obtain

$$\left(\hat{\mathbf{E}} \cdot \hat{\mathbf{r}}\right)^2 = \left(1 + 2/\lambda_e^3\right)^{-1}, \quad \gamma = \sqrt{\frac{\lambda_e^2 + 2/\lambda_e}{3n}} \tag{3.0.0.7}$$

for each of the chains. Then, using (3.0.0.5), (3.0.0.6), and (3.0.0.7), we obtain the free energy density.

Since the deformation and electric field are homogeneous, the minimization can be carried out point wise and amounts to a line search. We used Brent's method [Bre72] for the line search to determine the equilibrium λ_e [MR18]. The λ_e which minimizes the free energy density for various κ is shown in Figure 3.2. Figure 3.2 shows that the model predicts a spontaneous deformation of the DE film, even in the absence of pressure from the top and bottom electrodes. When $\kappa > 0$, that is, when the chain is made up of TI monomers, the film is compressed in the direction of $\hat{\mathbf{E}}$ (i.e. $\lambda_e < 1$). Alternatively,

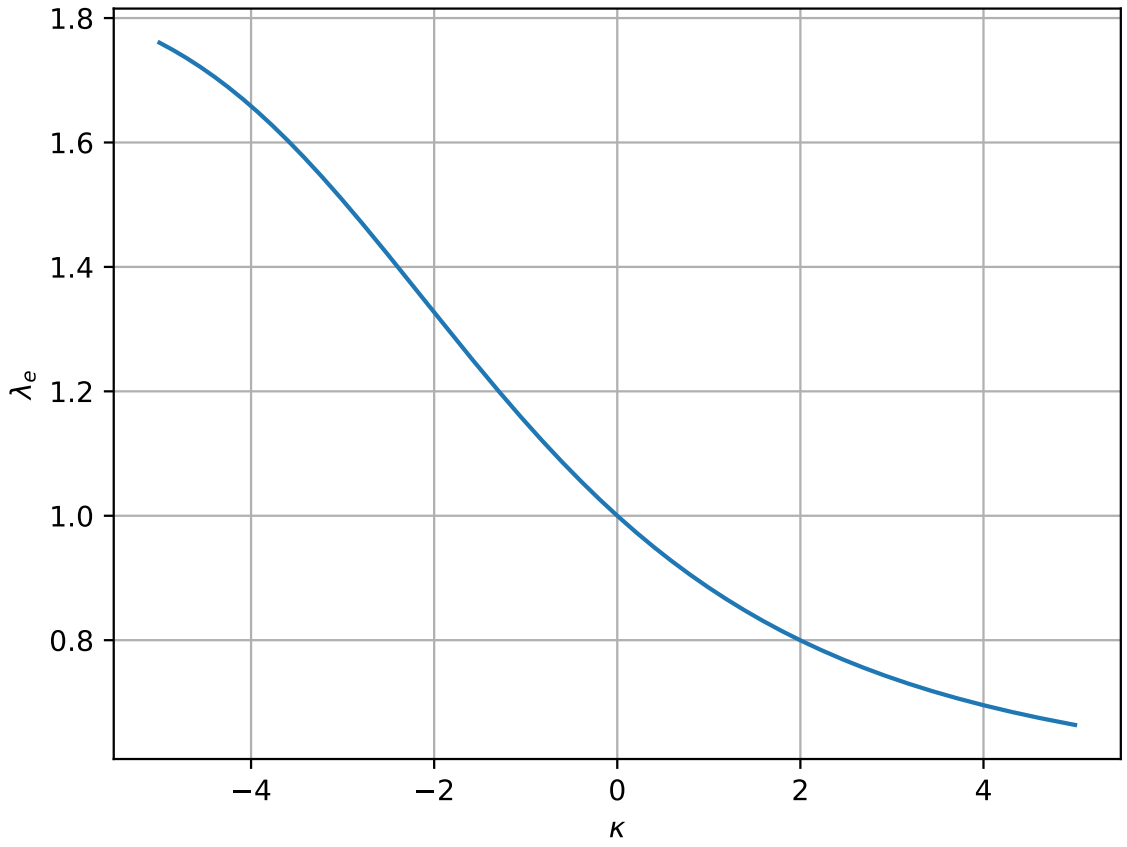

Figure 3.2: Stretch across the thickness of the DE film for various electrical inputs, κ. By free energy minimization, one sees a spontaneous deformation occurs despite the fact that the Maxwell stress has been counteracted.

when $\kappa < 0$ (chain consists of uniaxial monomers), the film actually elongates in the $\hat{\mathbf{E}}$ direction ($\lambda_e > 1$). This is likely not observed in experiments because the material and experimental parameters are such that the attractive force between the electrodes is always greater than stresses in the DE film due to this effect.

Although it has been pointed out that, at the continuum scale, this additional contribution to electrostriction can occur when the permittivity is a function of deformation [ZS08, Suo10, Cd16], the exact nature of the cause of this electrostriction at the macromolecular scale has not been adequately explained. The short explanation is that the deformation occurs because there is a net torque on each DE chain in the network that is similar to the torque on a dipole in an electric field. In fact, let ψ_r denote the angle between the electric field and the chain end-to-end vector; then it can be shown that

$$-\frac{\partial\left(\mathcal{A}^*/kT\right)}{\partial\psi_r} = \mathbf{p}\times\mathbf{E}$$

Due to empirical reasons, we assume the macroscopic deformation will be incompressible; and because of this constraint on the form of $\mathbf{F}$, chains can only rotate if the chains stretch as well. The confluence of the DE chain torque and incompressible nature of the material leads to the deformation observed in the above thought experiment. For a chain consisting of uniaxial monomers, for instance, some of its polarization is in the direction of its end-to-end vector (i.e. $\mathbf{p}\cdot\mathbf{r} \neq 0$). As a result, there is a torque that is forcing the chain to either align or anti-align with $\hat{\mathbf{E}}$. It is clear that such rotations of the chains would lead to an elongation in the $\hat{\mathbf{E}}$–which is exactly what is shown by Figure 3.2. The reasoning is similar for chains consisting of TI monomers, but instead the torque forces these chains into the plane orthogonal to $\hat{\mathbf{E}}$, which causes the film to compress in the $\hat{\mathbf{E}}$ direction.

Interestingly, although the chain torque is nonzero for each individual chain, the average over the eight chains vanishes (i.e. $\langle\mathbf{p}\times\mathbf{E}\rangle_{\tilde{\mathbf{r}}} = \mathbf{0}$). Thus, there is no net torque or "body couple" for this scenario. However, in the next example, we will consider a case in which the average torque does not vanish and a so-called body couple is present, which gives rise to a novel electromechanical coupling.

Again a thin DE film is considered with compliant electrodes on its top and bottom surfaces. How-

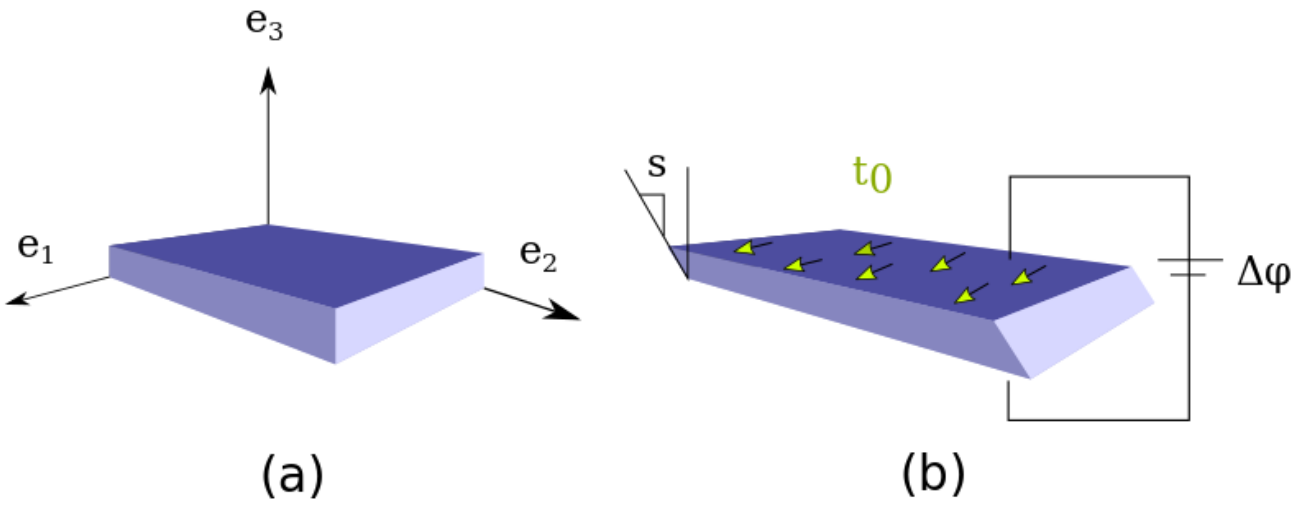

Figure 3.3: DEA constrained such that it can only undergo shear deformation: (a) undeformed reference configuration; (b) a shear prestress, $\mathbf{t_0}$, is applied and held, and then a voltage difference is applied across the top and bottom surfaces.

ever, in this example we assume the film is constrained such that it can only undergo homogeneous simple shear deformation. (This could be implemented by bonding the top surface of the DE film to an apparatus with rollers constraining its motion in the plane of shear). We also assume that the electric field is fixed and across the thickness of the film–which, neglecting fringe effects, would be realized by applying a voltage difference across the electrodes. The setup is shown in Figure 3.3.

For simple shear, the deformation gradient is of the form $\mathbf{F} = \mathbf{I} + s\mathbf{e}_1 \otimes \mathbf{e}_3$. Let $\lambda_s = \frac{1}{2}\left(\sqrt{4+s^2}+s\right)$. Then the principal directions are given by

$$\mathbf{c_1} = \left\{1 \quad 0 \quad \lambda_s\right\} / \sqrt{1+\lambda_s^2}, \qquad \mathbf{c_2} = \left\{0 \quad 1 \quad 0\right\},$$
$$\mathbf{c_3} = \left\{-\lambda_s \quad 0 \quad 1\right\} / \sqrt{1+\lambda_s^2}$$

Notice that $\hat{\mathbf{E}}$ is no longer aligned with any of the principal directions.

The last term in the brackets of (3.0.0.5) contains all the information regarding chain orientations. Since each of the chains stretches the same amount, this last term is the only one in which the averaging

must be explicitly calculated. In particular,

$$\left\langle \left(\hat{\mathbf{E}} \cdot \hat{\mathbf{r}} \right)^2 \right\rangle_{\tilde{\mathbf{r}}} = \frac{1 - \lambda_s^2 + \lambda_s^4}{1 + \lambda_s^2 + \lambda_s^4} \tag{3.0.0.8}$$

which is an even function of s, as expected. We will also be interested in the DE polarization (i.e. dipole moment per unit of volume in the current configuration).

$$\mathbf{P} = -\frac{\partial \mathcal{W}^*}{\partial \mathbf{E}} = N \left\langle \frac{\partial \mathcal{A}^*}{\partial \mathbf{E}} \right\rangle_{\tilde{\mathbf{r}}} = N \left\langle \mathbf{p} \left(\boldsymbol{\Phi}^T \boldsymbol{\Lambda} \tilde{\mathbf{r}}, \mathbf{E} \right) \right\rangle_{\tilde{\mathbf{r}}} \tag{3.0.0.9}$$

Having developed the kinematics, we now turn to the free energy. Let a traction, $\mathbf{t_0} = \begin{Bmatrix} t_0 & 0 & 0 \end{Bmatrix}$, be applied to the top surface of the film. Then, the free energy is given by

$$\int_{\Omega_0} \left(\mathcal{W}^* - \sigma_{t_0} s \right) \tag{3.0.0.10}$$

where, again, the energy density of the electric field is neglected because it does not do work on the dielectric elastomer (another way to justify this is that the electric field is held constant and volume is conserved–thus, the energy density of the electric field remains constant for any shear deformation) and σ_{t_0} is the stress induced by the traction. Again, by homogeneity (of both the deformation and electric field), we minimize (3.0.0.10) by minimizing the integrand.

Now we consider the following experiment: (1.) the traction is applied before any voltage difference is applied and is held constant; (2.) the traction causes initial shear strain, s_0; (3.) a voltage difference is applied across the electrodes such that there is some electric field, $\mathbf{E}$, in the DE film; (4.) for each $\mathbf{E}$, a shear strain s is observed such that a relationship $s = s(\mathbf{E})$ is determined. The $s = s(\mathbf{E})$ is shown in Figure 3.4. Note however that the relationship is shown in terms of κ instead of $\mathbf{E}$. This is because $s(\mathbf{E}) = s(-\mathbf{E})$ and, hence, s can be expressed as a function of κ without loss of generality; also the quantity κ is already nondimensionalized.

Figure 3.4 shows a shear electromechanical coupling. It can be seen that DEs with chains consisting of uniaxial monomers ($\kappa < 0$) spontaneously increase deformation with respect to an increasing elec-

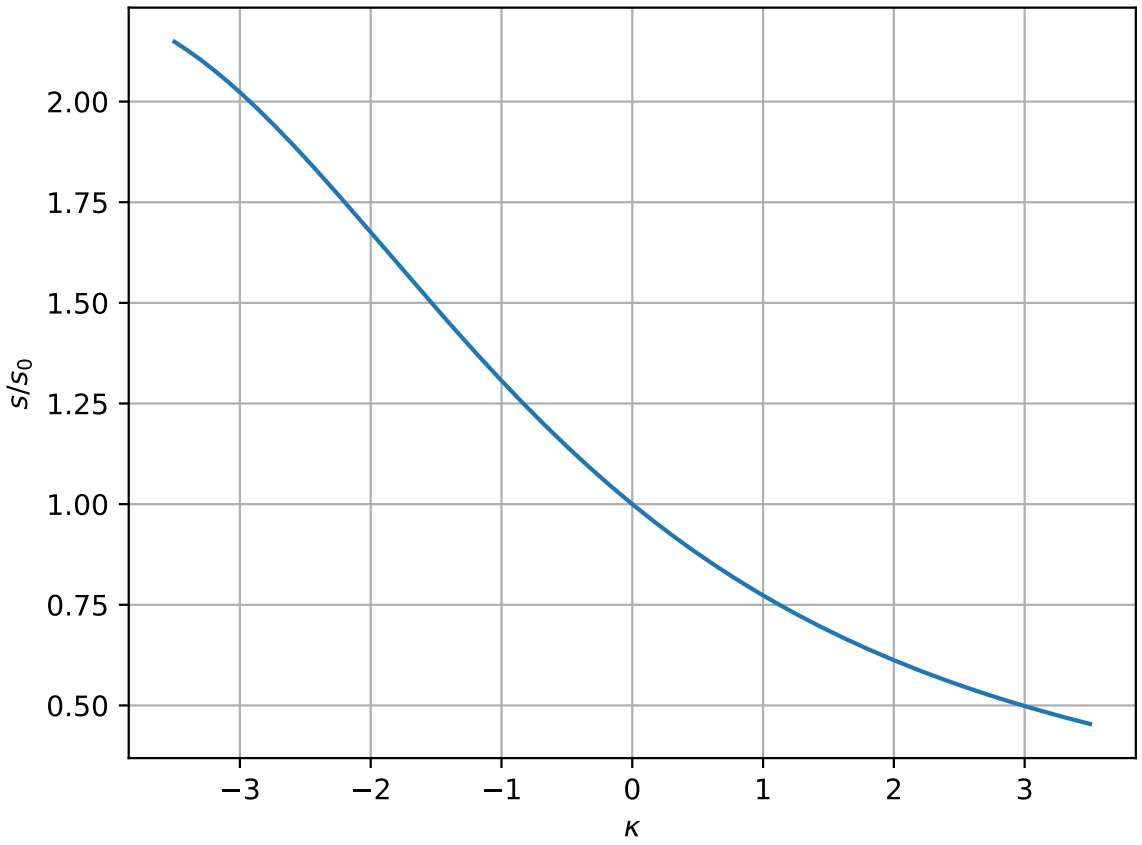

Figure 3.4: Shear electromechanical coupling due to the affect of deformation on polarization. Normalized shear strain, $\frac{s}{s_0}$, vs κ.

tric field while DEs with TI chains stiffen with increasing electric field such that the shear deformation decreases. This can be understood in terms of energy minimization by inspection of (3.0.0.8); that is, when shear deformation increases, the average of the chain alignment or anti-alignment with the electric field increases (i.e. $\left\langle \left(\hat{\mathbf{E}}\cdot\hat{\mathbf{r}}\right)^2\right\rangle_{\tilde{\mathbf{r}}}$ increases monotonically with $|s|$). It is energetically favorable for uniaxial chains to align with the electric field; hence, the increase in shear deformation–vice versa for TI chains.

Alternatively, we can think in terms of chain torque and so-called body couples. It is typical to decompose the total stress tensor of dielectric materials into mechanical and electrical parts (i.e. the Maxwell stress) [PKK00, Cd16, TM14, HZS09, HCB13, HLCF+12, BPK+12, KZSK12, Kof08, WM07, ZHS07]. While conservation of angular momentum requires that the total stress tensor be symmetric, the mechanical and electrical contributions need not be. The skew-symmetric parts of the mechanical and electrical stresses must be equal and opposite and can be thought of in terms of a body couple and a resistance to the said couple. As pointed out in [Coh18], when the electric field is not aligned with the principal frame, the mechanical and electrical stresses become asymmetric and a body couple is present. The reason why this occurs manifests itself at the macromolecular level. Just as in the case of biaxial deformation, there is a torque on each of the eight chains individually. However in the present case, the average torque does not vanish. And, in fact, the average torque over the 8-chains is precisely the skew-symmetric part of the Maxwell stress tensor. Indeed, since the Maxwell stress is the sum of a rank one tensor and a symmetric tensor, we can obtain its skew-part by the Levi-Civita tensor, ε_{ijk}, by $\varepsilon_{ijk}\left(P_iE_j+\frac{\epsilon_0}{2}E_mE_m\right)=\langle\mathbf{p}\times\mathbf{E}\rangle_{\tilde{\mathbf{r}}}=\boldsymbol{\omega}$ where we let $\boldsymbol{\omega}$ denote the chain torque. The nonzero component of $\boldsymbol{\omega}$ is the $\mathbf{e}_2$ component (the direction about which the torque occurs)

$$\omega_2 = nkT\kappa\left(3\gamma/\mathcal{L}^{-1}(\gamma)-1\right)\frac{\lambda_s\left(\lambda_s^2-1\right)}{1+\lambda_s^2+\lambda_s^4} \tag{3.0.0.11}$$

Notice that the sign of the torque is determined by κ, as expected, so that the direction of the torque depends only on whether the chains consist of uniaxial or TI monomers.

Finally, it is worth considering the difference between our model and some of those that exist in the

literature to isolate what gives rise to this newly predicted behavior in the context of the continuum picture. It is typical to, upon decomposing the stress into mechanical and electrical parts, model the mechanical part through a hyperelastic model [TM14, HZS09, HCB13, HLCF+12, BPK+12, KZSK12, Kof08, WM07, ZHS07]. The electrical part is captured through the Maxwell stress. Thus, one needs a constitutive model for the polarization response of the DE:

$$\boldsymbol{\sigma} = \boldsymbol{\sigma}_{\text{mech}} + \boldsymbol{\Sigma} = \boldsymbol{\sigma}_{\text{mech}} + \mathbf{P}\left(T, \mathbf{E}, \mathbf{F}, ...\right) \otimes \mathbf{E} + \frac{\epsilon_0}{2}|\mathbf{E}|^2\mathbf{I}$$

where, by the notation $\mathbf{P} = \mathbf{P}\left(T, \mathbf{E}, \mathbf{F}, ...\right)$, we mean to emphasize that the polarization response may be a function of T, $\mathbf{E}$, $\mathbf{F}$, and other state variables. Often, citing the isotropic nature of elastomers, it is typically assumed: $\mathbf{P}\left(T, \mathbf{E}\right) = \mathcal{X}\left(T\right)\mathbf{E}$, where $\mathcal{X}$ is a scalar quantity representing the polarization susceptibility of the material [TM14, HZS09, HCB13, HLCF+12, BPK+12, KZSK12, Kof08, WM07, ZHS07]. However, while this has a solid empirical basis, it results in the polarization always being aligned with $\hat{\mathbf{E}}$; and yet it is clear from (3.0.0.11) that such a constitutive model would not result in a body couple. What we have predicted is that, although DEs tend to behave isotropically in their stress-free state, the symmetry of the material is broken when deformed. This can be understood by considering that, while chain end-to-end vectors may be isotropically oriented in the stress free network, they will, in general, not be isotropically oriented after deformation. This breaking of symmetry means that the polarization is no longer restricted to be aligned with the local electric field.

What is more is that we have derived this anisotropic polarization constitutive response through statistical mechanics and network theory; however, if, instead of using numerical methods or an approach like the asymptotic matching approach used in the current work, one used a Gaussian-like approximation (i.e. small chain stretch approximation) and Taylor expanded the unknown multiplier related to the kinematic constraint, $\boldsymbol{\tau}$, out of the exponential (see [CDd16, Cd16])–for instance $\rho \approx C\left[1 + \boldsymbol{\tau}\cdot\hat{\mathbf{n}} + \frac{1}{2}\left(\boldsymbol{\tau}\cdot\hat{\mathbf{n}}\right)^2 + ...\right]\exp\left[-u/kT\right]$ results in the prediction: $\mathbf{P}\left(T, \mathbf{E}, \mathbf{F}\right) = \mathcal{X}\left(T, \mathbf{F}\right)\mathbf{E}$, where although $\mathcal{X}$ is a function of deformation, it is still a scalar quantity and results in an isotropic response. So it is clear that the anisotropic susceptibility and the prediction of the type of shear electromechanical coupling discussed above, is a result of the nonlinear relationship between the chain

end-to-end vector and polarization at the macromolecular level. For completeness, we remark that, although we do not artificially decompose the total stress into mechanical and electrical parts, our approach does result in a polarization response of the form: $\mathbf{P}\left(T, \mathbf{E}, \mathbf{F}\right) = \boldsymbol{\mathcal{X}}\left(T, \mathbf{F}\right)\mathbf{E}$, where $\boldsymbol{\mathcal{X}}$ is a second-order tensor and the direction of the polarization can vary from being aligned with $\hat{\mathbf{E}}$. Of course, we also recovered the limiting isotropic behavior in the absence of strain.

To recap, we have presented a multiscale theoretical model of dielectric elastomers which predicts and explains new types of electromechanical couplings: (1.) a biaxial electromechanical coupling of a thin film DE actuator–despite the Coulomb attraction between the electrodes being counteracted and (2.) a shear electromechanical coupling where the electric field is orthogonal to the plane of shear. Each of these electromechanical couplings is a continuum scale manifestation of chain torques in the DE network due to their interaction with an electric field; the interaction is analogous to a dipole in an electric field. Although chain torque is the driving factor in these couplings, it is balanced by the incompressibility of the network and the entropic elasticity of the individual chains.

Chapter 4

Design and optimization of the material architecture of dielectric elastomers

4.1 Design parameters

Manufacturing technologies have been progressing at a rapid rate and provide a means for finer and finer control of the structural details of materials. The goal of this work is to make useful suggestions about how the properties of DEs may be controlled by altering its molecular and macromolecular structure in specific ways–such that, manufacturers and other researchers may leverage advanced manufacturing to produce novel DEs with enhanced material properties. If this goal is to be achieved, it is important that the gap between what is suggested and what can be realized is not too great. With this in mind, we aim to identify design parameters such that:

1. The parameters are readily understood in the sense of structure rather than response (e.g. it is more useful to, when designing a structure against high speed winds, suggest that the structure not exceed a certain height or aspect ratio than to describe an abstract, response-type property such as “it would be desirable that it not sway much”. While the latter is true, it is much less clear how to achieve “not sway much” than it is to achieve a geometric property.) Thus, we aim

to identify direct, concrete properties, as opposed to abstractions.

2. There is some notion for how each of the parameters may be controlled. It would perhaps not be all that useful to give a blueprint for the ideal molecular structure if the design cannot be manufactured, even with modern technology, or if it can be manufactured but it is unlikely that the benefits will outweigh the costs.

One design parameter that we will consider, in particular, is the architecture of the chains that make up the cross-linked network–where by architecture we mean the geometrical features of the chain, the types of monomers the chain consists of, and the various sequences that the monomer types are arranged in. Figure 4.1 shows a few examples of polymer chain architectures. In architectures that are not a linear sequence of monomers (examples of linear chains are (a), and (b); examples of non-linear are (c) and (d)), we divide the monomers into two groups: (1.) those that make up the backbone of the chain, n_b, and (2.) those that make up the loose ends of the chain, n_l. By backbone of the chain, we mean those monomers that span from cross-link to cross-link and by loose ends, we mean the remaining monomers in the chain. We make this distinction because it allows us to consider monomers which interact through the end-to-end vector constraint separately from those that do not need to satisfy such a constraint. Further, we take linear chains with some amount of loose ends as our fundamental building block of the network. So in regards to a more complex architecture such as the star polymer ((d) in Figure 4.1), if each appendage of the star has a cross-link at its end, we say that this architecture actually consists of five separate (linear) chains and no loose end monomers.

4.1.1 Linear chains and the weakly interacting assumption

The importance of the above distinctions will become clear after the following definition. We say that two systems A and B are in *weak interaction* with each other if $|\mathcal{H}^{A\leftrightarrow B}| << |\mathcal{H}^{A}|\ |\mathcal{H}^{B}|$ where the Hamiltonian of the two systems, $\mathcal{H} = \mathcal{H}^{A} + \mathcal{H}^{B} + \mathcal{H}^{A\leftrightarrow B}$ have been broken into the contributions: $\mathcal{H}^{A}$, the Hamiltonian of system A as if it were in isolation; $\mathcal{H}^{B}$, the Hamiltonian of system B as if it were in isolation; and $\mathcal{H}^{A\leftrightarrow B}$, a correction term due to interactions between system A and system B; that

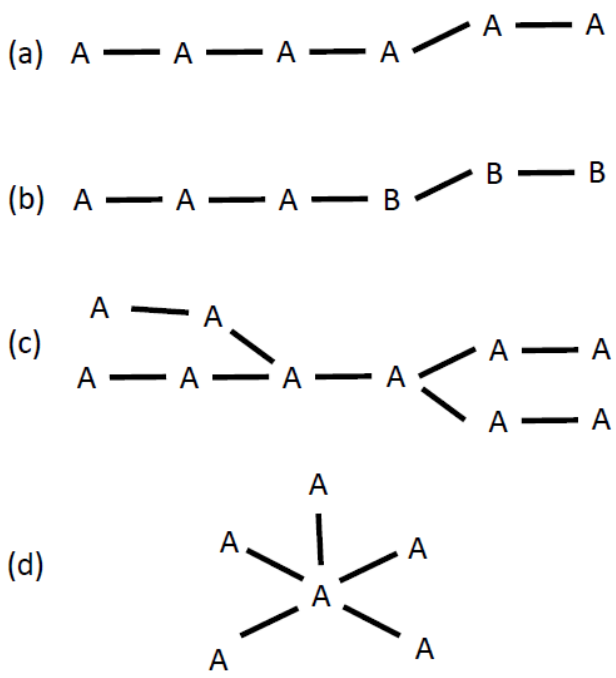

Figure 4.1: (a) Linear polymer chain (b) (linear) block copolymer chain (c) branched polymer (d) star polymer

is, we say the systems are in weak interaction if the interaction term is negligible (see [TM11] section 7.3.3, for example). If one neglects the interaction term, then the free energy of the two systems is simply a sum of their individual free energies (as if they were in isolation). When systems are in weak interaction with each other then we can break up the whole system into simpler pieces and combine their contributions later. Next, we make the assumption that loose end monomers are in weak interaction with the backbone monomers and that separate chains are in weak interaction with each other. This is justified as follows: in regards to the electrical energy of the system, we made the assumption that dipole-dipole interactions within a chain are negligible compared to dipole interactions with the electric field; thus, to maintain consistency we should also neglect dipole-dipole interactions between loose end monomers and between monomers of different chains. In regards to what might be considered the mechanical portion of the energy of the system, monomers within a chain interact through the enforcement of the end-to-end vector constraint. However, loose end monomers, by definition, do not take part in this constraint; and obviously monomers in separate chains do not interact through such

a constraint. (Note that the assumption of weakly interacting chains is often used in rubber elasticity, see [Tre75] Section 4.2. The weakly interacting assumption could be violated if chains are "too short" such that a significant portion of monomers in the chain are neighboring another chain, if long range potentials between monomers are present, and/or if excluded volume effects between chains becomes relevant.)

In summary, we have reduced all chain architectures to collections of weakly interacting linear chains with some fraction of loose ends, $\alpha = n_l/n$. However, the orientation of these chains (with respect to local electric field) influence the electroelastic response of the network. As a result, in contrast to explicitly analyzing different complex architectures such as the star polymer, we instead think of all networks as weakly interacting linear chains and take the distribution of these linear chains within the network as the design variable. More specifically, let $\mathrm{P} = \mathrm{P}(\tilde{\mathbf{r}})$ denote a probability density function which describes the fraction of chains with reference end-to-end vector $\tilde{\mathbf{r}}$. Then P is one of our design parameters.

4.1.2 Mass density and cross-linking properties

In addition, we will also consider the parameters: the density of chains per unit volume (in the reference configuration), N_0; the number of monomers per chain, n; and the fraction of loose end monomers– together with the pdf P, we will say that these variables describe the microstructure of our elastomer. As an aside, clearly $\chi_{\parallel}$ and $\chi_{\perp}$ will vary, in general, from monomer-type to monomer-type. However, we do not consider these as design variables because it is not apparent how one might control these properties, especially continuously, beyond measuring them for different molecules and cataloging their various values. In regards to controlling the considered design variables: we envision P as being controlled either by cross-linking while under an applied electric field (with the idea being that the field will introduce preferred chain directions) or by some type of advanced 3D printing. And in terms of controlling N_0 and n, it is perhaps easier to think in terms of the product $N_0 n$ and the ratio N_0/n. The former is related to the mass density of the material and the latter is a function of the density of

cross-links (per unit volume) for a fixed mass density.

4.1.3 Chain pdf

Having established some parameters of interest, we now turn our attention to P. The purpose of a network model is relate deformation at the continuum scale to chain deformations. Similarly, given a pdf, P, we need to establish how chains map into the current configuration. Following [Tre75], we assume that cross-links (so-called "junction points" in [Tre75]) are mapped under the local deformation gradient, $\mathbf{F}$. Treloar refers to this as the affine deformation assumption. The key difference between the affine deformation assumption and the 8-chain model [AB93, BA00] is that it is assumed that the representative volume element (or cell, as it is called in [AB93]) rotates such that its edges are stretched (by the principal stretches) in the principal frame; that is, the basis that consists of the principals directions of the right Cauchy-Green tensor. [1] We forego the nuanced differences between the affine deformation assumption and the principal frame assumption in this work by considering diagonal deformation gradients only; in this case, the two competing assumptions are equivalent.

Let Ω_0 denote the body of our DE in the reference configuration and $\Omega = \boldsymbol{\Upsilon}(\Omega_0)$ the body in the current configuration, where $\boldsymbol{\Upsilon}$ is the deformation mapping. The position of a material point in the reference configuration, $\mathbf{X}$, is mapped to a position in the current configuration by the deformation

[1] The argument in favor of rotation of the representative volume element such that it is stretched in the principal frame is given in [BA00] as follows:

> The 8-chain model was found to be predictive of the biaxial data and indeed to provide a better prediction than the full network model. The full network model predicts a biaxial stress-stretch response that falls between that predicted by the 8-chain and that predicted by the 3-chain model. The somewhat surprising lack of success of the full network model lies in its assumption of affine deformation of all chains in the non-Gaussian regime. In a real network, chains which lie along the maximum principal stretch direction would begin to stretch less with continuing deformation once they begin to approach their limiting extensibility; at that point, other chains in the network will stretch more than that predicted by affine deformation in order to accommodate the total applied stretch. Therefore, the affineness of chain deformation will be lost. The full network model assumes affine deformation of all chains and therefore, at large stretches, the contribution to the stress-stretch behavior from chains along the principal stretch direction is overestimated. We note that the 8-chain model does not assume affine deformation of all chains, but captures an effective network response.

There was, at one time, some controversy regarding this, as Treloar was not convinced that this rotation had proper physical justification [Tre75]. To the authors' knowledge, this assumption has not been observed directly through experiments. It seems the principal motivation for this assumption is the agreement of the 8-chain model with experimental data.

mapping, i.e. $\mathbf{x} = \boldsymbol{\Upsilon}(\mathbf{X})$; and the deformation gradient is given by $\mathbf{F} = \text{Grad}\boldsymbol{\Upsilon}$.

Then given some boundary conditions, $\mathbb{B}$, and some external work, $\mathbb{W}$, the equilibrium configuration of the DE body is given by the minimization of the Gibbs free energy such that the boundary conditions are satisfied; that is:

$$\begin{aligned} \Psi\left[\mathbf{F}, \tilde{\mathbf{P}}\right] &= \int_{\Omega_0} \mathcal{W}\left(\mathbf{F}, \tilde{\mathbf{P}}\right) \mathrm{d}V - \mathbb{W} \\ \left\{\mathbf{F}^{\mathrm{eq}}, \tilde{\mathbf{P}}^{\mathrm{eq}}\right\} &= \arg\min_{\mathbf{F}, \tilde{\mathbf{P}}} \Psi\left[\mathbf{F}, \tilde{\mathbf{P}}\right] \text{ subject to } \mathbb{B} \end{aligned} \tag{4.1.3.1}$$

Thus, the constitutive response of our design DE is encoded in the form of the Helmholtz free energy density function, $\mathcal{W}$. Because of the weakly interacting assumption, $\mathcal{W}$ is given by

$$\mathcal{W}\left(\mathbf{F}, \tilde{\mathbf{P}}; T\right) = \mathcal{W}^*\left(\mathbf{F}, \mathbf{E}; T\right) + J^{-1}\tilde{\mathbf{P}} \cdot \mathbf{E} \tag{4.1.3.2}$$

$$\mathcal{W}^* = N\left\langle \mathcal{A}^*\left(\mathbf{F}\tilde{\mathbf{r}}, \mathbf{E}; T\right)\right\rangle_{\tilde{\mathbf{r}}} = N\int_{\mathbb{R}^3} \mathrm{d}^3\tilde{r}\, \mathrm{P}\left(\tilde{\mathbf{r}}\right) \mathcal{A}^*\left(\mathbf{F}\tilde{\mathbf{r}}, \mathbf{E}; T\right) \tag{4.1.3.3}$$

where $\tilde{\mathbf{P}} = J\mathbf{P}$ is the pullback of the (continuum-scale) polarization and $\mathcal{W}^*$ is the Legendre transform of the Helmholtz free energy density (in the $\tilde{\mathbf{P}}$ slot)–which we will call LTHP for short. (This claim is justified in Appendix A.) Physically, the significance of the LTHP free energy is that it has a minimum principle at constant temperature and constant electric field.

The design space of P is the space of all probability measures on $\mathbb{R}^3$; and hence, an infinite dimensional space. However, there are rational ways in which to reduce our search. First, we assume that the length of all chains depends only on n and b; specifically, we assume $|\tilde{\mathbf{r}}| = b\sqrt{n}$, which is the expectation of the length of a random walk of n steps with step length b. This choice is obviously motivated by probability theory but it will also be justified further later on in this section when we discuss residual stresses.

Having reduced the support of P to the surface of a sphere of radius $b\sqrt{n}$, we next consider the symmetries inherent in the physical problem. For instance, in regards to chain statistical mechanics: $\mathcal{A}^*(\mathbf{r}, ...) = \mathcal{A}^*(-\mathbf{r}, ...)$; or, in other words, although chains have well defined ends (cross-linking

points), there is no difference between calling one end the start and the other the finish and vice versa. This reduces the information needed to specify a P to values on a half sphere.

So far our thinking has been quite general, but now we consider specific applications of interest. Our primary focus will be on a thin film dielectric elastomer actuator (DEA), where the voltage difference is applied across the thickness of the film. Physically, there are three orthogonal directions that are significant. We therefore restrict our attention to $\mathrm{P} = \mathrm{P}(\phi, \theta)$ of the form

$$\mathrm{P}(\phi, \theta) = \mathrm{P}_\phi(\phi)\,\mathrm{P}_\theta(\theta) \tag{4.1.3.4}$$

where

$$\begin{aligned} \mathrm{P}_\phi(\phi) &= \mathrm{P}_\phi(\pi - \phi) \\ \mathrm{P}_\theta(\theta) &= \mathrm{P}_\theta(\pi - \theta) \end{aligned} \tag{4.1.3.5}$$

and the polar axis is taken as the direction of the electric field, $\hat{\mathbf{E}}$, and ϕ is the angle relative to the $\mathbf{e}_1$ direction. The form given by (4.1.3.4) is consistent with the symmetry of the DEA while (4.1.3.5) is consistent with the $\mathbf{r} \to -\mathbf{r}$ symmetry. For materials with the above symmetries and the BVP associated with a thin film DEA, we expect a homogeneous deformation of the form $\mathbf{F} = \mathrm{diag}(\lambda_1, \lambda_2, \lambda_3)$, which is diagonal as desired.

That concludes the discussion regarding the symmetries of P. From a more practical perspective, we will take the following as an ansatz of P:

$$\begin{aligned} \mathrm{P} = C &\left\{ \exp\left[-\frac{(\theta - \theta_0)^2}{2\sigma_\theta^2} \right] + \exp\left[-\frac{(\pi - \theta - \theta_0)^2}{2\sigma_\theta^2} \right] \right\} \times \\ &\left\{ \exp\left[-\frac{(\phi - \phi_0)^2}{2\sigma_\phi^2} \right] + \exp\left[-\frac{(\pi - \phi - \phi_0)^2}{2\sigma_\phi^2} \right] \right\} \end{aligned} \tag{4.1.3.6}$$

where, when considering transversely isotropic materials, reduces to:

$$\mathrm{P}(\phi, \theta) = \mathrm{P}_\theta(\theta; \theta_0, \sigma) = C \left\{ \exp\left[-\frac{(\theta - \theta_0)^2}{2\sigma^2} \right] + \exp\left[-\frac{(\pi - \theta - \theta_0)^2}{2\sigma^2} \right] \right\}. \tag{4.1.3.7}$$

where C is a normalization constant such that $\int \mathrm{P} = 1$. The reasons for this choice of ansatz are as follows: the properties of Gaussian distributions are well understood; (2) ease of integration (e.g. when evaluating (4.1.3.3)); (3) the symmetries given by (4.1.3.4) and (4.1.3.5) are satisfied; (4) it reduces our search space from an infinite dimensional space to a finite dimensional space (specifically, four dimensional: θ_0, σ_θ, ϕ_0, and σ_ϕ); and (5) it is consistent with some of the ideas that were previously mentioned about how the direction of chains may be controlled. For instance, if some advanced form of 3D printing were indeed used, then it would be necessary to consider manufacturing error tolerances. The error tolerances could be modeled by placing lower bounds on σ_θ and σ_ϕ. Alternatively, if chain directions were controlled by an applied electric field, then the above ansatz is likely the only possible form of P that could be manufactured.

Now, for the case of the uniform distribution (i.e. $\mathrm{P} = 1/4\pi$) or the 8-chain model [AB93]:

$$\begin{aligned}\mathrm{P} = \frac{1}{8}\left[\delta\left(\theta_{iso} - \theta\right) + \delta\left(\pi - \theta_{iso} - \theta\right)\right] \times \\ \left[\delta\left(\pi/4 - \phi\right) + \delta\left(3\pi/4 - \phi\right) + \delta\left(5\pi/4 - \phi\right) + \delta\left(7\pi/4 - \phi\right)\right]\end{aligned} \tag{4.1.3.8}$$

(where $\theta_{iso} = \arctan\sqrt{2}$)) and in the absence of external loads ($\mathbf{E} = \mathbf{0}$, $P_1 = P_2 = P_3 = 0$), then by symmetry $\lambda_1 = \lambda_2 = \lambda_3$. Elastomers are typically incompressible (or approximately so); this, together with the symmetry of the chain distribution is enough to enforce that, in the absence of external loads, $\mathbf{F}^{\mathrm{eq}} = \mathbf{I}$, as expected. What is interesting is that this is not true, in general, for anisotropic P (with $|\tilde{\mathbf{r}}| = \text{const.}$). Since the hypothetically manufactured P is not in mechanical equilibrium when $\mathbf{F} = \mathbf{I}$ and in the absence of external loads, this is analogous to residual stresses that are introduced during the manufacturing process. The procedure we envision is as follows then:

1. Chose design variables: P; mass density (i.e. $N_0 n$); density of cross-links (i.e. n/N_0); fraction of loose-ends, α. Recall: $\chi_\parallel$ and $\chi_\perp$ are determined by the monomer-type and its chemical composition.

2. The DE is manufactured to its design specifications.

3. The DE is allowed to relax to a stress-free, polarization-free deformation $\mathbf{F} = \mathbf{F}^\star$; that is, $\mathbf{F}^\star$

minimizes the Helmholtz free energy density of the DE in the absence of external loads; or, in the language of our analogy, the residual stresses are relieved. Note: since the material is homogeneous, the minimization (in (4.1.3.1)) can be done point-wise. This results in some uniform shape change that should be taken into account when manufacturing to specific dimensions.

4. Properties of interest, A, B, ..., etc., are measured in the stress-free, polarization-free state and are denoted by: $A^\star$, $B^\star$, ..., etc. It will also be useful to develop expressions for these properties as functions of deformation and polarization.

It is for this reason that we remarked earlier that assuming fixed $|\tilde{\mathbf{r}}| = b\sqrt{n}$ would be further justified. This justification lies in the fact that it is apparent that chain lengths and orientations cannot be controlled independently of each other–they are related through the relaxation of the residual stresses.

In regards to the material properties of interest, we consider the Taylor expansion of the free energy density about the relaxed configuration (i.e. $\left\{\mathbf{F} = \mathbf{F}^\star, \tilde{\mathbf{P}} = 0\right\}$):

$$\begin{aligned}\mathcal{W}\left(\mathbf{F}, \tilde{\mathbf{P}}\right) =& \mathcal{W}\left(\mathbf{F}^\star, 0\right) + \frac{\partial \mathcal{W}}{\partial F_{ij}}\left(\mathbf{F} - \mathbf{F}^\star\right)_{ij} + \frac{\partial \mathcal{W}}{\partial \tilde{P}_k}\tilde{P}_k \\ &+ \frac{1}{2}\frac{\partial^2 \mathcal{W}}{\partial F_{ij}\partial F_{kl}}\left(\mathbf{F} - \mathbf{F}^\star\right)_{ij}\left(\mathbf{F} - \mathbf{F}^\star\right)_{kl} + \frac{\partial^2 \mathcal{W}}{\partial F_{ij}\partial \tilde{P}_k}\left(\mathbf{F} - \mathbf{F}^\star\right)_{ij}\tilde{P}_k + \frac{1}{2}\frac{\partial^2 \mathcal{W}}{\partial \tilde{P}_i \partial \tilde{P}_j}\tilde{P}_i\tilde{P}_j \\ &+ \mathcal{O}\left(\epsilon_1^3\right) + \mathcal{O}\left(\epsilon_1^2\epsilon_2\right) + \mathcal{O}\left(\epsilon_1\epsilon_2^2\right) + \mathcal{O}\left(\epsilon_2^3\right)\end{aligned} \tag{4.1.3.9}$$

where $\epsilon_1 = |\mathbf{F} - \mathbf{F}^\star|$ and $\epsilon_2 = |\tilde{\mathbf{P}}|$. We assume $\mathcal{W}$ is convex in $\tilde{\mathbf{P}}$ and its minimum is $\tilde{\mathbf{P}} = \mathbf{0}$ (this is justified empirically for general DEs). This, along with the definition of $\mathbf{F}^\star$, means that the linear terms in (4.1.3.9) vanish. Since we are only interested in energy differences, in the neighborhood of $\left\{\mathbf{F} = \mathbf{F}^\star, \tilde{\mathbf{P}} = 0\right\}$, the constitutive response of the DE is governed by $\frac{\partial^2 \mathcal{W}}{\partial \mathbf{F} \partial \mathbf{F}}$, $\frac{\partial^2 \mathcal{W}}{\partial \tilde{\mathbf{P}} \partial \tilde{\mathbf{P}}}$, and $\frac{\partial^2 \mathcal{W}}{\partial \mathbf{F} \partial \tilde{\mathbf{P}}}$. These quantities correspond to the stiffness tensor, the inverse of the polarization susceptibility tensor (i.e. $\boldsymbol{\mathcal{X}}^{-1}$)–which is a measure of the bond stiffness between charges bound to the DE–and the cross modulus tensor, respectively. The magnitude of the cross modulus signifies the electromechanical coupling of the material itself; that is, the electromechanical coupling irrespective of external loads.

Thus, we will be interested in how our design variables affect these three quantities. As a note: we will not, strictly speaking, seek to optimize all of these properties. In particular, a desirable feature of DEs is their compliance (i.e. inverse stiffness). So it will often be a goal to control the stiffness within some operational range while optimizing the susceptibility and the cross modulus.

4.1.4 Incompressibility

As a final note to this section, we make a few remarks regarding the incompressibility of our hypothetical, anisotropic DEs. It is true that most elastomers are incompressible to a very good approximation. However, in terms of modeling these materials, their incompressibility is empirically motivated and taken as an assumption in both statistical mechanics-based and continuum mechanics-based models. Since we are proposing to design an anisotropic material–which may or may not be fundamentally different from existing elastomers–and since incompressibility has not, to the authors' knowledge, been connected to the molecular-scale or macromolecular-scale physics of elastomers, it is not obvious that incompressibility will remain a very good, or even an adequate, approximation for our designed materials. For simplicity, we will continue to assume that the anisotropic DEs are incompressible. We simply note that it may prove, upon the proper experimentation, that the model and results derived herein need to be generalized in order to take differential changes in volume into account.

4.2 Design analysis

4.2.1 Mathematical prelude

One must evaluate the integral in (4.1.3.3) to determine the constitutive response associated with a pdf, P. For this reason, it will be useful to develop approximations for the integral:

$$I_k\left[\mu,\sigma\right] := \int_0^\pi \mathrm{d}x \left(\exp\left[-\frac{\left(x-\mu\right)^2}{2\sigma^2}\right] + \exp\left[-\frac{\left(\pi-x-\mu\right)^2}{2\sigma^2}\right]\right)\sin\left(kx\right)$$

where $k \in \mathbb{N}$, $\mu \in \left[0, \frac{\pi}{2}\right]$, and $\sigma \in [0, \infty]$. In the limit of $\sigma << 1$, we have that

$$I_k\left[\mu, \sigma\right] \approx I_k^0\left[\mu, \sigma\right] = 2\sqrt{2\pi}\sigma \exp\left[-\frac{k^2\sigma^2}{2}\right] \sin\left(k\mu\right) \tag{4.2.1.1}$$

This is derived by bringing the sine term into the exponential (by using $\sin\left(kx\right) = \mathrm{Im}\left(e^{ix}\right)$) and changing the bounds of integration to $-\infty$ and ∞. In the limit of $\sigma >> 1$, we have that

$$I_k\left[\mu, \sigma\right] \approx I_k^\infty\left[\mu, \sigma\right] = \frac{\sin\left(\frac{k\pi}{2}\right)}{k^3\sigma^2}\left\{2k\pi\cos\left(\frac{k\pi}{2}\right) + \left[k^2\left(\pi^2 - 2\pi\mu + 2\mu^2 - 4\sigma^2\right)\right]\sin\left(\frac{k\pi}{2}\right)\right\} \tag{4.2.1.2}$$

which is derived by Taylor expanding the exponential to linear order in its argument.

We will also use a result which can be derived by recognizing that $\left(\cos\left(x\right) + i\sin\left(x\right)\right)^k = \cos\left(kx\right) + i\sin\left(kx\right)$:

$$\sin^3\left(x\right) = \frac{3}{4}\sin\left(x\right) - \frac{1}{4}\sin\left(3x\right) \tag{4.2.1.3}$$

4.2.2 Elasticity

We begin by isolating and focusing on the mechanical behavior of a design DE. Let $\mathbf{E}\left(\mathbf{x}\right) = 0$ for all $\mathbf{x} \in \Omega$. Then $U = 0$ and consequently:

$$\mathcal{A}^* = \mathcal{A} = -T\mathcal{S} = nkT\left[\gamma\mathcal{L}^{-1}\left(\gamma\right) + \ln\left(\frac{\mathcal{L}^{-1}\left(\gamma\right)}{4\pi\sinh\left(\mathcal{L}^{-1}\left(\gamma\right)\right)}\right)\right]$$

(where the final expression was first derived in [KG42], and subsequent derivations can be found in [Tre75, D+72]). Since, in this work, our kinematic assumption is equivalent to $\mathbf{r} = \mathbf{F}\tilde{\mathbf{r}}$, the Helmholtz free energy density is given by:

$$\mathcal{W} = N\int_0^\pi \mathrm{d}\theta \int_0^{2\pi} \mathrm{d}\phi\, \mathrm{P} \times \left(nkT\left[\frac{|\mathbf{F}\tilde{\mathbf{r}}|}{nb}\mathcal{L}^{-1}\left(\frac{|\mathbf{F}\tilde{\mathbf{r}}|}{nb}\right) + \ln\left(\frac{\mathcal{L}^{-1}\left(\frac{|\mathbf{F}\tilde{\mathbf{r}}|}{nb}\right)}{4\pi\sinh\left(\mathcal{L}^{-1}\left(\frac{|\mathbf{F}\tilde{\mathbf{r}}|}{nb}\right)\right)}\right)\sin\theta\right]\right) \tag{4.2.2.1}$$

where $\tilde{\mathbf{r}} = b\sqrt{n}\,(\cos\phi\sin\theta, \sin\phi\sin\theta, \cos\theta)$. This integral, however, is difficult to evaluate given the inverse Langevin function and the square root terms implicit in $|\mathbf{F}\tilde{\mathbf{r}}|$. The integrand simplifies significantly if we Taylor expand $\mathcal{L}^{-1}(\gamma)$ in powers of γ:

$$\mathcal{W} = \frac{3}{2}NkT\int_0^{\pi}\mathrm{d}\theta\int_0^{2\pi}\mathrm{d}\phi\,\mathrm{P}(\phi,\theta)\left(\gamma_r^2 + \mathcal{O}\left(\gamma^4 n\right)\right)\sin\theta \tag{4.2.2.2}$$

where $\gamma_r = |\mathbf{r}|/|\tilde{\mathbf{r}}| = |\mathbf{r}|/b\sqrt{n}$. For the remainder of this section, we neglect higher order terms in (4.2.2.2). As mentioned previously, we assume $\mathbf{F}$ of the form: $\mathbf{F} = \mathrm{diag}(\lambda_1, \lambda_2, \lambda_3)$; thus,

$$\gamma_r^2 = \lambda_1^2\cos^2\phi\sin^2\theta + \lambda_2^2\sin^2\phi\sin^2\theta + \lambda_3^2\cos^2\theta.$$

First, let $\mathrm{P} = 1/4\pi$ or the 8-chain pdf (given explicitly in (4.1.3.8)). It is easy to show that in either case,

$$\mathcal{W} = \frac{G_{iso}}{2}\left(\lambda_1^2 + \lambda_2^2 + \lambda_3^2\right)$$

where $G_{iso} \coloneqq NkT$ is the shear modulus that is predicted by the Gaussian chain approximation in classical rubber elasticity [Tre75, BA00]. (Note: the above form of $\mathcal{W}$ is equivalent to the neo-Hookean model.) This result is to be expected since we took a Taylor expansion of the Langevin chain statistics (4.2.2.1) about zero stretch and because the chosen form of P is isotropic. Clearly then, for isotropic elastomers, the stiffness–for a constant mass density, $N_0 n$–increases with the density of cross-links; that is, increases with the ratio N_0/n. Moreover, the slope of the inverse Langevin function is a monotonically increasing function of its argument. Its argument in (4.2.2.1) is $\mathcal{O}(n^{-1})$, so increasing the density of cross-links for fixed mass density–which effectively lowers n–also increases the stiffness through higher order terms in (4.2.2.2). Physically, this is because the higher order terms account for the finite extensibility of the chain and, as n decreases, so does the maximum length of a chain. Similarly, the stiffness increases with the fraction of loose end monomers (for fixed n) because, as α increases, the maximum length of the chain, $n_b b$, decreases and finite extensibility effects are more relevant for shorter stretches.

Next we consider a transversely isotropic elastomer. In this case, we take P to be uniform in ϕ

such that it is given by the form (4.1.3.7). Using (4.2.1.3), the average square relative stretch and the Helmholtz free energy density are

$$\left\langle \gamma_r^2 \right\rangle_{\tilde{\mathbf{r}}} = \frac{1}{4}\left\{ \frac{\lambda_1^2+\lambda_2^2}{2}\left(3-\frac{I_3\left[\theta_0,\sigma\right]}{I_1\left[\theta_0,\sigma\right]}\right)+\lambda_3^2\left(1+\frac{I_3\left[\theta_0,\sigma\right]}{I_1\left[\theta_0,\sigma\right]}\right)\right\} \tag{4.2.2.3}$$

$$\mathcal{W}\left(\lambda_1,\lambda_2,\lambda_3;\theta_0,\sigma\right) = \frac{3}{8}NkT\left\{ \frac{\lambda_1^2+\lambda_2^2}{2}\left(3-\frac{I_3\left[\theta_0,\sigma\right]}{I_1\left[\theta_0,\sigma\right]}\right)+\lambda_3^2\left(1+\frac{I_3\left[\theta_0,\sigma\right]}{I_1\left[\theta_0,\sigma\right]}\right)\right\} \tag{4.2.2.4}$$

We can approximate the Helmholtz free energy density in the limits of $\sigma << 1$ and $\sigma >> 1$ by using (4.2.1.1) and (4.2.1.2), respectively.

Incompressible materials

As mentioned previously, there does not appear to be a good theory which connects the molecular structure of elastomers to their effective Poisson's ratio. Instead, incompressibility is generally taken as an assumption. In this section, we make the same assumption; that is, we assume that $\lambda_3 = 1/\left(\lambda_1\lambda_2\right)$. Further, let us consider a uniaxial stress-strain experiment. Specifically, we imagine loading our DE in a hard device (i.e. strain controlled) in the direction of the axis of symmetry (i.e. in our coordinate system, direction of the polar axis) and measuring the stress. Let the deformation, in this case, be given by $\mathbf{F} = \mathrm{diag}\left(1/\sqrt{\lambda}, 1/\sqrt{\lambda}, \lambda\right)$. Given the stress-strain curve, the instantaneous slope of the curve at any given point is a measure of its *Young's modulus* in the direction of the axis of symmetry. We denote this property as $Y_{\parallel}$ (we adopt this notation, as opposed to the standard notation of E, so as not to be confused with the electric field). Similarly, the Young's modulus in the plane orthogonal to the axis of symmetry is denoted by $Y_{\perp}$. In the limit of $\sigma << 1$, our model predicts:

$$Y_{\parallel} = \frac{\partial^2\mathcal{W}}{\partial\lambda^2} = \frac{3}{4}N_0kT\left\{1+3\lambda^{-3}+e^{-4\sigma^2}\left[1-\lambda^{-3}+2\left(1-\lambda^{-3}\right)\cos\left(2\theta_0\right)\right]\right\} \tag{4.2.2.5}$$

which shows a strain hardening in compression and a strain softening in tension–except when $\theta_0 = 0$ and $\sigma = 0$. Interestingly, $(\theta_0, \sigma) = (0, 0)$ recovers the isotropic elastic modulus; as does any (θ_0, σ) at $\lambda = 1$. At first glance, this seems physically unreasonable and a possible indication that there has been

something wrong with our approach, as one would expect changing the distribution of chain directions in the network to affect the stiffness in various directions. However, recall from our discussion in Section 4.1.3 that $\lambda = 1$ is no longer the equilibrium configuration in the absence of external loads. Indeed, let $\lambda^\star$ be such that $\frac{\partial \mathcal{W}}{\partial \lambda}\Big|_{\lambda=\lambda^\star} = 0$; then,

$$\lambda^\star = \left(\frac{3 - [1 + 2\cos(2\theta_0)]\, e^{-4\sigma^2}}{2 + [2 + 4\cos(2\theta_0)]\, e^{-4\sigma^2}} \right)^{1/3}. \tag{4.2.2.6}$$

Equation (4.2.2.6) is shown in Figure 4.2 as a function of θ_0 for $\sigma = 0, \pi/32$ and $\pi/16$. When $\theta_0 < \theta_{iso}$, $\lambda^\star < 1$. This is because there is simultaneously a higher density of chains that are oriented more toward the direction of stretch (i.e. the axis of symmetry) and a lower density of chains oriented more orthogonal to the direction of stretch. The elasticity of polymer chains, to a good approximation, is due entirely to entropy; the effect of this is that chains are in tension, at any finite temperature, if their end-to-end vector is finite. Put differently, the maximum chain entropy is given by a vanishing end-to-end vector; thus, chains want to contract. Neglecting excluded volume effects, the reason why network models in classical rubber elasticity do not predict a sudden and spontaneous collapse of the network in on itself is because incompressibility is taken as an additional assumption. When incompressibility is enforced, then for chains to contract in one direction there must be an expansion of the network in another directions, causing other chains to stretch. Incompressibility, along with the balancing of chain entropy differences when attempting to stretch in any particular direction, is why isotropic networks have the property that $\lambda^\star = 1$. When $\theta_0 < \theta_{iso}$, $\lambda^\star < 1$ and thus there is a contraction in the direction of the axis of symmetry, because there are more chains oriented toward this direction and hence a net increase in entropy can be gained from some $\lambda^\star < 1$. When $\theta_0 > \theta_{iso}$, vice versa; that is, since there are less chains in the direction of the axis of symmetry, a net increase in entropy can be gained by contracting orthogonal to the axis and thereby stretching in the direction of the axis. Actually, this effect leads to singularities at $(\theta_0 = 0, \sigma = 0)$ and $(\theta_0 = \pi/2, \sigma = 0)$; and the effect is of course dampened by increasing σ, as can be seen in Figure 4.2.

We return our attention to the elastic modulus. In particular, we are interested in $Y_\parallel^\star := Y_\parallel(\lambda = \lambda^\star)$;

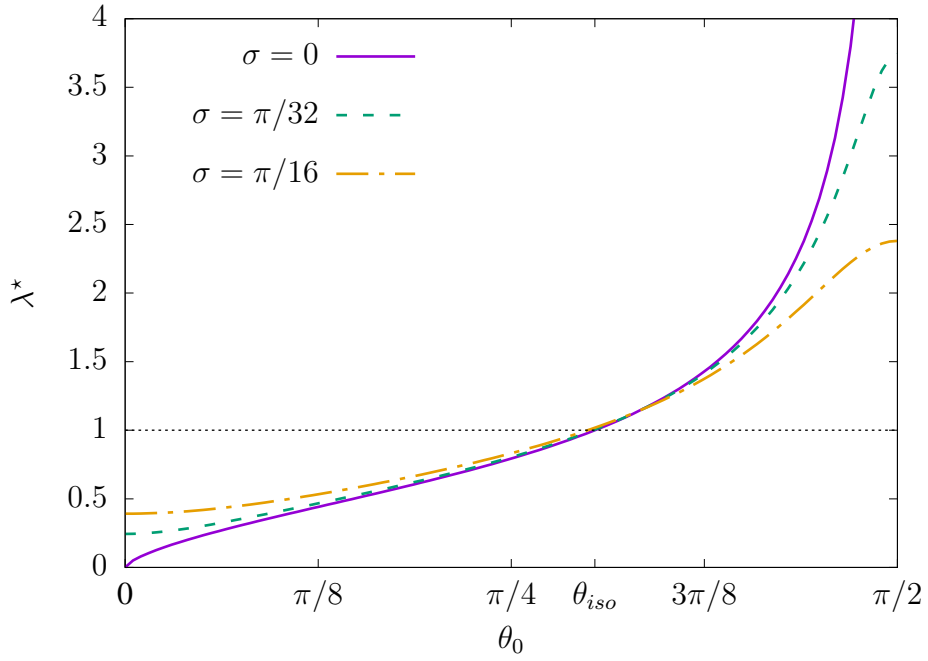

Figure 4.2: The load-free equilibrium stretch in the direction of the axis of symmetry for a transversely isotropic, incompressible elastomer. The stretch, $\lambda^\star$, is shown as a function of the angle, θ_0, that the (upper) Gaussian is centered about.

that is, the stiffness of the material at its load-free, equilibrium state. Plugging (4.2.2.6) into (4.2.2.5), we obtain:

$$Y_{\parallel}^{\star}(\theta_0, \sigma) = \frac{9}{4} NkT \left\{ 1 + [1 + 2\cos(2\theta_0)]\, e^{-4\sigma^2} \right\} \tag{4.2.2.7}$$

Similarly, let $Y_{\perp} := \frac{1}{4} \frac{\partial^2 \mathcal{W}}{\partial \left(1/\sqrt{\lambda}\right)^2}$, where the $\frac{1}{4}$ is a material and geometric factor related to the number of dimensions that are being stretched when $\mathbf{F} \to \mathbf{F} + \epsilon\, \mathrm{diag}\left(1/\sqrt{\lambda}, 1/\sqrt{\lambda}, 0\right)$ (i.e. 2) and the Poisson's ratio, $\frac{1}{2}$. Then,

$$Y_{\perp}^{\star}(\theta_0, \sigma) = \frac{9}{8} NkT \left\{ 3 - [1 + 2\cos(2\theta_0)]\, e^{-4\sigma^2} \right\}. \tag{4.2.2.8}$$

As expected, the maximum $Y_{\parallel}^{\star}$ occurs at $(\theta_0, \sigma) = (0, 0)$–as this is the case which has the maximum amount of chains oriented in the direction of the axis of symmetry for a given N_0. Interestingly, although, as previously mentioned, there is a singularity at $(\theta_0, \sigma) = (0, 0)$ such that $\lambda^\star = 0$, the Young's modulus is finite. The maximum $Y_{\parallel}^{\star}$ is given by $9NkT$, which is *the number of spatial dimensions times the Young's modulus for an isotropic network* ($Y_{iso} = Y_{\parallel}(\theta_{iso}, 0) = Y_{\perp}(\theta_{iso}, 0) = 3G_{iso} = 3NkT$). Once again, as expected, $Y_{\parallel}^{\star}$ is a minimum and, more specifically, vanishes at

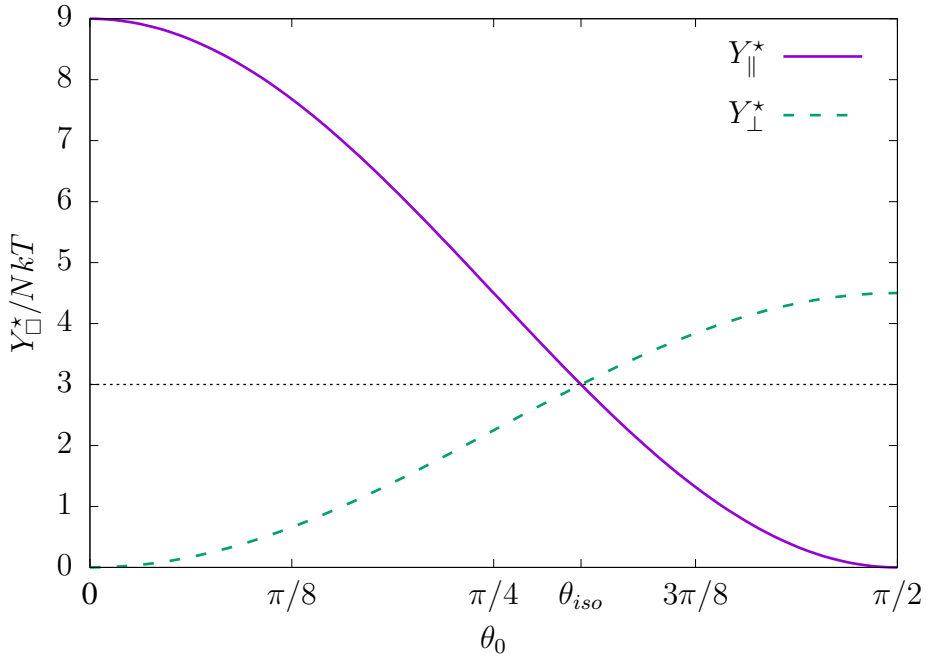

Figure 4.3: The dimensionless Young's moduli in the directions of the axis of symmetry, $Y^\star_\parallel$, and orthogonal to the axis of symmetry, $Y^\star_\perp$, as a function of the upper Gaussian center, θ_0, when $\sigma = 0$. The dashed, black line represents the Young's modulus for an isotropic network, $Y_{iso} = 3G_{iso} = 3NkT$

$(\theta_0, \sigma) = (\pi/2, 0)$. Similarly, $Y^\star_\perp$ is a maximum at $(\theta_0, \sigma) = (\pi/2, 0)$ and vanishes at its minimum $(\theta_0, \sigma) = (0, 0)$.

This analysis establishes theoretical upper bounds for $Y^\star_\parallel$ and $Y^\star_\perp$ as $9NkT$ and $\frac{9}{4}NkT$, respectively; and shows that theoretically, zero stiffness can be achieved. However, as previously mentioned, there are many applications, such as soft robotics, when it will be desirable to control the DE stiffness within some bounds while optimizing over other properties. In this case, (4.2.2.7) and (4.2.2.8) can be used as design tools in the limit when $\sigma << 1$; that is, when directionality in the network is highly controlled.

We now carry out a similar analysis in the limit of weak directional control (i.e. the limit of $\sigma >> 1$).

In this case, $I_k\left[\theta_0,\sigma\right] \approx I_k^{\infty}\left[\theta_0,\sigma\right]$, where $I_k^{\infty}\left[\theta_0,\sigma\right]$ is given in (4.2.1.2). In this case:

$$\begin{aligned} Y_{\parallel,\infty} &= NkT\left[\frac{\left(2+\lambda^3\right)f\left(\theta_0,\sigma\right)-28\lambda^3-80}{\lambda^3\left(f\left(\theta_0,\sigma\right)-36\right)}\right] \\ \lambda^{\star} &= \left[\frac{f\left(\theta_0,\sigma\right)-40}{f\left(\theta_0,\sigma\right)-28}\right]^{1/3} \\ Y_{\parallel,\infty}^{\star} &= 3NkT\left[\frac{f\left(\theta_0,\sigma\right)-28}{f\left(\theta_0,\sigma\right)-36}\right] \\ Y_{\perp,\infty}^{\star} &= 3NkT\left[\frac{f\left(\theta_0,\sigma\right)-40}{f\left(\theta_0,\sigma\right)-36}\right] \\ f\left(\theta_0,\sigma\right) &= 18\sigma^2-18\pi\sigma-36\theta_0^2+9\pi^2 \end{aligned} \tag{4.2.2.9}$$

Approximations for the nondimensional Young's moduli, $Y_{\parallel}/NkT$ and $Y_{\perp}/NkT$, are shown in Figure 4.4 for $\sigma = 4\pi/3$ and $3\pi/2$. Clearly, (4.2.2.9) recovers $Y_{\parallel,\infty}^{\star} = Y_{\perp,\infty}^{\star} = Y_{iso}$ in the limit of $\sigma \to \infty$, as expected. The approximations in (4.2.2.9) share the same physical character as the $\sigma << 1$ approximations in the sense that, when σ is large enough, $Y_{\parallel,\infty}^{\star}$ is at its maximum (on the interval $[0,\pi/2]$) at $\theta_0 = 0$ and minimum at $\theta_0 = \pi/2$ (this can also be seen in Figure 4.4). The situation is reversed for $Y_{\perp,\infty}^{\star}$; that is, its maximum is at $\theta_0 = \pi/2$ and its minimum is at $\theta_0 = 0$. Again, this is due to the fact that there is a greater stiffness in the directions of higher chain densities. Lastly, note that the approximations in (4.2.2.9) predict a nonphysical singularity on the interval $\theta_0 \in [0,\pi/2]$ when σ is not large enough ($\sigma \lessapprox \pi$). This can result in, incorrectly, predicting negative and/or diverging $Y_{\parallel}$ or $Y_{\perp}$. Thus, one should take care that σ is large enough when using (4.2.2.9) for design of transversely isotropic elastomers.

To recap: we derived theoretical approximations for how changing P would change the elastic properties of a polymer network. We did this analysis primarily in the context of transversely isotropic, incompressible materials–although a similar analysis could be carried out for a general Poisson function and/or an anisotropic material with multiple special directions (as opposed to just one).

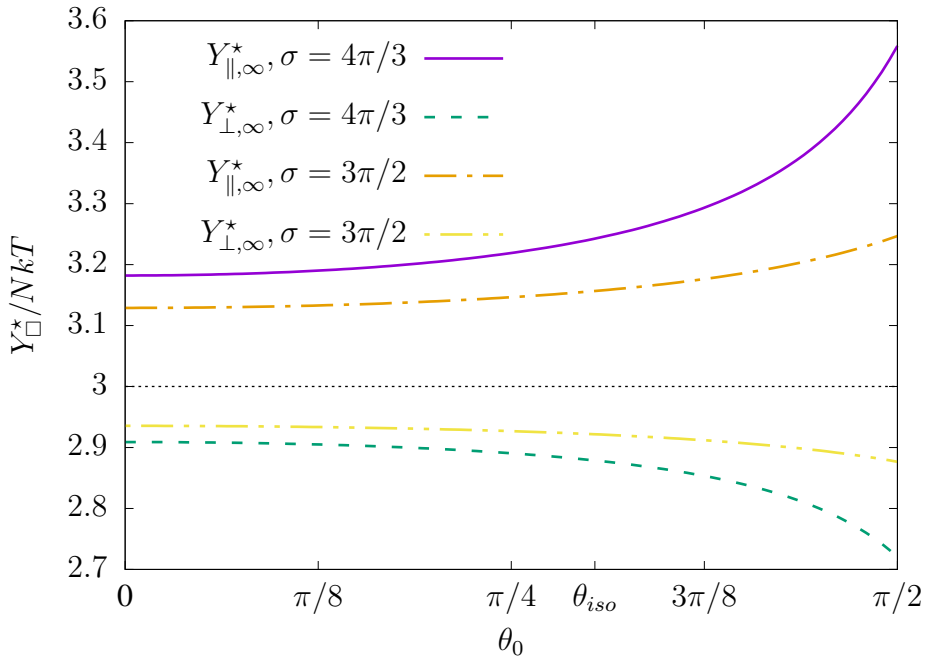

Figure 4.4: The dimensionless Young's moduli in the directions of the axis of symmetry, $Y^\star_\parallel$, and orthogonal to the axis of symmetry, $Y^\star_\perp$, as a function of the upper Gaussian center, θ_0, for finite σ: $4\pi/3$ and $3\pi/2$. The dashed, black line represents the Young's modulus for an isotropic network, $Y_{iso} = 3G_{iso} = 3NkT$.

4.2.3 Susceptibility

Physical prelude

We will consider, in this section, the affect of the network architecture on the polarization response of the DE. In Section 4.1.3 we made the claim that, for linear dielectric elastomers, the inverse susceptibility tensor: $\boldsymbol{\chi}^{-1} \coloneqq \frac{\partial^2 \mathcal{W}}{\partial \mathbf{P} \partial \mathbf{P}}$. However, we have derived $\mathcal{W}^*$; that is, the Legendre transform of $\mathcal{W}$ in the polarization slot. Further, although it is clear that $\mathcal{W}(\mathbf{F}, \mathbf{P}) = \mathcal{W}^*(\mathbf{F}, \mathbf{E}(\mathbf{P})) + \mathbf{P} \cdot \mathbf{E}(\mathbf{P})$ where by $\mathbf{E}(\mathbf{P})$ we mean the electric field as a function of polarization, it is not straightforward to write out $\mathcal{W}$ in its explicit form given $\mathcal{W}^*$. This is because, while we have derived the polarization as a function of the electric field in our approach, we are unable to invert this function, for general $\mathbf{F}$ and $\mathbf{P}$, to obtain $\mathbf{E} = \mathbf{E}(\mathbf{P})$. While symmetries can often be exploited (e.g. in $\mathbf{F}$, $\mathbf{E}$, etc.) in order to invert $\mathbf{P}(\mathbf{E})$ and formulate $\mathcal{W}$ explicitly from $\mathcal{W}^*$, we instead look for a correspondence between derivatives of $\mathcal{W}$ and of $\mathcal{W}^*$ as such an approach would be much more readily generalized. The desired identity is as

follows:

$$-\frac{\partial^2 \mathcal{W}^*}{\partial \mathbf{E} \partial \mathbf{E}} = \left(\frac{\partial^2 \mathcal{W}}{\partial \mathbf{P} \partial \mathbf{P}} \right)^{-1} = \boldsymbol{\mathcal{X}}$$

A short proof is given in Appendix B.

Again, by the weakly interacting assumption, $\mathcal{W}^* = N \left\langle \mathcal{A}^* \right\rangle_{\tilde{\mathbf{r}}}$. However, upon inspection of (3.0.0.4), we have a similar difficulty to the one faced in Section 4.2.2; that is, the integration involved in $\left\langle \mathcal{A}^* \right\rangle_{\tilde{\mathbf{r}}}$ is difficult to evaluate exactly. Taylor expanding the inverse Langevin function about zero stretch (and subsequently out of the denominator, $\gamma / \mathcal{L}^{-1}(\gamma) = \frac{1}{3} - \frac{1}{5}\frac{\gamma_r^2}{n} + \mathcal{O}(\gamma^4)$), we obtain the approximation:

$$\mathcal{W}^*(\mathbf{F}, \mathbf{E}) = NkT \Bigg\{ n \left[w_f^*(\kappa) - \kappa_\perp \right] + \left[\frac{3}{2} + \frac{2\kappa}{15} - w_f^*(\kappa) \right] \left\langle \gamma_r^2 \right\rangle_{\tilde{\mathbf{r}}} + \frac{3\kappa}{5} \left\langle \gamma_r^2 \left(\hat{\mathbf{E}} \cdot \hat{\mathbf{r}} \right)^2 \right\rangle_{\tilde{\mathbf{r}}} + \left\langle \mathcal{O}\left(\gamma^4 n\right) \right\rangle_{\tilde{\mathbf{r}}} \Bigg\} \tag{4.2.3.1}$$

where

$$w_f^*(\kappa) = \ln \left(\frac{2\sqrt{\kappa}}{\sqrt{\pi}\, \mathrm{erf}\left(\sqrt{\kappa}\right)} \right). \tag{4.2.3.2}$$

The four terms in (4.2.3.1) can be understood as follows: (1.) the first term is the LTHP free energy density of a collection of (Nn) monomers that are kinematically free; that is, monomers that are not constrained to satisfy some end-to-end vector; (2.) a correction to the first term that is related to the average magnitude of chain stretch; (3.) another correction that takes into account the average amount that the chain is stretched parallel to the direction of the electric field; and (4.) higher order terms related to the finite extensibility of the chain. Note that the first term is invariant when changing the cross-linking density at fixed mass density. The second and third terms contribute to electromechanical coupling, while only the third term captures the effect of chain torque. Interestingly, if one neglects $\mathcal{O}(\gamma^4 n)$ terms in (4.2.3.1), then it is invariant under α. Therefore changing the fraction of loose end monomers can only have an effect on higher order terms, terms which are related to the finite extensibility of the chain.

We return our attention to the first term in (4.2.3.1)–the term that corresponds to a dielectric that consists of monomers that are unconstrained. We call this the *free polarization*. The ratio of free

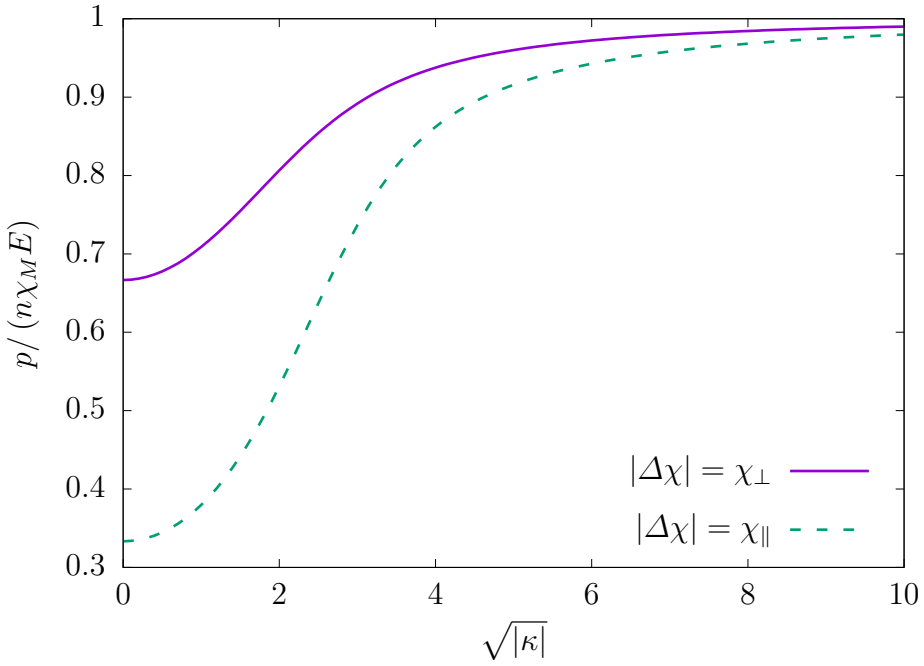

Figure 4.5: The nondimensional lab susceptibility per monomer for a collection of kinematically free monomers–or, in other words, the ratio of chain polarization to the characteristic scale, $n\chi_M E$, where $\chi_M \coloneqq \max\left(\chi_\parallel, \chi_\perp\right)$–shown as a function of $\sqrt{|\kappa|}$. The chains consist of TI ($|\Delta\chi| = \chi_\perp$) and uniaxial ($|\Delta\chi| = \chi_\parallel$) monomers. In the limit of small electric field or large temperature (i.e. $\sqrt{|\kappa|} \to 0$), the nondimensional (lab) susceptibility per monomer is $2/3$ for TI monomers and $1/3$ for uniaxial monomers. In the limit of large electric field or small temperature, the chain polarization approaches its theoretical maximum: $n\chi_M E$.

chain polarization to its maximum theoretical value is shown in Figure 4.5 as a function of the applied electric field. The quantity of polarization per applied electric field corresponds with what we typically consider the susceptibility of the material. In this work, in order to reason in precise terms we make the following definition: consider a series of experiments in which you apply three linearly independent electric fields, $\mathbf{E}_1, \mathbf{E}_2$ and $\mathbf{E}_3$, and measure three corresponding polarizations: $\mathbf{P}_1, \mathbf{P}_2$ and $\mathbf{P}_3$; then we say the *lab susceptibility*, $\boldsymbol{\mathcal{X}}_{lab}$, is given by:

$$\boldsymbol{\mathcal{X}}_{lab} = \mathbf{P}_{mat}\mathbf{E}_{mat}^{-1} \tag{4.2.3.3}$$

where $\mathbf{E}_{mat} = (\mathbf{E}_1, \mathbf{E}_2, \mathbf{E}_3)$ and $\mathbf{P}_{mat} = (\mathbf{P}_1, \mathbf{P}_2, \mathbf{P}_3)$. But in general, as can be seen in Figure 4.5, $\boldsymbol{\mathcal{X}}_{lab}$ is a function of $\mathbf{E}$. Thus, to determine $\boldsymbol{\mathcal{X}}_{lab}$ for a specific $\mathbf{E}$, the experiment in (4.2.3.3) should be carried out in a limiting fashion until $\mathbf{E}_1, \mathbf{E}_2$ and $\mathbf{E}_3$ are arbitrarily close to each other.

For the analysis considered in the remainder of this work, it will often be the case that $\mathbf{P}$ is proportional to $\mathbf{E}$. For instance, this is true when an electric field is applied in the direction of the axis of symmetry for a transversely isotropic DE. When $\mathbf{P}$ is proportional to $\mathbf{E}$, the lab susceptibility (for that some direction $\hat{\mathbf{E}}$) simplifies to:

$$\mathcal{X}_{lab,\hat{\mathbf{E}}} = P/E, \tag{4.2.3.4}$$

which is conceptually similar to what is shown in Figure 4.5 for free polarization.

Clearly $\boldsymbol{\mathcal{X}}_{lab} \neq \boldsymbol{\mathcal{X}} = -\frac{\partial^2 \mathcal{W}^*}{\partial \mathbf{E} \partial \mathbf{E}}$ in general; in fact, $\boldsymbol{\mathcal{X}} = \boldsymbol{\mathcal{X}}_{lab} + \frac{\partial \boldsymbol{\mathcal{X}}_{lab}}{\partial \mathbf{E}} \mathbf{E}$. It is only the case that the two are equivalent for all applied electric fields when the dielectric is linear[2]; that is, when $\boldsymbol{\mathcal{X}}_{lab}$ is not a function of $\mathbf{E}$. Otherwise, $\boldsymbol{\mathcal{X}}_{lab}$ and $\boldsymbol{\mathcal{X}}$ are only equivalent at relative extrema of $\boldsymbol{\mathcal{X}}_{lab}$.

All of the dielectric nonlinearity in our DE materials is encoded in the function w_f^*, which is a per monomer contribution to the LTHP free energy for an unconstrained polymer chain (see (4.2.3.2)). In fact, the LTHP free energy of an unconstrained polymer chain is, $nkT\left(w_f^* - \kappa_\perp\right)$. Negating the derivative with respect to E and then dividing by E, we arrive at the result shown in Figure 4.5. The y-axis corresponds to the lab susceptibility for a DE with a single free chain per unit volume where the lab susceptibility is measured in units of $n\chi_M$ and $\chi_M \coloneqq \max\left(\chi_\parallel, \chi_\perp\right)$. In regards to the physical character of the lab susceptibility for the free chain, there are three regimes that can be seen in Figure 4.5. When $\sqrt{|\kappa|} \to 0$, then $\mathcal{X}_{lab}/n \to \left(\chi_\parallel + 2\chi_\perp\right)/3$. In this limit (i.e. $E \to 0$ and/or $kT \to \infty$), the pdf of monomer orientations is uniformly distributed over the unit sphere because the electrostatic energy is vanishingly small as compared to the thermal energy. The factors of $1/3$ for $\chi_\parallel$ and $2/3$ for $\chi_\perp$ correspond to the dimensionality of each dipole susceptibility: the monomers are in three dimension space while $\chi_\parallel$ is the dipole susceptibility along a line (i.e. $\operatorname{span} \hat{\mathbf{n}}$) and $\chi_\perp$ is the dipole susceptibility in the plane orthogonal to $\hat{\mathbf{n}}$. (In addition, note that $\mathcal{X}_{lab}$ does not vanish as $kT \to \infty$.

[2] It is well known that the concept of stored energy can be ill-defined for many nonlinear systems (for discussion of this specific to dielectrics, see [Gri89] section 4.4.3). This is because the nonlinearity can result in a path dependence for the work required to assemble the system. However, the work required to assemble the polarized nonlinear dielectrics considered in this work is not path dependent and there is a clear understanding of how the energy is stored in the system. In terms of electrostatics, it was establish in Section **??** that the energy is stored in (1.) the electrostatic potential of monomer dipoles and (2.) in the bond energy associated with stretching bound charges in the monomer relative to each other in order to form dipoles. The dielectric nonlinearity of our DE materials arises because the average alignment of the monomers is determined by a balancing of electrostatic potential energy and the entropy, and because the dipole susceptibility of a monomer depends on its alignment with respect to the applied electric field

This is because $\boldsymbol{\chi}_\mu$ is quadratic in $\hat{\mathbf{n}}$. Even though $\hat{\mathbf{n}}$ is uniformly distributed, the polarization does not cancel.) When $\sqrt{|\kappa|} \to \infty$, then $\mathcal{X}_{lab}/n \to \max\left(\chi_\parallel, \chi_\perp\right)$. In this limit (i.e. $E \to \infty$ and/or $kT \to 0$), the monomers are frozen in their energy minimum orientation; that is, $\hat{\mathbf{n}} = \pm\hat{\mathbf{E}}$ when $\chi_\parallel > \chi_\perp$ and $\hat{\mathbf{n}}$ such that $\hat{\mathbf{n}} \cdot \hat{\mathbf{E}} = 0$ when $\chi_\perp > \chi_\parallel$. In this case, the chain has reached its maximum theoretical lab susceptibility. Finally, there is a transition regime between the limits of $\sqrt{|\kappa|} \to 0$ and $\sqrt{|\kappa|} \to \infty$. There are two main takeaways that are relevant to this discussion: (1.) the dielectric nonlinearity of our DE materials arises because the average alignment of the monomers is determined by a balancing of electrostatic potential energy and the entropy, and because the dipole susceptibility of a monomer depends on its alignment with respect to the applied electric field; and (2.) despite this nonlinearity, we have $\mathcal{X} = \mathcal{X}_{lab}$ in the limits of $\sqrt{|\kappa|} \to 0$ and $\sqrt{|\kappa|} \to \infty$. Moving forward, we will consider both $\mathcal{X}$ and $\mathcal{X}_{lab}$; as they will both prove useful. Specifically, $\mathcal{X}$ is particularly relevant to material stability while $\mathcal{X}_{lab}$ is relevant to the capacitance–and hence, electromechanical coupling–for a given thin film DEA geometry. Moreover, for convenience, we make the definitions:

$$\boldsymbol{\mathcal{X}}^h \coloneqq \lim_{\sqrt{|\kappa|}\to 0} \boldsymbol{\mathcal{X}} = \lim_{\sqrt{|\kappa|}\to 0} \boldsymbol{\mathcal{X}}_{lab}$$

$$\boldsymbol{\mathcal{X}}^c \coloneqq \lim_{\sqrt{|\kappa|}\to \infty} \boldsymbol{\mathcal{X}} = \lim_{\sqrt{|\kappa|}\to \infty} \boldsymbol{\mathcal{X}}_{lab}$$

We now consider what we have learned about free polarization in the context of the design of anisotropic dielectric elastomers. When used for a DEA, it is desirable that the lab susceptibility of the DE be as large is possible. This is because the susceptibility serves to increase the capacitance of the DEA. The increased capacitance means a greater accumulation of charge on the electrodes for a given voltage difference–which leads to a greater Coulomb attraction between the electrodes and hence a greater electromechanical coupling of the DEA. Now, for illustrative purposes, consider a single chain. If the chain is allowed to contract to zero stretch, then all the terms in (4.2.3.1) vanish except the first one–which is consistent with our previous discussion. In this case, it is also clear from the previous discussion, that the susceptibility is isotropic and is such that $\boldsymbol{\mathcal{X}}_{lab} = \mathcal{X}_{lab}\mathbf{I}, \mathcal{X}_{lab} \in Nn\left[\frac{\chi_\parallel + 2\chi_\perp}{3}, \max\left(\chi_\parallel, \chi_\perp\right)\right]$. Recall (Figure 4.5) that the lab susceptibility is

maximized at low temperature or large electric field (i.e. $\sqrt{|\kappa|} >> 1$). This is an issue, from a practical standpoint, because we would prefer not to need to operate our DEA under these conditions. Controlling temperature is not always an option and at a minimum requires energy, while a large applied electric field requires larger and more expensive electromotive force devices.

Now consider this same chain, but in the reference, load-free state of an isotropic network such that $\gamma_r = 1$. Then the second and third terms–the electromechanical terms–are $\mathcal{O}(1)$ while the first is of $\mathcal{O}(n)$. This means, for a dielectric elastomer that consists of "long chains" (i.e. $n >> 1, n \gtrsim 1000$), that the electromechanical terms are negligible when the elastomer is in the load-free state (and in many cases, they are even negligible at large macroscopic deformations). Thus, if we are to significantly improve on the small $\sqrt{|\kappa|}$ lab susceptibility in the load-free state, then one may first want to increase the density of cross-links of the elastomer (i.e. increase N_0/n)–while keeping in mind that the stiffness also scales with the density of cross-links. Before moving on, it is also worth recalling the discussion on the "residual stresses" of our hypothetical anisotropic elastomers. Since the load-free state has some initial deformation to "relieve" the "residual stresses", $\gamma_r \neq 1$ in general. At first glance, one may consider this as an opportunity to increase $\left(\mathcal{X}^h\right)^\star$. However, it is easy to show that $\langle \gamma_r^2 \rangle_{\tilde{\mathbf{r}}}^\star \leq 1$ and that equality only holds for an isotropic network. The key is that, in the absence of electrical loads, the relaxed state should maximize the entropy of the elastomer and, by our approximation, the chain entropy as proportional to $-\gamma_r^2$; thus, for entropy to not decrease with respect to the manufactured state (i.e. $\langle -\gamma_r^2 \rangle_{\tilde{\mathbf{r}}} = 1$), we require $\langle \gamma_r^2 \rangle_{\tilde{\mathbf{r}}}^\star \leq 1$. Similarly, the lower bound on $\left\langle \gamma_r^2 \left(\hat{\mathbf{E}} \cdot \hat{\mathbf{r}} \right)^2 \right\rangle_{\tilde{\mathbf{r}}}^\star$ is clearly zero since it is strictly nonnegative and it vanishes when the elastomer is manufactured such that all of the chains are orthogonal to the eventual direction of the applied electric field. The upper bound, however, is much less clear and warrants further investigation. For the purposes of this investigation, we split the susceptibility into two contributions: one associated with free monomers, $\mathcal{X}_{\text{free}}$, and a correction term due to the electromechanical coupling of the material, $\check{\boldsymbol{\mathcal{X}}}$; that is:

$$\boldsymbol{\mathcal{X}} = \mathcal{X}_{\text{free}} \mathbf{I} + \check{\boldsymbol{\mathcal{X}}}.$$

Taking derivatives of (4.2.3.1) with respect to E and taking the appropriate limits, we obtain:

$$\check{\mathcal{X}}_{\parallel}^{h} = \frac{N\left(\Delta\chi\right)}{5}\left(\left\langle\gamma_r^2\right\rangle_{\tilde{\mathbf{r}}} - 3\left\langle\gamma_r^2\left(\hat{\mathbf{E}}\cdot\hat{\mathbf{r}}\right)^2\right\rangle_{\tilde{\mathbf{r}}}\right), \tag{4.2.3.5}$$

and

$$\check{\mathcal{X}}_{\parallel}^{c} = -\frac{N\left(\Delta\chi\right)}{15}\left(2\left\langle\gamma_r^2\right\rangle_{\tilde{\mathbf{r}}} + 9\left\langle\gamma_r^2\left(\hat{\mathbf{E}}\cdot\hat{\mathbf{r}}\right)^2\right\rangle_{\tilde{\mathbf{r}}}\right). \tag{4.2.3.6}$$

Design for susceptibility

We again consider transversely isotropic materials such that we take (4.1.3.7) as our ansatz for P. Using our ansatz, some basic trigonometry, and (4.2.1.3), we obtain the result:

$$\left\langle\gamma_r^2\left(\hat{\mathbf{E}}\cdot\hat{\mathbf{r}}\right)^2\right\rangle_{\tilde{\mathbf{r}}} = \frac{\lambda^2}{4}\left(1 + \frac{I_3\left[\theta_0,\sigma\right]}{I_1\left[\theta_0,\sigma\right]}\right). \tag{4.2.3.7}$$

In the limit of $\sigma << 1$, we have the approximation:

$$\left\langle\gamma_r^2\left(\hat{\mathbf{E}}\cdot\hat{\mathbf{r}}\right)^2\right\rangle_{\tilde{\mathbf{r}}} \approx \frac{\lambda^2}{4}\left[1 + e^{-4\sigma^2}\left(1 + 2\cos\left(2\theta_0\right)\right)\right]$$

We can then derive, using (4.2.3.7) and (4.2.2.3), $\mathcal{W}^*$ for transversely isotropic DEs. Instead, we turn our attention directly to $\check{\mathcal{X}}_{\parallel}^{h}$. In the limit of $\sigma << 1$, we have the approximation:

$$\frac{\left(\check{\mathcal{X}}_{\parallel,0}^{h}\right)^{\star}}{N\left(\Delta\chi\right)} = 0$$

where again, $\square^{\star}$ denotes a quantity evaluated at $\lambda = \lambda^{\star}$. Interestingly, the electromechanical correction term vanishes at $\lambda^{\star}$ for all θ_0 and σ when $\sigma << 1$; and hence, at least in the limit of the load-free state, the DE effectively behaves as a collection of free monomers.

Similarly, by plugging (4.2.1.2) into (4.2.2.3) and (4.2.3.7), then subsequently (4.2.3.5) and (4.2.2.9), we arrive at an approximation of $\left(\check{\mathcal{X}}_{\parallel}^{h}\right)^{\star}$ in the limit of weak directional control (i.e. $\sigma >> 1$). This

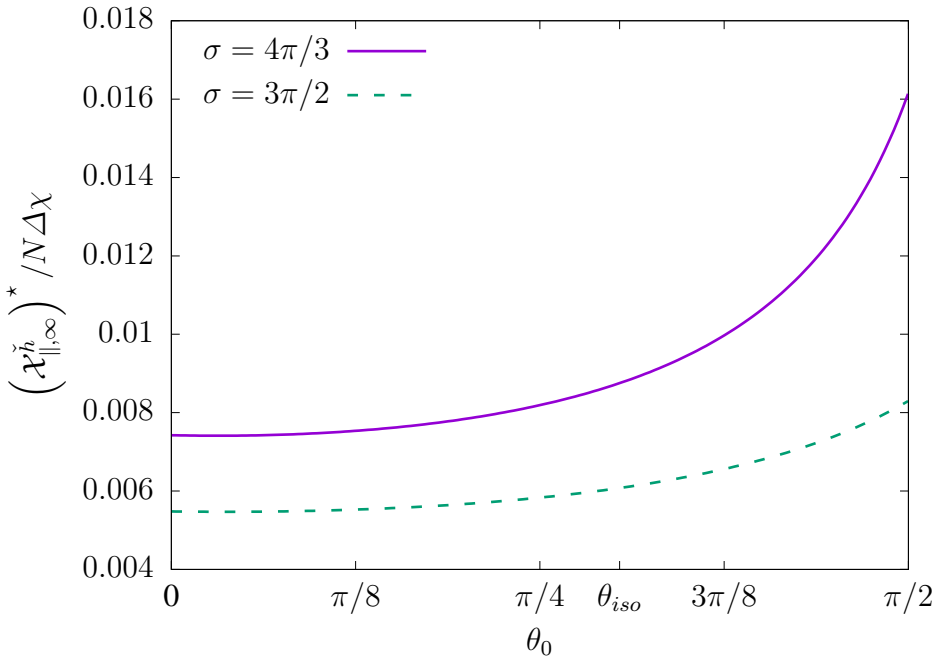

Figure 4.6: Correction to the free monomer susceptibility in the load-free state in the limit of $\sigma >> 1$. The correction to the free monomer susceptibility is much less in this limit than the $\sigma << 1$ limit, and it vanishes as $\sigma \to \infty$.

approximation is:

$$-\frac{16\Delta\chi\left(\theta_0-\sigma\right)\left[\pi-3\left(\theta_0+\sigma\right)\right]}{5\left(2\theta_0^2-2\pi\theta_0-4\sigma^2+\pi^2-4\right)\left[f\left(\theta_0,\sigma\right)-40\right]^{1/3}\left[f\left(\theta_0,\sigma\right)-28\right]^{2/3}}$$

where f was first defined in (4.2.2.9). The approximation is shown in Figure 4.6. Notice that, while the electromechanical correction (at $\lambda = \lambda^\star$) does not vanish, $\left(\check{\mathcal{X}}^h_{\parallel,\infty}\right)^\star / N\Delta\chi$ is small compared to 1 in the limit of $\sigma >> 1$. Since the free monomer susceptibility is $\mathcal{O}\left(Nn\right)$, this correction term is negligible; and, what is more, is that it vanishes as $\sigma \to \infty$.

The electromechanical correction to the susceptibility in the load-free state, $\left(\check{\mathcal{X}}^h_{\parallel}\right)^\star$, vanishes in the limit of $\sigma << 1$ and is negligible in the limit of $\sigma >> 1$. It would seem then that there is little hope for increasing the initial susceptibility of our design DEs. However, it is clear from (4.2.3.5) that $\check{\mathcal{X}}^h_{\parallel}$ is deformation dependent. It is worth considering whether or not $\check{\mathcal{X}}^h_{\parallel,0}$, for instance, vanishes when $\lambda \neq \lambda^\star$. To this end, we visualize $\check{\mathcal{X}}^h_{\parallel,0}$ for $\sigma = 0$ and $\lambda = 1$ in Figure 4.7. Notice that, in this case, $\check{\mathcal{X}}^h_{\parallel,0}$ does not vanish and is, in fact, has a positive contribution of $\mathcal{O}\left(N\right)$ when $\Delta\chi > 0$ and $\theta_0 \to \pi/2$, and

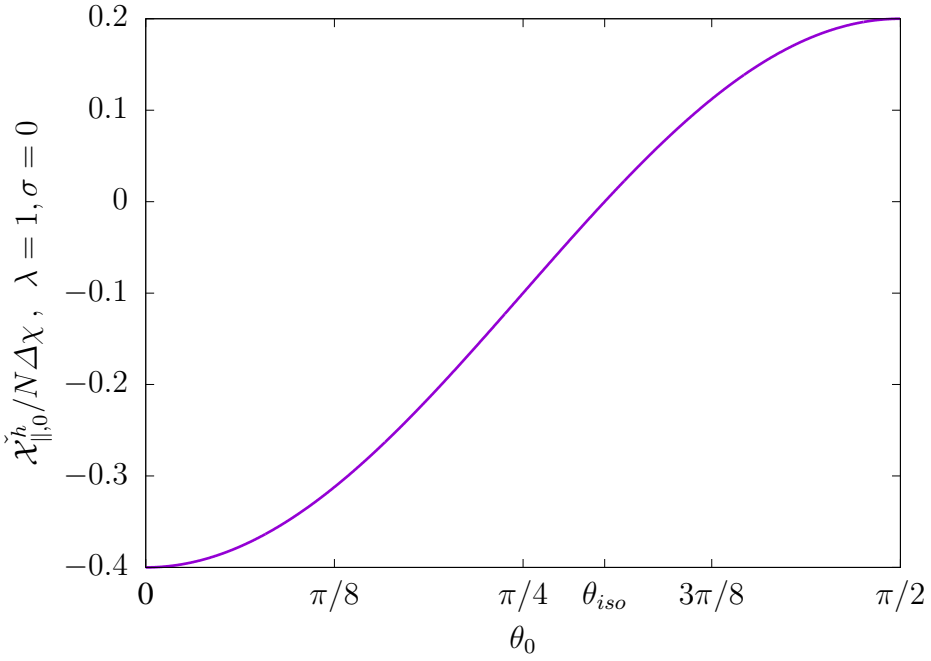

Figure 4.7: Approximate $\check{\mathcal{X}}^h_{\parallel,0}$ for $\sigma = 0$ and $\lambda = 1$. In this case, $\check{\mathcal{X}}^h_{\parallel,0}$ does not vanish and is $\mathcal{O}(N)$.

when $\Delta\chi < 0$ and $\theta_0 \to 0$. Thus, to maximize $\left(\check{\mathcal{X}}^h_{\parallel,0}\right)^\star$, one must find a way to alter the polarization properties while simultaneously maintaining a (nearly) mechanically isotropic network.

Hybrid networks: maximizing the operating susceptibility

It was clear, particularly in Figure 4.7, that $\left(\check{\mathcal{X}}^h_{\parallel}\right)^\star$ could be made greater if somehow the initial, load-free deformation, $\lambda^\star$, could be as close to unity as possible. For this reason, we propose the following (rough) manufacturing process and design algorithm for optimizing $\left(\check{\mathcal{X}}^h_{\parallel}\right)^\star$. First, imagine that we have two types of polymer chains that are compatible with each other in the sense that they can be cross-linked together in a network. Further, imagine that the monomers for the one type of chain are such that $\Delta\chi > 0$ and the other are such that $\Delta\chi < 0$. Call these type A and type B, respectively. Now, if an electric field is applied in a constant direction just prior to and during cross-linking, then the density of A chains oriented orthogonal to the electric field direction will increase, as will the density of B chains oriented parallel to the electric field. Let σ_A and σ_B be the design standard deviations for chains of type A and type B, respectively. Then, clearly, σ_A and σ_B would depend on the magnitude of the applied electric field; and, σ_A and σ_B would likely not be able to be controlled independently

of each other–or rather, the envisioned manufacturing process would need to be specialized further in order to control the two independently of each other. In this scenario, the monomer susceptibilities $\chi_{\perp}^{A}$, $\chi_{\parallel}^{A}$, $\chi_{\perp}^{B}$, and $\chi_{\parallel}^{B}$ are given; or at best, selected from a catalog of possible monomer types. Then the design variables consist of N_0^A, n^A, θ_0^A, σ_A, N_0^B, n^B, θ_0^B, σ_B, where N_0^A is the number of chains of type A per unit volume, n^A is the number of monomers per chain in chains of type A, θ_0 is the center of the Gaussian in the upper half of the unit sphere for chains of type A, σ_A is the standard deviations of the pdf for chains of type A, and the remaining quantities are the same but for chains of type B. The LTHP free energy density for this hybrid DE is:

$$\mathcal{W}^* = J^{-1}\left(N_0^A \left\langle \mathcal{A}^* \right\rangle_{\tilde{\mathbf{r}}}^{A} + N_0^B \left\langle \mathcal{A}^* \right\rangle_{\tilde{\mathbf{r}}}^{B}\right)$$

where

$$\left\langle \mathcal{A}^* \right\rangle_{\tilde{\mathbf{r}}}^{\square} = C^{\square} \int_0^{\pi} \mathrm{d}\theta \int_0^{2\pi} \mathrm{d}\phi \left(\left\{ \exp\left[-\frac{\left(\theta - \theta_0^{\square}\right)^2}{2\sigma_{\square}^2} \right] + \exp\left[-\frac{\left(\pi - \theta - \theta_0^{\square}\right)^2}{2\sigma_{\square}^2} \right] \right\} \times \mathcal{A}^*\left(\mathbf{F}\tilde{\mathbf{r}}, \mathbf{E}; n^{\square}, \chi_{\perp}^{\square}, \chi_{\parallel}^{\square}\right) \sin\theta \right).$$

The design space for this problem is of a higher dimension than those that we have considered thus far. As a consequence, using the tools that we have employed through much of this work–basic calculus and graphical methods–will prove difficult. Instead, we proceed by using some of the intuition that we have gained thus far. By Figure 4.7, we reason that an optimal $\left(\mathcal{X}_{\parallel}^{h}\right)^{\star}$ will result from taking $\theta_0^A = \pi/2$, $\theta_0^B = 0$, and $\sigma_A = \sigma_B = 0$. Now let $\mathcal{N}_0^m \coloneqq N_0^A n^A + N_0^B n^B$ be the number of monomers per unit volume in the reference configuration and $\mathcal{N}^m \coloneqq J^{-1}\mathcal{N}_0^m$ be the number of monomers per unit volume in the current configuration. The free monomer susceptibility scales with the number of monomers per unit volume; thus, assume that $\mathcal{N}_0^m$ is already taken as large as possible or desired given some range of acceptable DE mass density. Similarly, $\check{\mathcal{X}}_{\parallel}^{h}$ scales with N_0, but so does the stiffness. Thus, one should take N_0 as large as possible while still keeping the stiffness within some desired range. Let $\Xi^A \coloneqq N_0^A/N_0$ so that $N_0^B = \Xi^B N_0 = \left(1 - \Xi^A\right) N_0$. Again, considering Figure 4.7, we

want to pick $\Xi^A \in [0,1]$ such that $\lambda^\star = 1$. In other words, we require that Ξ^A satisfies:

$$\frac{\partial}{\partial \lambda}\left[\left(\Xi^A \left\langle \mathcal{A}^* \right\rangle^A_{\tilde{\mathbf{r}}} + \left(1-\Xi^A\right)\left\langle \mathcal{A}^* \right\rangle^B_{\tilde{\mathbf{r}}}\right)\right]\Big|_{\lambda=1} = 0,$$

which sets $\Xi^A = 2/3$.

Next, we need to pick n^A and n^B. We define the ratios $\xi^A \coloneqq N_0 n^A/\mathcal{N}_0^m$ and $\xi^B \coloneqq N_0 n^B/\mathcal{N}_0^m$. Since, by assumption, the total number of monomers is already given, by definition, we require:

$$\mathcal{N}_0^m = N_0^A n^A + N_0^B n^B.$$

Consequently: $\xi^A \in \left[0, 1/\Xi^A\right]$ and $\xi^B = \left(1-\Xi^A\xi^A\right)/\left(1-\Xi^A\right)$. Because the only contribution to $\mathcal{X}_\parallel^h$ that depends on $\mathcal{N}^m$ is the free monomer susceptibility, if $\left(\chi_\parallel^A + 2\chi_\perp^A\right) > \left(\chi_\parallel^B + 2\chi_\perp^B\right)$ then we try to reach the limit $\xi^A \to 1/\Xi^A$. Where as, if $\left(\chi_\parallel^A + 2\chi_\perp^A\right) < \left(\chi_\parallel^B + 2\chi_\perp^B\right)$ then we try to reach the limit $\xi^A \to 0$. Lastly, if $\left(\chi_\parallel^A + 2\chi_\perp^A\right) = \left(\chi_\parallel^B + 2\chi_\perp^B\right)$ then, in our truncated theory, $\mathcal{X}_{\text{free}}^h$ is invariant with respect to ξ^A (in this case, it is likely best to let $n^A = n^B = \mathcal{N}^m/N_0$). Let $M = \arg^\square\max\left[\chi_\parallel^A + 2\chi_\perp^A, \chi_\parallel^B + 2\chi_\perp^B\right]$. If the limiting process is successfully carried out such that $\mathcal{X}_{\text{free}}^h$ is maximized, then:

$$\begin{aligned}
\left(\mathcal{X}_\parallel^h\right)^\star &= \left(\mathcal{X}_{\text{free}}^h\right)^M + \frac{N}{5}\left[\Xi^A|\Delta\chi^A| + 2\left(1-\Xi^A\right)|\Delta\chi^B|\right], \\
&= \frac{\mathcal{N}^m}{3}\left(\chi_\parallel^M + 2\chi_\perp^M\right) + \frac{N}{5}\left[\Xi^A|\Delta\chi^A| + 2\left(1-\Xi^A\right)|\Delta\chi^B|\right], \\
&= N\left\{\frac{n^A+n^B}{3}\left(\chi_\parallel^M + 2\chi_\perp^M\right) + \frac{2}{15}\left[|\Delta\chi^A| + |\Delta\chi^B|\right]\right\}.
\end{aligned} \tag{4.2.3.8}$$

In summary, the proposed design process for maximizing $\mathcal{X}_\parallel^h$ is as follows:

1. Choose a preferred mass density, $\mathcal{N}_0^m$.
2. Let $\theta_0^A = \pi/2$ and $\theta_0^B = 0$. Try to approach $\sigma \to 0$.
3. Let $\Xi^A = 2/3$ and, consequently, $\Xi^B = 1/3$.

4. Maximize $N_0/\mathcal{N}_0^m$ without exceeding the desired stiffness threshold(s). Note, when $\Xi^A = 2/3, \Xi^B = 1/3$:

$$Y_{\parallel} = NkT\left(1 + 2\lambda^{-3}\right)$$
$$Y_{\perp} = NkT\left(\frac{1}{2} + \frac{5}{2}\lambda^{3}\right)$$

5. Choose ξ^A; let $\xi^B = \left(1 - \Xi^A\xi^A\right) / \left(1 - \Xi^A\right)$:

   (a) The target ξ^A should be determined by:

$$\xi^A = \begin{cases} 1/\Xi^A & \chi_{\parallel}^A + 2\chi_{\perp}^A > \chi_{\parallel}^B + 2\chi_{\perp}^B \\ 0 & \chi_{\parallel}^A + 2\chi_{\perp}^A < \chi_{\parallel}^B + 2\chi_{\perp}^B \\ \mathcal{N}_0^m/N_0 & \chi_{\parallel}^A + \chi_{\perp}^A \approxeq \chi_{\parallel}^B + \chi_{\perp}^B \end{cases}$$

   (b) However, approaching either the upper limit of ξ^A, which would result in chains of type B to be "short" (i.e. n^B small) or the lower limit of ξ^A, which would result in chains of type A to be "short", may affect the electromechanical response of the DE. This is because, as chains become shorter, higher order terms in (4.2.3.1) become more relevant at even moderate deformations. Specifically, these higher order terms would cause monomers to be constrained toward the direction of chain stretch more quickly as the DE deforms. This will lead to an increase in both strain hardening and electromechanical coupling. An additional consideration is the effect of chain length on the validity of the weakly interacting assumption; it could be that, as chain lengths become shorter, interactions between chains become more important. Thus, either limit should be approached iteratively until it is determined how closely the limit can be approached without affecting the desired stiffness properties.

We have shown that $\left(\mathcal{X}_{\text{free}}^h\right)^\star$ can theoretically be improved upon by deliberately designing and manufacturing the network architecture of a dielectric elastomer. However, practically speaking, it can be

seen from (4.2.3.8) that, unless the network has a high density of cross-links and therefore consists of "short chains" (i.e. $\mathcal{N}_0^m/N_0 \leq 10$) the increase is modest at best (e.g. $\lesssim 1\%$ for $\mathcal{N}_0^m/N_0 \gtrsim 100$); and a high density of cross-links may not be desirable because the stiffness per mass density scales linearly with the density of cross-links. Not to mention: the theoretical improvement may be lost entirely once manufacturing error inevitably occurs.

One may wonder then why we bothered spending so much time detailing and analyzing the proposed manufacturing and design processes. The answer to this is two-fold: (1.) despite such modest gains, it is still worth carefully exploring the theoretical limitations of what can be achieved through the design of dielectric elastomer network architectures and (2.) although the gains have been modest for improving $\left(\mathcal{X}^h_{\text{free}}\right)^\star$, it is still to be determined whether the same can be said for the electromechanical coupling of the designed network–which is, after all, the main goal of this work. Indeed, recall that $\mathcal{X}^h_{\text{free}}$ is also a function of deformation; so that larger increases in susceptibility may be realized at deformations such that $\lambda \neq \lambda^\star$. This effect will be investigated in the next subsection.

Mechanically induced susceptibility

The susceptibility of dielectric elastomers is deformation dependent because deformation can cause chains in the network to rotate, thereby changing the average monomer orientation in each of the chains, and cause chains to stretch, thereby increasing the concentration of monomers oriented toward the direction of stretch for a given chain. Using the results developed thus far, we consider a few examples. First, as a baseline, we consider an isotropic dielectric elastomer such that $\mathrm{P} = 1/4\pi$. Using (4.2.2.3), (4.2.3.7), and (4.2.3.5):

$$\check{\mathcal{X}}^{h\,uni}_{\parallel} = \frac{2N}{15}\left(\Delta\chi\right)\left(\lambda^{-1} - \lambda^2\right) \tag{4.2.3.9}$$

Notice that when $\Delta\chi > 0$, $\check{\mathcal{X}}^{h\,uni}_{\parallel}$ increases (relative to the reference configuration) when the DE is compressed in the direction of the axis of symmetry ($\lambda < 1$) and decreases when stretched; when $\Delta\chi < 0$, vice versa. (Also, $\theta_0 = \theta_{iso}$, $\sigma = 0$ recovers the same correction term as (4.2.3.9).)

For the hybrid network, where $\theta_0^A = \pi/2, \theta_0^B = 0, \sigma_A = \sigma_B = 0, \Xi^A = 2/3, \Xi^B = 1/3$, we have:

$$\check{\mathcal{X}}_{\parallel}^{h\,hybrid} = \frac{2N}{15}\left(|\Delta\chi^A|\lambda^{-1} + |\Delta\chi^B|\lambda^2\right) \tag{4.2.3.10}$$

Interestingly, since both coefficients are strictly nonnegative and physically we require $\lambda > 0$, it is the case that $\check{\mathcal{X}}_{\parallel}^{h\,hybrid}$ is semi-convex in λ for the domain of admissible λ. Further, it is convex when $|\Delta\chi^A| \neq 0$ and $|\Delta\chi^B| \neq 0$. This is significant because it means that when either compressing (i.e. $\lambda < 1$) or stretching (i.e. $\lambda > 1$)–even though initially there may be a drop in $\check{\mathcal{X}}_{\parallel}^{h}$–eventually $\check{\mathcal{X}}_{\parallel}^{h}$ will begin increasing again and do so monotonically. *The electromechanical increase of $\mathcal{X}_{\parallel}^{h}$ is bidirectional for the hybrid network.* If $|\Delta\chi^A| = 2|\Delta\chi^B|$, then $\check{\mathcal{X}}_{\parallel}^{h}$ has its minimum at $\lambda = 1$ so that any deformation increases $\check{\mathcal{X}}_{\parallel}^{h}$. Also, importantly, (4.2.3.9) and (4.2.3.10) show that, not only is mechanically induced susceptibility unidirectional for a uniformly distributed network and bidirectional for the hybrid network (by unidirectional, we mean that, depending on the sign of $\Delta\chi$, the susceptibility is only increased for either compression or stretching but not both), but, also, the mechanically induced susceptibility of the hybrid network is greater than that of the uniform network for all admissible deformations, λ.

Next, in contrast to either a uniformly distributed network or the hybrid network, we consider a network that consists of a single type of monomer and has been manufactured in the limit of high control, i.e. $\sigma << 1$. In this case: using (4.2.1.1), (4.2.2.3), (4.2.3.7), and (4.2.3.5):

$$\begin{aligned}\check{\mathcal{X}}_{\parallel,0}^{h} = -\frac{N}{20}(\Delta\chi)\Big\{&\left[\left(1+2\cos\left(2\theta_0\right)\right)e^{-4\sigma^2} - 3\right]\lambda^{-1} + \\ &\left[2\left(1+2\cos\left(2\theta_0\right)\right)e^{-4\sigma^2} + 2\right]\lambda^2\Big\}\end{aligned} \tag{4.2.3.11}$$

As to be expected, when $\theta_0 = 0$ the coefficient of λ^{-1} vanishes and when $\theta_0 = \pi/2$ the coefficient of λ^2 vanishes. This is expected because the sign and coefficient of λ^{-1} and λ^2 determine the effect of compression and stretching, respectively, on $\check{\mathcal{X}}_{\parallel}^{h}$. The above equation could be used as a design tool for anisotropic elastomers that consist of a single monomer type. For further physical insight, we let

$\sigma = 0$. Then (4.2.3.11) simplifies to:

$$\check{\mathcal{X}}^{h}_{\parallel,0}\Big|_{\sigma=0} = -\frac{N(\Delta\chi)}{10}\left\{\left[\cos(2\theta_0) - 1\right]\lambda^{-1} + 2\left[\cos(2\theta_0) + 1\right]\lambda^{2}\right\}.$$

Importantly, the theoretical factor for mechanically induced susceptibility can be larger in this case than it is for the uniform or hybrid networks. That is because, in this case, we can orient all of the chains in their preferred electromechanical susceptibility direction instead of a portion. The maximum factors occur at $\theta_0 = 0$ and $\theta_0 = \pi/2$, as expected. At $\theta_0 = 0$, the λ^{-1} factor (i.e. compression factor) vanishes and the λ^2 factor (i.e. expansion factor) is maximized–its value being $2N/5$. And at $\theta_0 = \pi/2$, the λ^2 factor vanishes and the λ^{-1} factor is maximized–its value being $N/5$. These factors are $3/2$ and 2 times larger than the hybrid network factors, respectively. However, recall that $Y_\perp$ vanishes as $\theta_0 \to 0$ and $Y_\parallel$ vanishes as $\theta_0 \to \pi/2$. Thus, while a greater mechanically induced susceptibility can be achieved (over the uniform and hybrid networks), there is a trade-off in terms of stiffness and mechanical stability. The implications of this in terms of the electromechanical coupling, operation, and failure of DEAs will be explored in the next section.

4.2.4 Dielectric elastomer actuators

In this section, we explore the effect of our design parameters on the deformation and usable work obtained from a dielectric elastomer actuator as a function of its electrical input. There are two main goals associated with this design: (1.) we would like to maximize the deformation and/or usable work that results from a fixed electrical input so that we maximize the efficiency of our DEAs and minimize the size of the electrical generator (e.g. battery) required to operate the DEA; and (2.) we would prefer, in many cases, to maximize the deformation and/or usable work that the DEA can produce before its failure. Since we are interested in the mechanics, the usable work, and the failure of the DEA, we will model its behavior using thermodynamics and free energy minimization. Since the pioneering work of [Tou56], there has been a lot of work recently in variational methods and formulations for electroelasticity [Tou56, SZG08, Suo10, BDO09, DO06, DO14, Liu13, Liu14]. Similarly, for the

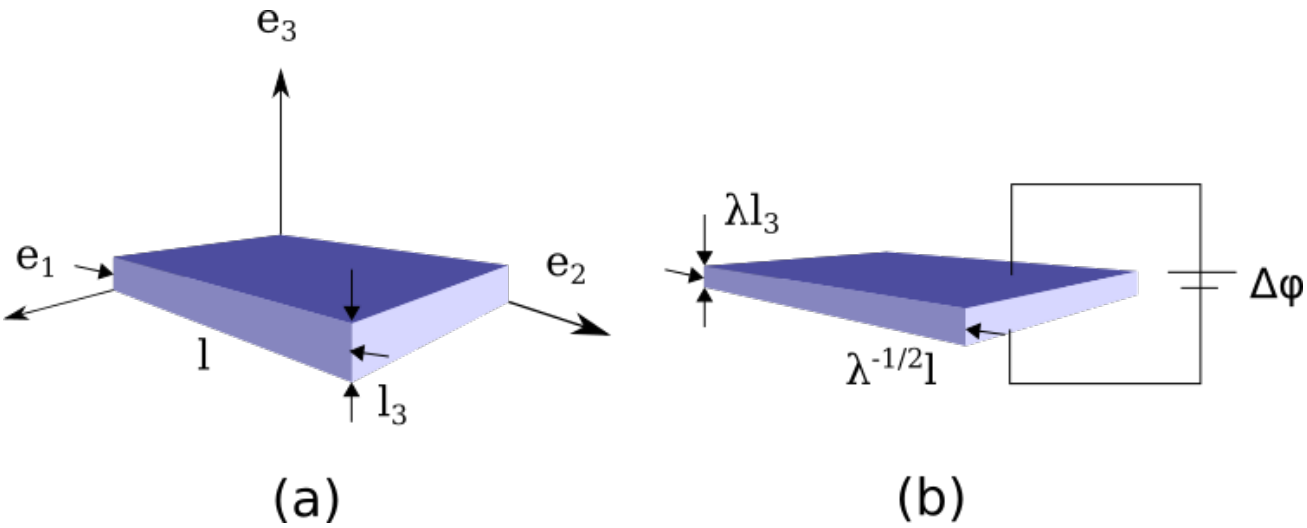

Figure 4.8: Dielectric elastomer actuator in the reference configuration (a) and deformed state (b). A voltage difference is applied across the top and bottom surfaces, which are then attracted to each other in accordance with Coulomb's law. The attraction between the electrodes compresses the film across its thickness. Additional stress develops as a result of the electromechanical coupling of the material itself [Cd16, Suo10].

theory and analysis of the stability of DEAs, see [ZDDP17, YZS17, ZS07].

Let the dimensions of the DEA in the reference configuration be $l \times l \times l_3$ where $l_3 <<$ is the thickness of the DE film. The top and bottom surfaces of the DE film are assumed to be covered with compliant electrodes–compliant such that they have negligible stiffness. When operating the DEA, a voltage difference, $\Delta\varphi$, is applied across the top and bottom surfaces. Equal and opposite net charges, $\pm Q$, accumulate on the top and bottom surfaces, which are then attracted to each other in accordance with Coulomb's law. The attraction between the electrodes compresses the film across its thickness. And an additional stress develops as a result of the electromechanical coupling of the material itself [Cd16, Suo10]. The DEA setup is shown in Figure 4.8

Following [YZS17] and [ZS07], the free energy of a DEA undergoing homogeneous deformation, $\mathbf{F} = \mathrm{diag}\left(\lambda^{-1/2}, \lambda^{-1/2}, \lambda\right)$, is:

$$\Psi = l^2 l_3 \left(\mathcal{W} + \frac{1}{2}E^2\right) - (\Delta\varphi)\, Q \tag{4.2.4.1}$$

where the first term in the parentheses is the free energy density of the DE film and the second term

in the parentheses is the energy density of the electric field; and the last term in (4.2.4.1) is the work of the battery. (Note: (4.2.4.1) is in Gaussian units, i.e. $\epsilon_0 = 1$.) However, (4.2.4.1) is in terms of $\mathcal{W}$ instead of $\mathcal{W}^*$. Recalling that $\mathcal{W} = \mathcal{W}^* + \mathbf{P} \cdot \mathbf{E}$ and using Gauss's law:

$$\Psi = l^2 l_3 \left(\mathcal{W}^* - \frac{1}{2} E^2 \right). \tag{4.2.4.2}$$

We have already implicitly assumed that E is constant inside the DE film–which is a good approximation when $l_3 << l$ and the DE film has homogeneous material properties. Further, to a good approximation, $E = -\left(\Delta\varphi\right)/\lambda l_3$.

Now, as mentioned previously, there is an initial relaxation, in general, after manufacturing an anisotropic dielectric elastomer. We do not want this initial deformation to bias our results in any way. Therefore, we propose the following process:

1. The DE film is manufactured; it relaxes to some $\lambda = \lambda^\star$. In anticipation of this relaxation, its initial, pre-relaxation thickness is $l_3/\lambda^\star$.
2. A voltage difference, $\Delta\varphi$, is applied across the electrodes.
3. The DE film deforms further by some amount λ' such that $\lambda = \lambda'\lambda^\star$.

To model this process, we reformulate (4.2.4.2) as:

$$\Psi\left(\lambda'\right) = l^2 l_3 \left[\mathcal{W}^* \left(\lambda^\star \lambda', \tilde{E} \lambda'^{-1} \right) - \frac{1}{2} \tilde{E}^2 \lambda'^{-2} \right] \tag{4.2.4.3}$$

where $\tilde{E} = \Delta\varphi/l_3$. The stable equilibrium states of the DEA are given by $\frac{d\Psi}{d\lambda'} = 0, \frac{d^2\Psi}{d\lambda'^2} > 0$; the DEA becomes unstable when $\frac{d\Psi}{d\lambda'} = 0, \frac{d^2\Psi}{d\lambda'^2} \leq 0$. The equation $\frac{d\Psi}{d\lambda'} = 0$, however, is a highly nonlinear function of λ'. Even if one Taylor expands the $w_f^* \left(\tilde{E}^2 \lambda'^{-2} \left(\Delta\chi\right)/2kT \right)$ terms (see (4.2.3.2)) (about $\tilde{E} = 0$) and truncates higher order terms, the equilibrium equation still requires solving for the roots of a 5th order polynomial. Instead, moving forward, we use Newton's method with an initial guess of $\lambda' = 1$.

DEA deformation

Let $\mathcal{E} \coloneqq \tilde{E}\sqrt{n\mathcal{X}^h_{\text{free}}/kT}$. This is a nondimensional measure of the electric field (similar to the dimensionless electric field used in [ZHS07, ZDDP17]). Because we would like to emphasize optimization, in this section, as opposed to control, we will focus on three types of networks: a uniform (isotropic) network–as a baseline, network designs in the limit of $\sigma = 0$, and the aforeproposed hybrid network. Similarly, because (for unitype networks) elastomers that consist of TI monomers will have an greater electromechanically induced susceptibility than elastomers consisting of uniaxial monomers, we will consider elastomers such that $\Delta\chi = \chi_\perp$ for the uniform and $\sigma = 0$ networks.

First, Figure 4.9 shows λ' vs θ_0 contours of constant $\mathcal{E}$. It can be seen in Figure 4.9 that, for each of the contours, $\theta_0 = \theta_{iso}$ has the least amount of deformation. In fact, the contours are symmetric about θ_{iso}. However, while the deformation increases as θ_0 has a larger deviation from θ_{iso}, the DEA also fails at smaller $\mathcal{E}$. Thus, there is a trade-off between the maximizing the deformation for a fixed $\mathcal{E}$ and maximizing the operating $\mathcal{E}$ before failure–and, consequently, the maximum deformation possible. Put differently, there is a trade-off between electromechanical efficiency and stability. Note that it can be seen from numerical examples that $\theta_0 = \theta_{iso}$ has an equivalent electromechanical response to the uniform network. Thus, $\theta_0 = \theta_{iso}$ represents our isotropic baseline.

Next, we consider the hybrid network within this context. Figure 4.10 compares the DEA deformation of the hybrid network to the unitype networks with $\sigma = 0$. For a given $\mathcal{E}$, the hybrid network deforms more than the unitype isotropic network (i.e. $\theta_0 = \theta_{iso}$). However, for $\mathcal{E}$ low enough, there is always some $\theta_0, \sigma = 0$ for which the unitype network has a larger induced deformation than the hybrid network.

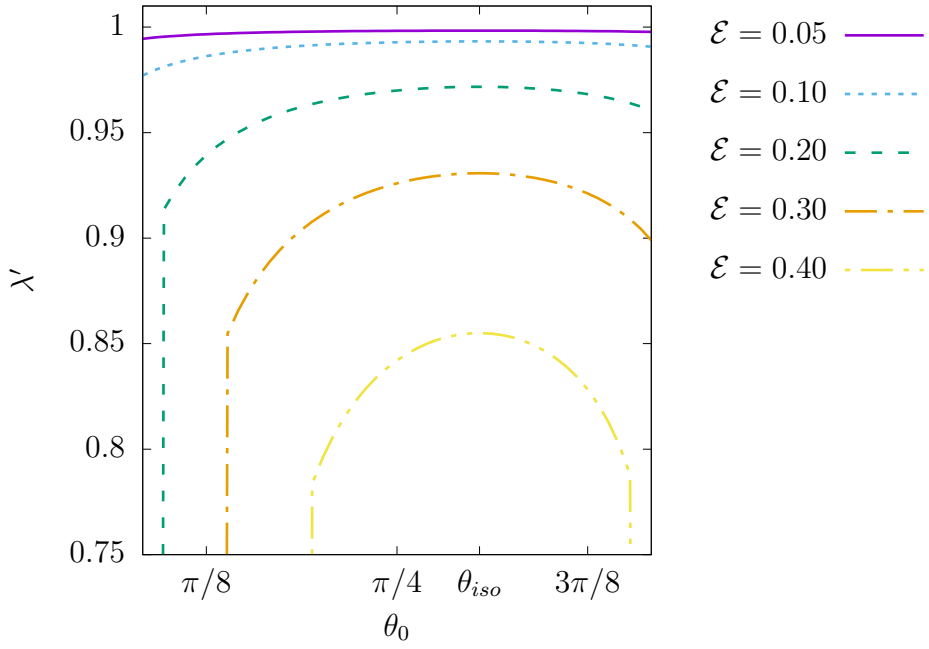

Figure 4.9: λ' vs θ_0 contours of constant $\mathcal{E}$. For each of the contours, $\theta_0 = \theta_{iso}$ has the least amount of deformation and the contours are symmetric about θ_{iso}. However, while the deformation increases as θ_0 has a larger deviation from θ_{iso}, the DEA also fails at smaller $\mathcal{E}$. Note that $\theta_0 = \theta_{iso}$ has an equivalent electromechanical response to the uniform network–so $\theta_0 = \theta_{iso}$ represents our isotropic baseline.

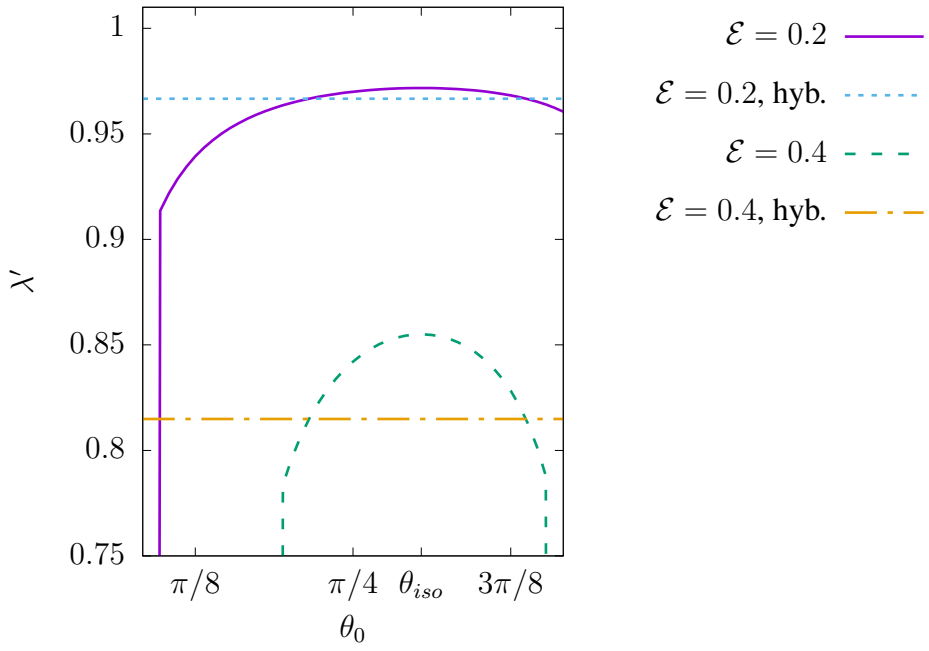

Figure 4.10: Comparison of the DEA deformation of the hybrid network to the unitype networks with $\sigma = 0$. The unitype networks have varying θ_0. Notice: for a given $\mathcal{E}$, the hybrid network deforms more than the unitype isotropic network (i.e. $\theta_0 = \theta_{iso}$). However, for $\mathcal{E}$ low enough, there is always some $\theta_0, \sigma = 0$ for which the unitype network has a large induced deformation than the hybrid network.

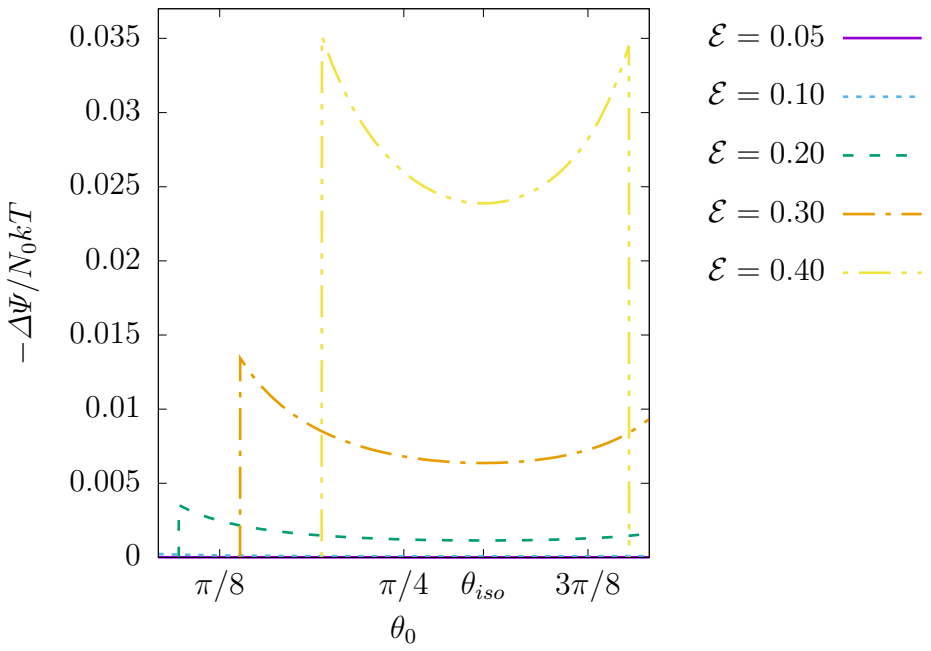

Figure 4.11: $-\Delta\Psi/N_0kT$ vs θ_0 contours of constant $\mathcal{E}$. For each of the contours, $\theta_0 = \theta_{iso}$ has the least amount of usable work and the contours are symmetric about θ_{iso}. However, while the deformation increases as θ_0 has a larger deviation from θ_{iso}, the DEA also fails at smaller $\mathcal{E}$. Note that $\theta_0 = \theta_{iso}$ has an equivalent electromechanical response to the uniform network–so $\theta_0 = \theta_{iso}$ represents our isotropic baseline.

DEA usable work

Another performance metric for our DEAs is the amount of usable work that can be derived from the system. We will use $-\Delta\Psi$ as a measure of the usable work, where

$$\Delta\Psi = \Psi\left(\lambda^\star\lambda', \mathcal{E}\right) - \Psi\left(\lambda^\star, \mathcal{E}\right).$$

Figure 4.11 shows $-\Delta\Psi/N_0kT$ vs θ_0 contours of constant $\mathcal{E}$. Similar to the case of deformation, it can be seen that, for a given $\mathcal{E}$, the usable work can be maximized by picking the θ_0 such that $|\theta_{iso} - \theta_0|$ is maximized without an instability occurring.

Next, consider the usable work of the hybrid network compared to the unitype $\sigma = 0$ networks. Figure 4.12 shows $-\Delta\Psi/N_0kT$ as a function of $\mathcal{E}$ for $\sigma = 0; \theta_0 = \pi/6, \pi/4, \theta_{iso}, \pi/3$ and the hybrid network. Again, it can be seen that for a fixed $\mathcal{E}$, a unitype network with properly chosen θ_0

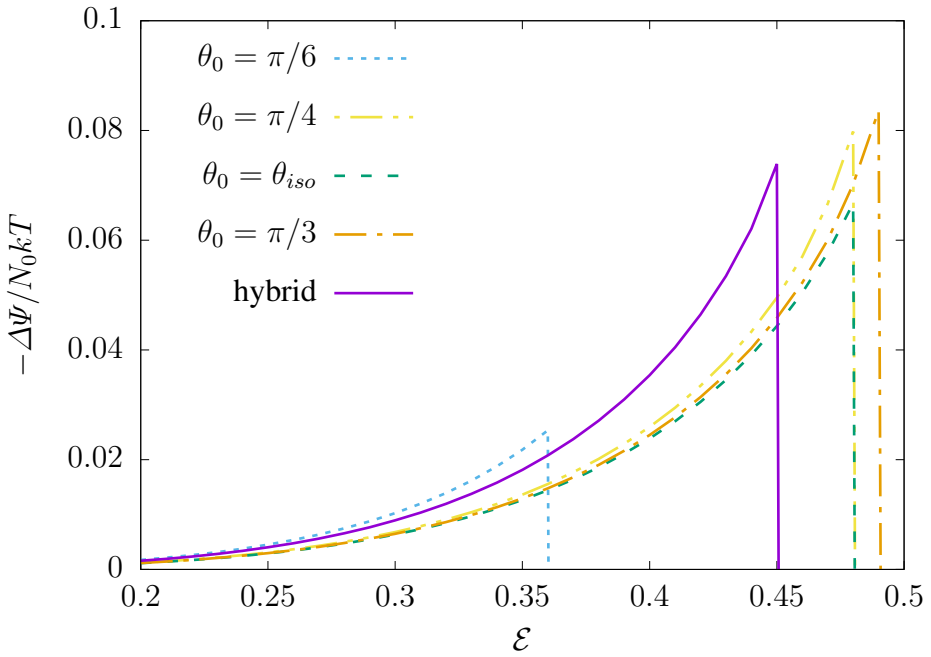

Figure 4.12: Comparison of the DEA usable work of the hybrid network to the unitype networks with $\sigma = 0$. While the most usable work can be derived from a unitype, $\sigma = 0$ network with properly chosen θ_0 for a given $\mathcal{E}$, the hybrid network combines both stability and an enhanced usable work. In fact, the hybrid network performs $\approx 75\%$ better than the isotropic network.

can outperform the hybrid network. However, the hybrid network combines both a higher electromechanical coupling (than the isotropic network) and maintains its stability at larger $\mathcal{E}$. In particular, *the hybrid network shows* $\approx 75\%$ *increase in usable work over the isotropic network for general* $\mathcal{E}$. While $\sigma = 0, \theta_0 = \theta_{iso}$ can endure a larger $\mathcal{E}$ before failure, the maximum usable work before failure of the hybrid network is still greater than that of the isotropic network. In summary the unitype, $\sigma = 0$ networks can be optimized for a specific electrical load more so than the hybrid network. However, the hybrid network is more stable and would be much more preferable than the unitype network when used in an application with a wider range of operating $\mathcal{E}$.

4.3 Conclusion

The theoretical design and analysis of anisotropic dielectric elastomers for enhanced electromechanical coupling was carried out. For this work, we proposed the following design parameters: the distribution

of chain end-to-end vectors in the network, P; the mass density (i.e. $N_0 n$); the density of cross-links (i.e. n/N_0); and the fraction of loose-end monomers, α. It turned out that, to a good approximation, the behavior of the network was invariant with respect to α. However, the stiffness of the material is proportional to the density of cross-links. And, in addition, the electromechanically induced susceptibility of the DE is proportional to the density of cross-links. Thus, as is analogous to many problems in soft multifunctional composites, there is a trade-off between compliance and electromechanical coupling in regards to the density of cross-links in a dielectric elastomer network. In addition to considering the effect of P on $Y_{\parallel}$ and $Y_{\perp}$, we also considered its effect on the DE susceptibility and the electromechanical coupling of the DEA. It was found that substantial gains in the deformation and usable work, for fixed electrical input, can be obtained by designing and manufacturing an anisotropic DE material. In addition, a so-called "hybrid network" was proposed which consisted of uniaxial chains oriented with $\hat{\mathbf{E}}$ and $-\hat{\mathbf{E}}$ and TI chains oriented orthogonal to $\hat{\mathbf{E}}$. The hybrid network preserved the isotropic stiffness and electromechanical stability of the DE, while increasing its usable work output by $\approx 75\%$. These results suggest concrete ways in which novel DEs with enhanced electromechanical coupling can be designed and manufactured for specific applications.

Chapter 5

Conclusion

5.1 Summary

A statistical mechanics-based, multiscale model of dielectric elastomers was developed and presented. The model showed some interesting physical phenomena such as: (1.) the interaction between electrostatics, chain orientation, and chain stiffness in DE chains, (2.) the presence of electrostatic chain torque in DE chains and its influence in the electromechanical coupling of DE networks, and (3.) the interaction between chain stretch and polarizability, which, at the macroscopic-scale, manifests itself as a deformation dependent susceptibility. The newly discovered phenomena inspired a comprehensive investigation at how the architecture of DE networks may be designed and manufactured in order to optimize their electromechanical coupling for different applications.

5.2 Future work

5.2.1 Experimental measurement of dielectric elastomer paramters

The multiscale model for the electroelastic behavior of dielectric elastomers requires the input of four molecular- and macromolecular-scale properties: the density of polymer chains per unit volume in the reference configuration, N_0; the number of monomers per chain, n; and the two susceptibility parameters, $\chi_{\parallel}$ and $\chi_{\perp}$. An important feature of a model is that its various parameters can be isolated and measured by simple, independent experiments. Therefore, we consider for a moment how one may reliably isolate and measure the aforementioned parameters for dielectric elastomers.

Firstly, in the absence of an externally applied electric field, the multiscale model presented herein recovers the Arruda-Boyce constitutive model for rubber elasticity [AB93]. The authors show that their model can be fit to experimental stress-strain data well. So while N_0 and n cannot be isolated from each other, they can be isolated from the susceptibility parameters. Thus, N and n can be determined by fitting stress-strain data in the absence of an applied electric field. While fitting two parameters at once is not ideal, one could make the fit more robust by fitting different modes of strain. For instance, one may choose to fit N and n by minimizing error for a uniaxial tension test and shear-strain test, simultaneously.

Having obtained N_0 and n separately, $\chi_{\parallel}$ and $\chi_{\perp}$ can then be determined. As mentioned previously, in general, the (bulk) susceptibility of the elastomer is not only a function of its monomer susceptibility parameters, but also a function of deformation. Therefore, one can run experiments where:

1. The DE specimen is put into a capacitor where it is loaded mechanically such that it deforms like $\mathrm{diag}\left(\lambda^{-1/2}, \lambda^{-1/2}, \lambda\right)$.

2. A voltage difference is applied across the capacitor plates such that a weak electric field is applied in the dielectric elastomer ("weak" can be achieved in a limiting fashion).

3. The deformation, λ, and polarization, P, are measured. Let $\mathcal{X}_{lab} = P/E$.

4. Repeating this procedure, a function $\mathcal{X}_{lab} = \mathcal{X}_{lab}(\lambda)$ is developed in the limit of weak electric field.

5. Using the previously fitted parameters, N_0 and n, and the measured curve, $\mathcal{X}_{lab} = \mathcal{X}_{lab}(\lambda)$, fit $\chi_{\parallel}$ and $\chi_{\perp}$.

5.2.2 Instability

The onset of instabilities and failure in DEAs has been studied recently [WZZ11, ZS07, ZDDP17, YZS17]. However, all of the aforementioned works model the dielectric elastomer as *ideal*; that is, they do not consider a deformation dependent susceptibility or an electrostatic dependent stiffness. It may be that if one were to use a DE constitutive relationship that considers these effects, like the one developed in this work, that one would predict novel modes of instabilities. Conducting such an investigation could be an avenue of future research.

5.2.3 Two-scale energetics

It was seen in Chapter 2 that the symmetry breaking that occurs when a chain end-to-end vector is not aligned with the electric field makes obtaining an exact solution of the chain free energy difficult. However, one can perhaps circumvent this difficulty by investigating the regime in which the electrostatic energy of the chain dominates the elastic (i.e. entropic) contribution. If the two energy scales can be separated, then the statistical mechanics of the electrostatics can be solved independently of the elasticity; and then, a Gaussian chain-like elasticity may be assumed about the electrostatic solution. Since considering the electrostatic problem independently of the elasticity problem makes the electrostatic statistics simpler, it may be possible to include dipole-dipole (i.e. monomer-monomer) interactions into the Hamiltonian and still obtain a closed-form solution (or approximation). Modeling molecular interactions is important for capturing phenomena such as phase transitions. Thus, such an approach may potentially lead to some interesting predictions regarding phase transitions in dielectric elastomer chains; and, subsequently, the phase transitions may be utilized to increase the

electromechanical coupling of the material.

5.2.4 Visco-electro-elasticity of dielectric elastomers

Many of the applications of DEs such as robotics, prothetics, energy harvesting, etc., are a part of a dynamic system. As a result, there has been some work in modeling the viscoelectroelastic constitutive behavior of DEs [HLCF+12]. However, results have only matched experiments qualitatively and not quantitatively. Again, as an alternative to phenomenological approaches, future work could involve modeling the nonequilibrium behavior of DEs using statistical mechanics through closed-form approximations and/or numerics. For closed-form solutions, Liouville's theorem, through a system of partial differential equations, describes how the density of (micro-) states of a thermodynamic system evolves in time. The initial conditions for the partial differential equations can be derived from work that has been proposed in previous sections. Specifically, the work which involves deriving the equilibrium statistical mechanics of an DE, will, for each set of macroscopic initial conditions of interest (e.g. electrical loading, mechanical loading, constraints, etc.), provide a corresponding set of initial conditions on the density of states of the system. Although the differential equations can prove difficult to solve for certain systems, there are various methods of solution that have been developed. For example, in [Pri17], it is pointed out that the Liouville operator is Hermitian. As a result, the partial differential equations governing the evolution of the density of states in time resemble the time dependent Schrödinger wave equation. A typical method for solving the evolution of a wave equation in time is to expand it in a linear superposition of energy eigenstates and recognize that the change in each eigenstate is determined by its corresponding eigenvalue. Similarly, the time dependent behavior of the density of states can be expanded in a linear superposition of eigenfunctions of the Liouville operator. If this approach proves to be infeasible, then there is also the so-called linear response theory (see for example [KTH12, Maz08]) which relates the equilibrium fluctuations of the system to its nonequilibrium behavior. Derivations using linear response theory are much simpler than the eigenfunction approach but rely on the assumption that the system is always *near* to equilibrium while it transitions from one macroscopic state to another. For numeric solutions, one could in principle ap-

proximate a solution to Liouville's equations using Finite Elements or Finite Differences. However, the dimensionality of the space ($6n$ where n is the number of monomers in a chain) would make such an approximation computationally expensive and scale poorly with mesh resolution. Instead, molecular simulation methods such as nonequilibrium molecular dynamics (for example, Ch. 8 of [AT17]) and kinetic Monte Carlo (e.g. [Vot07]) could prove more useful. Future work will include modeling the time-dependent and dissipative behavior of EAPs. Similar to Chapter 2, it may prove fruitful to model this behavior using closed-form approximations where possible and numerical methods as a way to compliment and aid in the development of such closed-form approximations. Lastly, a multiscale analysis similar to that performed in [Cd14] could be used to relate chain-scale dynamics to macroscopic dynamics.

5.2.5 Flexoelectricity

It has been pointed out that, soft materials may be designed and engineered in order to maximize their flexoelectric and the transverse piezoelectric effects [RBS19]. This is important because many applications of soft multifunctional materials (e.g. sensing and actuation in soft robotics) require a flexural electromechanical coupling. One reason, in particular, is that bending deformations typically have a lower resonance frequency and higher attainable strain [RBS19]. Future work could include looking at designing polarizable elastomers (with or without frozen in polarization) for optimal flexoelectric and tranverse piezoelectric couplings.

References

Bibliography

[AB93] Ellen M Arruda and Mary C Boyce. A three-dimensional constitutive model for the large stretch behavior of rubber elastic materials. *Journal of the Mechanics and Physics of Solids*, 41(2):389–412, 1993.

[AT17] Michael P Allen and Dominic J Tildesley. *Computer simulation of liquids*. Oxford university press, 2017.

[BA00] Mary C Boyce and Ellen M Arruda. Constitutive models of rubber elasticity: a review. *Rubber chemistry and technology*, 73(3):504–523, 2000.

[BC04] Yoseph Bar-Cohen. *Electroactive polymer (EAP) actuators as artificial muscles*. SPIE–The International Society for Optical Engineering, 2004.

[BDO09] Roger Bustamante, Alois Dorfmann, and Ray W Ogden. Nonlinear electroelastostatics: a variational framework. *Zeitschrift für angewandte Mathematik und Physik*, 60(1):154–177, 2009.

[BO13] Carl M Bender and Steven A Orszag. *Advanced mathematical methods for scientists and engineers I: Asymptotic methods and perturbation theory*. Springer Science & Business Media, 2013.

[BPK+12] Michael Bozlar, Christian Punckt, Sibel Korkut, Jian Zhu, Choon Chiang Foo, Zhigang

Suo, and Ilhan A Aksay. Dielectric elastomer actuators with elastomeric electrodes. *Applied physics letters*, 101(9):091907, 2012.

[Bre72] Richard Brent. *Algorithms for Minimization without Derivatives*. Prentice-Hall, 1972.

[CC60] Charles W Clenshaw and Alan R Curtis. A method for numerical integration on an automatic computer. *Numerische Mathematik*, 2(1):197–205, 1960.

[Cd14] Noy Cohen and Gal deBotton. Multiscale analysis of the electromechanical coupling in dielectric elastomers. *European Journal of Mechanics-A/Solids*, 48:48–59, 2014.

[Cd16] Noy Cohen and Gal deBotton. Electromechanical interplay in deformable dielectric elastomer networks. *Physical review letters*, 116(20):208303, 2016.

[CDd16] Noy Cohen, Kaushik Dayal, and Gal deBotton. Electroelasticity of polymer networks. *Journal of Mechanics Physics of Solids*, 92:105–126, 2016.

[CKSLA11] Federico Carpi, Roy Kornbluh, Peter Sommer-Larsen, and Gursel Alici. Electroactive polymer actuators as artificial muscles: are they ready for bioinspired applications? *Bioinspriation & Biommetics*, 6(4):045006, 2011.

[Coh18] Noy Cohen. A generalized electro-elastic theory of polymer networks. *Journal of the Mechanics and Physics of Solids*, 110:173–191, 2018.

[D$^+$72] HE Daniels et al. Kuhn-grün type approximations for polymer chain distributions. In *Proceedings of the Sixth Berkeley Symposium on Mathematical Statistics and Probability, Volume 3: Probability Theory*. The Regents of the University of California, 1972.

[DB81] N.G. De Bruijn. *Asymptotic Methods in Analysis*. Dover Publications, 1981.

[DO06] A Dorfmann and RW Ogden. Nonlinear electroelastic deformations. *Journal of Elasticity*, 82(2):99–127, 2006.

[DO14] Luis Dorfmann and Ray W Ogden. *Nonlinear theory of electroelastic and magnetoelastic interactions*. Springer, 2014.

[F+06] Glenn Fredrickson et al. *The equilibrium theory of inhomogeneous polymers*, volume 134. Oxford University Press on Demand, 2006.

[FR43] Paul J Flory and John Rehner. Statistical mechanics of cross-linked polymer networks. ii. *The Journal of Chemical Physics*, 11:521–526, 1943.

[Gri89] David J Griffiths. *Introduction to electrodynamics*. Prentice-Hall, 1989.

[HCB13] David L Henann, Shawn A Chester, and Katia Bertoldi. Modeling of dielectric elastomers: Design of actuators and energy harvesting devices. *Journal of the Mechanics and Physics of Solids*, 61(10):2047–2066, 2013.

[Hil86] Terrell L Hill. *An introduction to statistical thermodynamics*. Dover Publications, 1986.

[Hin91] E John Hinch. *Perturbation methods*. Cambridge university press, 1991.

[HLCF+12] Jiangshui Huang, Tiefeng Li, Choon Chiang Foo, Jian Zhu, David R Clarke, and Zhigang Suo. Giant, voltage-actuated deformation of a dielectric elastomer under dead load. *Applied Physics Letters*, 100(4):041911, 2012.

[HZS09] Tianhu He, Xuanhe Zhao, and Zhigang Suo. Dielectric elastomer membranes undergoing inhomogeneous deformation. *Journal of Applied Physics*, 106(8):083522, 2009.

[IKW18] Mikhail Itskov, Vu Ngoc Khiêm, and Sugeng Waluyo. Electroelasticity of dielectric elastomers based on molecular chain statistics. *Mathematics and Mechanics of Solids*, 2018.

[Jed17] Radosław Jedynak. New facts concerning the approximation of the inverse langevin function. *Journal of Non-Newtonian Fluid Mechanics*, 249:8–25, 2017.

[JG43] Hubert M James and Eugene Guth. Theory of the elastic properties of rubber. *The Journal of Chemical Physics*, 11(10):455–481, 1943.

[Joha] Steven G Johnson. The cubature integration package. https://github.com/stevengj/cubature. [Online; accessed 31-March-2018].

[Johb] Steven G Johnson. The NLopt nonlinear-optimization package. http://github.com/stevengj/nlopt. [Online; accessed 31-March-2018].

[KG42] Werner Kuhn and F Grün. Beziehungen zwischen elastischen konstanten und dehnungsdoppelbrechung hochelastischer stoffe. *Kolloid-Zeitschrift*, 101(3):248–271, 1942.

[Kof08] Guggi Kofod. The static actuation of dielectric elastomer actuators: how does pre-stretch improve actuation? *Journal of Physics D: Applied Physics*, 41(21):215405, 2008.

[Kra06] Werner Krauth. *Statistical mechanics: algorithms and computations*, volume 13. Oxford University Press, 2006.

[Kro15] Martin Kroeger. Simple, admissible, and accurate approximants of the inverse langevin and brillouin functions, relevant for strong polymer deformations and flows. *Journal of Non-Newtonian Fluid Mechanics*, 223:77–87, 2015.

[KT07] Kwang J Kim and Satoshi Tadokoro. Electroactive polymers for robotic applications. *Artificial Muscles and Sensors*, 23:291, 2007.

[KTH12] Ryogo Kubo, Morikazu Toda, and Natsuki Hashitsume. *Statistical physics II: nonequilibrium statistical mechanics*, volume 31. Springer Science & Business Media, 2012.

[KZSK12] Matthias Kollosche, Jian Zhu, Zhigang Suo, and Guggi Kofod. Complex interplay of nonlinear processes in dielectric elastomers. *Physical Review E*, 85(5):051801, 2012.

[Liu13] Liping Liu. On energy formulations of electrostatics for continuum media. *Journal of the Mechanics and Physics of Solids*, 61(4):968–990, 2013.

[Liu14] Liping Liu. An energy formulation of continuum magneto-electro-elasticity with applications. *Journal of the Mechanics and Physics of Solids*, 63:451–480, 2014.

[Maz08] Gene F Mazenko. *Nonequilibrium statistical mechanics*. John Wiley & Sons, 2008.

[MGL04] C Miehe, S Göktepe, and F Lulei. A micro-macro approach to rubber-like matrials–part i: the non-affine micro-sphere model of rubber elasticity. *Journal of the Mechanics and Physics of Solids*, 52(11):2617–2660, 2004.

[MR18] Patrick Kofod Mogensen and Asbjørn Nilsen Riseth. Optim: A mathematical optimization package for Julia. *Journal of Open Source Software*, 3(24):615, 2018.

[PKK00] Ron Pelrine, Roy Kornbluh, and Guggi Kofod. High-strain actuator materials based on dielectric elastomers. *Advanced Materials*, 12(16):1223–1225, 2000.

[Pri17] Ilya Prigogine. *Non-equilibrium Statistical Mechanics*. Dover, 2017.

[RBS19] Amir Hossein Rahmati, Siegfried Bauer, and Pradeep Sharma. Nonlinear bending deformation of soft electrets and prospects for engineering flexoelectricity and transverse (d 31) piezoelectricity. *Soft matter*, 15(1):127–148, 2019.

[Row90] Thomas Harvey Rowan. *Functional stability analysis of numerical algorithms*. PhD thesis, Ph. D. thesis, Department of Computer Sciences, Univ. of Texas, 1990.

[SA08] Ahmad Safari and E Koray Akdogan. *Piezoelectric and acoustic materials for transducer applications*. Springer Science & Business Media, 2008.

[Sto67] Walter H Stockmayer. Dielectric dispersion in solutions of flexible polymers. *Pure and Applied Chemistry*, 15(3-4):539–554, 1967.

[Suo10] Zhigang Suo. Theory of dielectric elastomers. *Acta Mechanica Solida Sinica*, 23(6):549–578, 2010.

[SW17] Kevin Shen and Zhen-Gang Wang. Electrostatic correlations and the polyelectrolyte self energy. *The Journal of chemical physics*, 146(8):084901, 2017.

[SZG08] Zhigang Suo, Xuanhe Zhao, and William H Greene. A nonlinear field theory of deformable dielectrics. *Journal of the Mechanics and Physics of Solids*, 56(2):467–486, 2008.

[TM11] Ellad B Tadmor and Ronald E Miller. *Modeling materials: continuum, atomistic and multiscale techniques*. Cambridge University Press, 2011.

[TM14] A Tutcuoglu and Carmel Majidi. Energy harvesting with stacked dielectric elastomer transducers: Nonlinear theory, optimization, and linearized scaling law. *Applied Physics Letters*, 105(24):241905, 2014.

[Tou56] R.A. Toupin. The elastic dielectric. *Journal of Rational Mechanics and Analysis*, 5(6):849–915, 1956.

[Tre75] L R G Treloar. *The physics of rubber elasticity*. Oxford University Press, 1975.

[Vot07] Arthur F Voter. Introduction to the kinetic monte carlo method. In *Radiation effects in solids*, pages 1–23. Springer, 2007.

[Wei12] Jerome Harris Weiner. *Statistical mechanics of elasticity*. Courier Corporation, 2012.

[WM07] Michael Wissler and Edoardo Mazza. Mechanical behavior of an acrylic elastomer used in dielectric elastomer actuators. *Sensors and Actuators A: Physical*, 134(2):494–504, 2007.

[WVDG93] PD Wu and Erik Van Der Giessen. On improved network models for rubber elasticity and their applications to orientation hardening in glassy polymers. *Journal of the Mechanics and Physics of Solids*, 41(3):427–456, 1993.

[WZZ11] Qiming Wang, Lin Zhang, and Xuanhe Zhao. Creasing to cratering instability in polymers under ultrahigh electric fields. *Physical review letters*, 106(11):118301, 2011.

[YZS17] Shengyou Yang, Xuanhe Zhao, and Pradeep Sharma. Revisiting the instability and bifurcation behavior of soft dielectrics. *Journal of Applied Mechanics*, 84(3):031008, 2017.

[ZDDP17] Giuseppe Zurlo, Michel Destrade, Domenico DeTommasi, and Giuseppe Puglisi. Catastrophic thinning of dielectric elastomers. *Physical review letters*, 118(7):078001, 2017.

[ZHS07] Xuanhe Zhao, Wei Hong, and Zhigang Suo. Electromechanical hysteresis and coexistent states in dielectric elastomers. *Physical review B*, 76(13):134113, 2007.

[ZS07] Xuanhe Zhao and Zhigang Suo. Method to analyze electromechanical stability of dielectric elastomers. *Applied Physics Letters*, 91(6):061921, 2007.

[ZS08] Xuanhe Zhao and Zhigang Suo. Electrostriction in elastic dielectrics undergoing large deformation. *Journal of Applied Physics*, 104(12):123530, 2008.

Appendix A

Polarization, $\frac{\partial \mathcal{A}^*}{\partial \mathbf{E}}$, and $\frac{\partial \mathcal{W}^*}{\partial \mathbf{E}}$

We show that a consequence of assuming (2.1.0.7) as the form of the monomer density function and enforcing the constraints given in (3.0.0.3), we arrive at the relationship: $\mathbf{p} = -\frac{\partial \mathcal{A}^*}{\partial \mathbf{E}}$.

Proof. Taking derivatives of both sides of (3.0.0.3) with respect to $\mathbf{E}$, we obtain:

$$\begin{aligned} \frac{\partial}{\partial \mathbf{E}} \int_{\mathbb{S}^2} \mathrm{d}A \, \rho\left(\hat{\mathbf{n}}\right) &= \int_{\mathbb{S}^2} \mathrm{d}A \, \frac{\partial \rho}{\partial \mathbf{E}} = \frac{\partial n}{\partial \mathbf{E}} = 0 \\ \frac{\partial}{\partial \mathbf{E}} \int_{\mathbb{S}^2} \mathrm{d}A \, \rho\left(\hat{\mathbf{n}}\right) \hat{\mathbf{n}} &= \int_{\mathbb{S}^2} \mathrm{d}A \, \frac{\partial \rho}{\partial \mathbf{E}} \hat{\mathbf{n}} = \frac{\partial \mathbf{r}/b}{\partial \mathbf{E}} = 0 \end{aligned} \tag{A.0.0.1}$$

We are able to interchange the operations of derivation and integration because of the smoothness of the integrands; and in the last equalities we use the fact that neither the number of the monomers in the chain nor the end-to-end vector constraint depend on $\mathbf{E}$.

Now, we obtain the desired result by taking derivatives of both sides of (3.0.0.4):

$$\begin{aligned}
-\frac{\partial \mathcal{A}^*}{\partial \mathbf{E}} &= -\frac{\partial}{\partial \mathbf{E}} \int_{\mathbb{S}^2} \mathrm{d}A \ (\rho u + kT\rho \ln \rho) \\
&= -\int_{\mathbb{S}^2} \mathrm{d}A \ \left[\frac{\partial \rho}{\partial \mathbf{E}} u + \rho \frac{\partial u}{\partial \mathbf{E}} + kT \frac{\partial \rho}{\partial \mathbf{E}} \ln \rho + \rho \left(\frac{\partial \rho}{\partial \mathbf{E}} / \rho \right) \right] \\
&= -\int_{\mathbb{S}^2} \mathrm{d}A \ \left[\frac{\partial \rho}{\partial \mathbf{E}} u + \rho \frac{\partial u}{\partial \mathbf{E}} + kT \frac{\partial \rho}{\partial \mathbf{E}} (\ln C - u/kT + \boldsymbol{\tau} \cdot \hat{\mathbf{n}}) + \frac{\partial \rho}{\partial \mathbf{E}} \right] \\
&= -\int_{\mathbb{S}^2} \mathrm{d}A \ \left[\rho \frac{\partial u}{\partial \mathbf{E}} + kT \frac{\partial \rho}{\partial \mathbf{E}} (\boldsymbol{\tau} \cdot \hat{\mathbf{n}}) + (kT \ln C + 1) \frac{\partial \rho}{\partial \mathbf{E}} \right] \\
&= -\int_{\mathbb{S}^2} \mathrm{d}A \ \rho \frac{\partial u}{\partial \mathbf{E}} - kT \boldsymbol{\tau} \cdot \left(\int_{\mathbb{S}^2} \mathrm{d}A \ \frac{\partial \rho}{\partial \mathbf{E}} \hat{\mathbf{n}} \right) - (kT \ln C + 1) \int_{\mathbb{S}^2} \mathrm{d}A \ \frac{\partial \rho}{\partial \mathbf{E}}
\end{aligned}$$

By (A.0.0.1), the last two terms vanish. Thus, recalling (2.2.1.9) and (2.2.1.7):

$$\begin{aligned}
-\frac{\partial \mathcal{A}^*}{\partial \mathbf{E}} &= -\int_{\mathbb{S}^2} \mathrm{d}A \ \rho \frac{\partial u}{\partial \mathbf{E}} \\
&= \int_{\mathbb{S}^2} \mathrm{d}A \ \rho \frac{\partial}{\partial \mathbf{E}} \left(\frac{1}{2} \mathbf{E} \cdot \boldsymbol{\chi}_\mu \mathbf{E} \right) \\
&= \int_{\mathbb{S}^2} \mathrm{d}A \ \rho \frac{1}{2} \left(\boldsymbol{\chi}_\mu \mathbf{E} + \boldsymbol{\chi}_\mu^T \mathbf{E} \right) \\
&= \int_{\mathbb{S}^2} \mathrm{d}A \ \rho \boldsymbol{\mu} \\
&= \mathbf{p}
\end{aligned}$$

as desired. □

It is obvious then that this is not true of all chains with polarizable monomers such that u includes a dipole-electric field interaction term (i.e. $-\boldsymbol{\mu} \cdot \mathbf{E}$). Instead, this follows from the fact that the dipole susceptibility tensor, $\boldsymbol{\chi}_\mu$, is symmetric; and also from the fact that: *the bond energy between bound charges in the monomer is a linear, spring-like bond energy* such that $u_{\text{bond}} = \frac{1}{2} \boldsymbol{\mu} \cdot \boldsymbol{\chi}_\mu^{-1} \boldsymbol{\mu}$ (again, note that by $\boldsymbol{\chi}_\mu^{-1}$ we mean the generalized inverse of $\boldsymbol{\chi}_\mu$).

Similarly, we show that

$$-\frac{\partial \mathcal{W}^*}{\partial \mathbf{E}} = \mathbf{P} \tag{A.0.0.2}$$

This follows as a consequence of $-\frac{\partial \mathcal{A}^*}{\partial \mathbf{E}} = \mathbf{p}$ and the assumption that chains in the network are in weak interaction (see Section 4.1.1). By the weakly interacting assumption, $\mathcal{W}^* = N \langle \mathcal{A}^* \rangle_{\tilde{\mathbf{r}}}$, where by $\langle \square \rangle_{\tilde{\mathbf{r}}}$ we mean the average over the chain pdf. Hence, taking derivatives of both sides:

$$-\frac{\partial \mathcal{W}^*}{\partial \mathbf{E}} = -\frac{\partial}{\partial \mathbf{E}} N \langle \mathcal{A}^* \rangle_{\tilde{\mathbf{r}}} = N \left\langle -\frac{\partial \mathcal{A}^*}{\partial \mathbf{E}} \right\rangle_{\tilde{\mathbf{r}}} = N \langle \mathbf{p} \rangle_{\tilde{\mathbf{r}}} = J^{-1} \tilde{\mathbf{P}}$$

as desired. The significance of this result is that it–along with the statistical mechanical foundation of how $\mathcal{W}^*$ was derived–establishes $\mathcal{W}^* (\mathbf{F}, \mathbf{E})$ as the Legendre transform of $\mathcal{W} \left(\mathbf{F}, \tilde{\mathbf{P}} \right)$, the Helmholtz free energy density.

As an aside, we mention that the proof of

$$\frac{\partial \mathcal{A}^*}{\partial \mathbf{r}} = \frac{kT}{b} \boldsymbol{\tau}$$

follows from a similar series of arguments as the proof for $-\frac{\partial \mathcal{A}^*}{\partial \mathbf{E}} = \mathbf{p}$. Physically, this means that $\boldsymbol{\tau}$ is a nondimensional measure of the tension in the chain.

Appendix B

Derivatives of $\mathcal{W}$ and $\mathcal{W}^*$

Let the following hold:

1. $\mathcal{W}(\mathbf{F}, \mathbf{P}) = \mathcal{W}^*(\mathbf{F}, \mathbf{E}(\mathbf{P})) + \mathbf{P} \cdot \mathbf{E}(\mathbf{P})$,
2. $\frac{\partial \mathcal{W}}{\partial \mathbf{P}} = \mathbf{E}$,
3. $\frac{\partial \mathcal{W}^*}{\partial \mathbf{E}} = -\mathbf{P}$.

Assume $\mathbf{E}(\mathbf{P})$ invertible such that $\mathbf{P} = \mathbf{P}(\mathbf{E})$, $\frac{\partial \mathbf{P}}{\partial \mathbf{E}}$ is invertible, and $\mathcal{W}$, $\mathcal{W}^*$, $\mathbf{E}(\mathbf{P})$ and $\mathbf{P}(\mathbf{E})$ are all smooth functions.

Proof. By assumption, $\frac{\partial \mathcal{W}}{\partial \mathbf{P}} = \mathbf{E}(\mathbf{P})$. Taking derivatives of both sides:

$$\frac{\partial^2 \mathcal{W}}{\partial \mathbf{P} \partial \mathbf{P}} = \frac{\partial \mathbf{E}}{\partial \mathbf{P}}.$$

Similarly, taking derivatives of both sides of $\frac{\partial \mathcal{W}^*}{\partial \mathbf{E}} = -\mathbf{P}$:

$$\frac{\partial^2 \mathcal{W}^*}{\partial \mathbf{E} \partial \mathbf{E}} = -\frac{\partial \mathbf{P}}{\partial \mathbf{E}}.$$

From the two above equations we can conclude that

$$-\frac{\partial^2 \mathcal{W}^*}{\partial \mathbf{E} \partial \mathbf{E}} = \left(\frac{\partial^2 \mathcal{W}}{\partial \mathbf{P} \partial \mathbf{P}} \right)^{-1}$$

as desired. □

The physical implication of the above result is that: $-\frac{\partial^2 \mathcal{W}^*}{\partial \mathbf{E} \partial \mathbf{E}} = \boldsymbol{\varkappa}$.